Non-orthogonal Multiple Access (NOMA) with Asynchronous Interference Cancellation

A Thesis Submitted to The University of Kent
For The Degree of Doctor of Philosophy
In Electronic Engineering

By

Huseyin Haci

March, 2015

Supervisor

Professor Jiangzhou Wang

Create knowledge, the whole world will benefit...

H. Haci

Dedication

To my family and loved ones

Acknowledgments

I would like to thank Prof Jiangzhou Wang for his invaluable contributions to my scientific and personal development. He always encouraged me to move forward, develop myself and take the further step. Without his comments and contributions the work of this thesis could not be achieved.

I would like to thank Dr Huiling Zhu for her insightful and constructive comments and contributions. Her suggestions were always of great help and improved the work of this thesis greatly.

I would like to thank Dr Wenlong Xu for his kind help during the preparation and presentation of this work.

Finally, I would like to thank the colleagues in the lab and school for their support and friendly environment.

List of publications

1. H. Haci, H. Zhu and J. Wang, "Performance of Non-orthogonal Multiple Access (NOMA) with a Novel Asynchronous Interference Cancellation Technique," submitted to *IEEE Transactions on Wireless Communications*.

2. L. Lopes, R. Sofia, H. Haci and H. Zhu, "A Proposal for Dynamic Frequency Sharing in Wireless Networks," *IEEE Transactions on Networking*, Under second revision.

3. H. Haci and H. Zhu, "Performance of Non-orthogonal Multiple Access with a Novel Interference Cancellation Method," *IEEE International Conference on Communications (ICC2015)*, June 2015, London, UK.

4. H.Haci, H. Zhu and J. Wang, "Resource Allocation in User-Centric Wireless Networks," Chapter in *User-Centric Networking: Future Perspectives*, LNSN, Springer, 2014.

5. P. Mendes, W. Moreira, T. Jamal, H.Haci and H. Zhu, "Cooperative Networking in User-Centric Wireless Networks," Chapter in *User-Centric Networking: Future Perspectives*, LNSN, Springer, 2014.

6. L. Lopes, R. Sofia, H. Osman and H. Haci, "A Proposal for Elastic Spectrum Management in Wireless Local Area Networks," *IEEE Conference on Computer Communications (INFOCOM2014) Demo Session*, April 2014, Toronto, Canada.

7. H. Haci, H. Osman, H. Zhu, R. Sofia and L. Lopes, "Method and apparatus for communication in a wireless network," Patent Application Number: Europe 13191667.8, 6 November 2013.

8. H. Haci and H. Zhu, "Novel Scheduling Characteristics for Mixture of Real-time and Non-real-time Traffic," *IEEE Wireless Communications and Networking Conference (WCNC2013)*, April 2013, Shanghai, China.

9. H. Haci, H. Zhu and J. Wang, "Novel Scheduling for a Mixture of Real-time and Non-real-time Traffic," *IEEE Global Communications Conference (GLOBECOM2012)*, December 2012, Anaheim, California, USA.

10. H. Haci, H. Zhu and J. Wang, "Resource Allocation in User-Centric Wireless Networks," *IEEE 75th Vehicular Technology Conference (VTC2012)*, May 2012, Yokohama, Japan.

Abstract:

Non-orthogonal multiple access (NOMA) allows allocating one carrier to more than one user at the same time in one cell. It is a promising technology to provide high throughput due to carrier reuse within a cell.

In this thesis, a novel interference cancellation (IC) technique is proposed for asynchronous NOMA systems, which uses multiple symbols from each interfering user to carry out IC. With the multiple symbol information from each interfering user the IC performance can be improved substantially. The proposed technique creates and processes so called "IC Triangles". That is, the order of symbol detection is based on detecting all the overlapping symbols of a stonger user before detecting a symbol of a weak user. Also, successive IC (SIC) is employed in the proposed technique. Employing IC Triangles together with the SIC suppresses co-channel interference from strong (earlier detected) signals for relatively weak (yet to be detected) signals and make it possible to achieve low bit error rate (BER) for all users. Further, iterative signal processing is used to improve the system performance. Employing multiple iterations of symbol detection which is based on exploiting a priori estimate obtained from the previous iteration can improve the detection and IC performances. The BER and capacity performance analyses of an uplink NOMA system with the proposed IC technique are presented, along with the comparison to orthogonal frequency division multiple access (OFDMA) systems. Performance analyses validate the requirement for a novel IC technique that addresses asynchronism at NOMA uplink transmissions. Also, numerical and simulation results show that NOMA with the proposed IC technique outperforms OFDMA for uplink transmissions.

It is also concluded from the research that, in the NOMA system, users are required to have large received power ratio to satisfy BER requirements and the required received power ratio increases with increasing the modulation level. Also, employing iterative IC provides significant performance gain in NOMA and the number of required iterations depend on the modulation level and detection method. Further, at uplink transmissions, users' BER and capacity performances strongly depend on the relative time offset between interfering users, besides the received power ratio.

Contents

1 Introduction **12**

1.1 Motivation 12

1.2 Challenges 17

1.3 Contribution of the Thesis 19

1.4 Structure of the Thesis 20

2 Background Theory and Literature Review **23**

2.1 Superposition Coding with Successive Interference Cancellation . . . 23

2.2 Uplink Channel Capacity 27

2.3 Iterative Succesive Interference Cancellation 30

2.4 Literature Review 33

3 System Model **38**

3.1 Uplink NOMA system and Received Signal Structure 38

3.2 Iterative Signal Processing at the Receiver 40

4 Triangular Successive Interference Cancellation (T-SIC) and Performance Analyses **44**

4.1 T-SIC Technique 44

4.2 Received Signal and Average BER Analyses 48

4.3 Shannon Capacity based Performance Comparison 58

4.3.1 NOMA Spectral Efficiency 58

4.3.2 OFDMA Spectral Efficiency 60

5 Numerical Results **62**

5.1 BER Results 62

5.2 Capacity Results 73

6 Conclusions and Future Research **80**

6.1 Summary and Conclusions 80

6.2 Future Research Directions 81

Appendices **83**

A The Mean Square Error of Detection at the lth iteration **84**

References

List of Figures

1.1 Illustration of the smart world concept 13
1.2 Illustration of uplink NOMA system and received signal structure. . . 18

2.1 SC of two 4-QAM symbols. 24
2.2 SC-SIC detection of two 4-QAM symbols. 27
2.3 Two-user uplink capacity region. 29
2.4 Iterative SIC for two-user system. 32

3.1 Received signal structure at time domain. 39
3.2 Iterative SIC and symbol detection processing for IC Triangles. 43

4.1 Flowchart of T-SIC algorithm. 46
4.2 T-SIC received signal structure. 48
4.3 Comparison of pdf of Gaussian distribution and convolution of i.i.d. uniform r.v.s. 54

5.1 Analysis versus simulation BER results at the 3rd iteration. 16-QAM, 2nd user's average received SNR=25dB. 63
5.2 Average BER performance. 65
5.2 Average BER performance. 66
5.3 BER performance for TO =10%. 68
5.3 BER performance for TO =10%. 69
5.4 BER performance for TO =35%. 70
5.4 BER performance for TO =35%. 71

5.5 Average BER performance at the 3rd iteration versus transmit SNR. 16 QAM. 73
5.6 |MAI/p_{k^*}| versus different average received SNR ratios (see Table 5.1). 75
5.7 Spectral efficiency versus different levels of asynchronism of users. . . 77
5.8 Sum spectral efficiency verus different user power ratios (see Table 5.1). 78
5.9 Spectral efficiency when users' average channel conditions are largely different (see Table 5.1). 79

6.1 Extended T-SIC concept. 82

List of Tables

5.1 Average received SNR of users. 74

List of abbreviations

5G	Fifth Generation
AWGN	Additive White Gaussian Noise
BER	Bit Error Rate
BS	Base Station
Conv-SIC	Conventional Successive Interference Cancellation
CSI	Channel State Information
FDMA	Frequency Division Multiple Access
GFDM	Generalized Frequency Division Multiplexing
IC	Interference Cancellation
ICed	Interference Cancelled
i.i.d.	Independent and Identically Distributed
MAI	Multiple Access Interference
MC	Multi Carrier
MIMO	Multiple Input Multiple Output
MMSE	Minimum Mean Square Error
MSE	Mean Square Error
NOMA	Non-orthogonal Multiple Access
OFDM	Orthogonal Frequency Division Multiplexing
OFDMA	Orthogonal Frequency Division Multiple Access
OMA	Orthogonal Multiple Access
PAPR	Peak to Average Power Ratio
PDF	Probability Density Function
PF	Proportional Fairness
PFS	Proportional Fairness Scheduler
PIC	Parallel Interference Cancellation
PSD	Power Spectral Density
QAM	Quadrature Amplitude Modulation
RHS	Right Hand Side

RRM	Radio Resource Management
r.v.s	Random Variables
SC	Superposition Coding
SCed	Superposition Coded
SCM	Superposition Coded Modulation
SC-SIC	Superposition Coding with Successive Interference Cancellation
SIC	Successive Interference Cancellation
SINR	Signal to Interference plus Noise Ratio
SNR	Signal to Noise Ratio
TO	Time Offset
ToT	Time Offset Triplet
T-SIC	Triangular Successive Interference Cancellation
w.r.t.	With Respect To

List of symbols

$(A \mid B)$	A condition on B
$\lvert \cdot \rvert$	Modulus operator
α_k	Magnitude of fading of the kth user
α^2_{access}	Squared magnitude of fading for the user accessing the subcarrier at OFDMA-based system
B	Bandwidth of the channel
B_k	Bandwidth of the kth user
$\mathfrak{c}$	Mean SNR of the desired symbol at OFDMA-based system
$\mathfrak{c}_{k^*}$	Mean SINR of the desired symbol at NOMA-based system
$\mathrm{c}_k^{(\mathfrak{L})}[\varsigma]$	Event that at the latest iteration the symbol of the interferer was correctly detected
C_k	Uplink single-user capacity of the kth user
C_k^*	Uplink multi-user capacity of the kth user under MAI
C_{NOMA}	NOMA uplink capacity region
C_{OMA}	OMA uplink capacity region
d_k	Distance between the BS and kth user
$\mathrm{D}_k^{(\mathfrak{L})}[\varsigma]$	Mean square error of the detection at the latest iteration for the ςth symbol of the kth user
de_{k^*}	Half of the distance between two nearest constellation points for the desired user
$\delta(\cdot)$	Dirac delta function
$\boldsymbol{\Delta}_{k^*}[s]$	Vector of interferers' time offset to the desired user
$\Delta_{k^*,k}[s,\varsigma]$	Percentage of the symbol time that the ςth symbol of the kth user overlaps with the desired symbol
$\mathrm{e}_k^{(\mathfrak{L})}[\varsigma]$	Event that at the latest iteration the symbol of the interferer was detected in error
$E[\cdot]$	Statistical expectation
$\eta_{k^*}[s]$	Total interference to the desired signal

$\eta_{k^*,k}[s,\varsigma]$	Interference from the ςth symbol of the kth user to the desired symbol
$\hat{\eta}^{(l)}_{k^*,k}[s,\varsigma]$	Reconstructed interference signal from the ςth symbol of the kth user to the desired symbol at the lth iteration
$\tilde{\eta}^{(l)}_{k^*}[s]$	Residual interference to the desired symbol at the lth iteration
$f^{\mathfrak{N}}_{\gamma}(\gamma)$	pdf of the instantaneous SINR for the desired symbol at NOMA-based system
$f^{\mathfrak{O}}_{\gamma}(\gamma)$	pdf of the instantaneous SINR for the desired symbol at OFDMA-based system
$\tilde{\gamma}^{(l)}_{k^*}[s]$	SINR for the desired symbol at the lth iteration
h_k	Channel state information of the kth user
i	Index of the permutation
I_{asyn}	Indicator parameter that shows if employed SIC technique uses a priori information from adjacent symbols of interferers
k	Interference user
k^*	Reference user
K	Total number of users in the system
l	Reference iteration of the signal processing
L	Maximum number of iterations of the signal processing
$\mathfrak{L}$	Iteration index of the latest version of estimate available at the priori symbol vector for the interfering symbol
λ	Propagation exponent
M	Modulation level
$\mathfrak{M}$	Symbol constellation
m_i	ith constellation point
$\lvert\text{MAI}/p_{k^*}\rvert$	Ratio of residual MAI to transmit power for the desired symbol
n	Number of subcarriers in the system
N	Amplitude of the noise
$N_0/2$	Power spectral density of AWGN
Ω	Set of users accessing the subcarrier

$\mathrm{P}\left(A \middle\vert B\right)$	Conditional probability of A given B
$\mathrm{P}(\mathrm{c}_{k^*}^{(l)}[s])$	Probability of correct detection for the desired symbol at the lth iteration
$\mathrm{P}(\mathrm{e}_{k^*}^{(l)}[s])$	Error probability for the desired symbol at the lth iteration
$\mathrm{P}_{\mathrm{bit},k^*}^{(l)}[s]$	BER for the desired symbol at the lth iteration
${}_i\mathrm{P}_{\mathbf{z}^{(\mathfrak{L})}}$	ith permutation of $\mathbf{z}^{(\mathfrak{L})}$
p_k	Average received power of the kth user
p_k^{tx}	Transmission power of the kth user
$\mathrm{Pr}_{i,k}^{(\mathfrak{L})}[\varsigma]$	Probability of the detection status, of the latest detection for the ςth symbol of the kth user, considered at the ith permutation of $\mathbf{z}^{(\mathfrak{L})}$
$\mathrm{Pr}_{\mathrm{access}}(k)$	Probability of the subcarrier to be allocated to the kth user at OFDMA-based system
$Q(\cdot)$	Q function
R_k	Data-rate of the kth user
s	Reference symbol
ς	Interference symbol
S	Total number of symbols transmitted during a scheduling period
$\mathbb{S}$	Set of users accessing the channel
T	Symbol period
τ_k	Time offset of the kth user to a reference time
τ_{max}	Maximum time offset
τ_{min}	Minimum time offset
θ_k	Phase of the kth user's received signal
$\theta_{k^*,k}$	Phase mismatch of the kth user's signal to the k^*th user
$\cup$	Union of sets operator
$\mathrm{Var}(\cdot)$	Statistical variance
$X_k[s]$	Complex symbol transmitted at the sth symbol of the kth user
$\hat{\mathbf{X}}_k^{(l)}$	Vector of estimated symbols of the kth user at the lth iteration
$\hat{X}_k^{(l)}[s]$	Complex symbol estimated for the sth symbol of the kth user at the lth iteration

$\mathbf{Y}$	Vector of the received signal
$Y_{k^*}[s]$	Received signal for the k^*th user at the sth symbol
$\hat{Y}_{k^*}^{(l)}[s]$	ICed signal for the desired symbol at the lth iteration
$\mathbf{z}^{(\mathfrak{L})}$	Vector of the latest indicator parameters
$\mathrm{z}_k^{(\mathfrak{L})}[\varsigma]$	Indicator parameter for the status of the latest detection for the symbol of the interferer, i.e. in error or correct
ζ	Sum spectral efficiency of a subcarrier
$\zeta_{k^*}^{\mathfrak{N}}[s]$	Spectral efficiency for the desired symbol at NOMA-based system
$\zeta_{k^*}^{\mathfrak{O}}[s]$	Spectral efficiency for the desired symbol at OFDMA-based system

Superscripts

$\mathfrak{N}$	NOMA-based system
$\mathfrak{O}$	OFDMA-based system
Th	Theoretical signal model

Chapter 1

Introduction

Contents

1.1 Motivation 12

1.2 Challenges 17

1.3 Contribution of the Thesis 19

1.4 Structure of the Thesis 20

1.1 Motivation

In future, people are expected to be surrounded by smart objects in smart homes, offices, streets, and cities; so in the smart world [1], as illustrated in Fig. 1.1 [2]. The smart world will result in tremendous increase at the number of connected devices, the data traffic demand and the variety of supported applications [3]. Examples of interesting applications include; smart monitoring and control [4], content sharing (e.g. social websites and device-to-device multimedia sharing [5]) and always-on always-up-to-date data (e.g. Cloud [6]). It is clear that, these applications require significant amount of information to be conveyed from the users' devices/end-nodes to the access network. Therefore, traffic demand in the uplink direction will very rapidly increase, as well as the downlink direction.

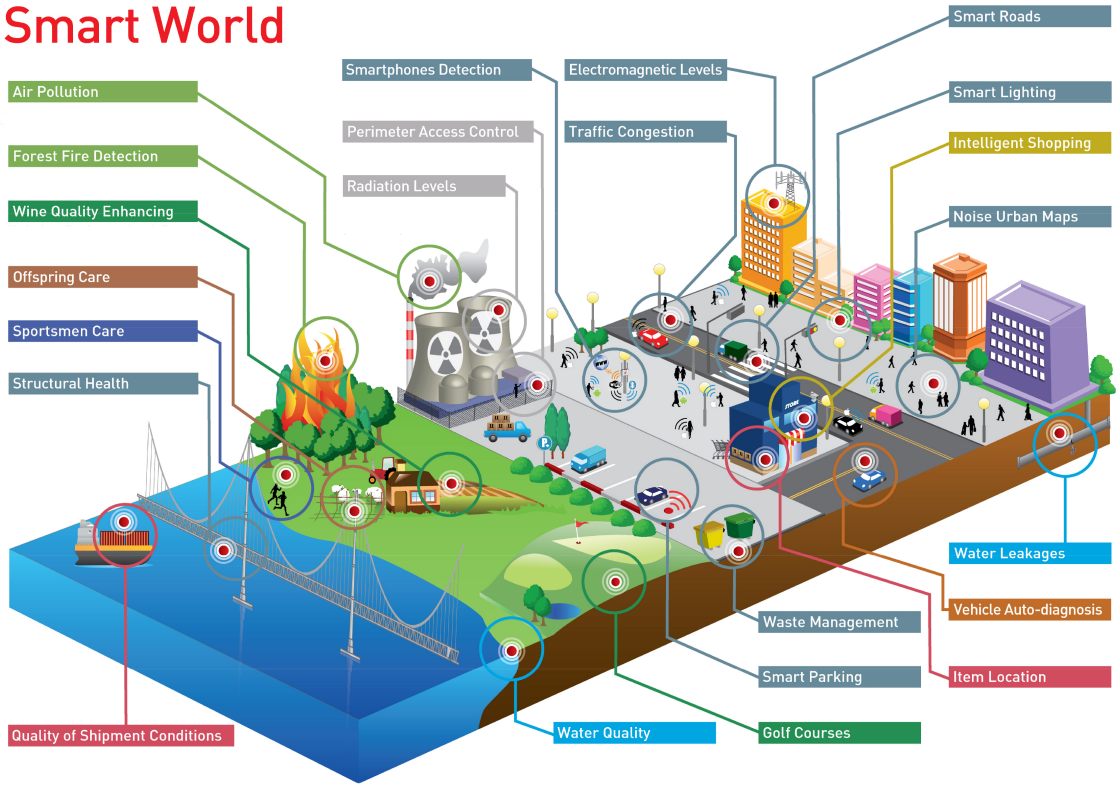

Figure 1.1: Illustration of the smart world concept [2].

However, the radio resources – the wireless spectrum and transmit power – are limited and current wireless communication technologies are not able to accommodate such increase in the traffic demand within the available resources [7]. For example, it is expected that the fifth generation (5G) mobile networks will require up to one thousand times (1000x) more area capacity than the current fourth generation long-term evolution networks [7]. Therefore, new technologies are needed to improve, in orders of magnitude, the channel capacity performance of the system. Much of the research effort in literature is devoted to improve downlink transmission performance [8–12]. But smart and interactive applications' performance also depend on the performance of the uplink transmission. For applications to perform well in the future wireless systems, there is need for more research effort to improve uplink transmission performance. This is the reason uplink transmissions is studied in this thesis.

A key technology that effects the channel capacity performance is the multiple ac-

cess scheme of a system [13]. At multi-carrier wireless communication systems, based on its advantage of transforming a frequency selective fading channel into a number of narrowband flat fading subchannels, orthogonal frequency division multiplexing (OFDM) [14] has been widely adopted as the multiplexing technique [15]. Wireless multiple access to OFDM based systems can be realized in two ways – orthogonal frequency division multiple access (OFDMA) [16] and non-orthogonal multiple access (NOMA) [17]. In OFDMA systems, the system throughput can be maximized by exploiting multiuser diversity gain [18]. That is, based on received channel state information (CSI) of all subchannels, allocating a subcarrier (or a chunk of subcarriers) only to one user which has the best condition on it. Despite the high system throughput, OFDMA has disadvantage in extra high data-rate communications. It does not allow frequency reuse within one cell [17], since a subcarrier in an OFDMA cell is allocated only to one user, which significantly limits cell throughput. Unlike OFDMA, NOMA technique can allocate a subcarrier to more than one user at the same time within one cell, which provides higher throughput due to subcarrier reuse within a cell. Therefore, NOMA is a promising technique in future wireless communications [19, 20].

It is hard for a single technology to improve the system performance, e.g. the data-rate, to meet the performance requirements in future wireless communications. Performance gains of multiple technologies, working in harmony, need to be combined to realize the extra high data-rate communications [21–24]. NOMA is an advantageous technology in this aspect as well. Since it can work in conjuction with various air interface technologies, such as multiple-input multiple-output (MIMO) [25–27] and distributed antenna systems [28–30], and networking platforms, such as small cells [31–33], proposed for future wireless communications without the need for any extra hardware. Employing NOMA on top of another technology will provide the additional frequency reuse gain to further improve the performance. An interesting application scenario of NOMA is envisioned to be used in conjuction with beamforming technology in the small cell environment [13]. The two advantages of reusing the limited (precious) spectrum and flexibility to be implemented in conjuction with

other promising technologies made NOMA increasingly attract academic and industrial attention, and NOMA has been recently considered for standardization in cellular systems for broadcasting [34]. Therefore NOMA is an increasingly interesting technology to research and develop for future wireless communications.

It should be noted that the use of NOMA technology is not limited to OFDM based systems. NOMA can be applied over broad range of multiplexing techniques, such as time division multiplexing [35], and waveforms, such as generalized frequency division multiplexing (GFDM) [36]. The application scenario of NOMA over OFDM is considered in this thesis due to the advantages and wide use of OFDM in current wireless communication systems.

Superposition coding (SC) is an effective technique to increase capacity in the NOMA system [20]. When SC is applied, multiple users' signals are multiplexed over the same subcarrier with different received power at the base station (BS). Then, in the BS, a superimposed signal is received on one subcarrier. The BS detects users' signals transmitted over the subcarrier, starting with the user having the strongest signal to noise ratio (SNR), in a descending order of users' SNR. Once the strongest signal is detected, the detected data is passed to the SIC algorithm. The SIC reconstructs the strongest signal by using its CSI, and subtracts it from the received superimposed signal. This suppresses co-channel interference from strong (earlier detected) signals for relatively weak (yet to be detected) signals. The principle of superposition coding with successive interference cancellation (SC-SIC) can be related to the concept of cognitive radio systems [37]. Where a reference NOMA user is viewed as the primary user and other NOMA users are viewed as secondary users. The NOMA system can be designed as to allow secondary users to share the spectrum with the primary user on the condition that primary user's performance will not be degraded more than the acceptable threshold. [38] investigated the impact of imperfect IC on the SC-SIC. [39] proved that among all possible signaling methods, superposition coded modulation (SCM) maximizes the output signal to interference plus noise ratio (SINR) in the linear minimum mean square error (MMSE) estimation. [40] studied the optimal number of users to be superposition-coded (SCed) on

a subcarrier, and concluded that at optimality there is a high probability that only a few (two to three) users are SCed on a subcarrier. [41] applied NOMA to cooperative transmissions and showed that cooperative NOMA can achieve the maximum diversity gain for all users at a cooperative transmission.

So far, the researches on NOMA only consider time-synchronous transmissions. Synchronous transmission is easily maintained for downlink transmissions since the BS controls timing of all transmissions for different users and since the desired and interfering signals travel same path to a reference receiver. However, synchronous transmission is impractical for uplink transmissions since users are geographically distributed and the mobile environment is dynamic. Moreover, signals from different users will propagate via different paths and encounter various channel effects. These result in different time offsets when signals from different users arrive at the BS. Although a closed-loop system with feedback channels from the BS to users may be employed to compensate for these time offsets and achieve synchronization [42], the cost of radio resources and channel dynamics in the feedback loop makes such a system inefficient. Asynchronism in the received signal causes disturbances to the SC-SIC. In the synchronous case, at the BS, the OFDM symbols in a subcarrier from different users are aligned in time domain. However in asynchronous case, symbols in a subcarrier from the different users are time misaligned, which can cause a symbol of a user overlapping with two symbols of each of the other users. Synchronous detection and SIC techniques, called conventional SIC (Conv-SIC) in this thesis, exploit information from only a single symbol of each user. However, the asynchronous communication requires information from multiple symbols when SIC is exploited. Detection and IC performances are significantly degraded if complete information of signals (desired and interfering) are not known in asynchronous communications. Therefore it is important to investigate NOMA in asynchronous communications.

1.2 Challenges

Asynchronism in NOMA introduces interference to a symbol from multiple symbols of each of the co-channel users. Therefore, the first challenge in asynchronous NOMA transmissions is how to obtain the complete information of the interference from the co-channel users. Without the complete information of the interference, there is strong residual interference among NOMA users and it is not possible to have reliable communications. The second challenge is how to remove the interference from the multiple symbols of the co-channel users. A novel IC technique is needed to exploit information of and suppress the interference from all the overlapping symbols of the co-channel users. Also, it is important to find out if it is worth to address the challenges of NOMA in asynchronous communications. Thus, performance analyses are necessary to evaluate the performance of NOMA with an IC technique that addresses asynchronism at uplink transmissions.

To demonstrate the challenges of NOMA in asynchronous communications, an uplink NOMA system is considered with a BS serving three geographically distributed users, as shown in Fig. 1.2 (a). Due to different distances and the dynamic channels from the users to the BS, asynchronous transmissions are assumed among users. Received signal structure in one subcarrier is illustrated in Fig. 1.2 (b), where three adjacent symbols $\{s-1, s, s+1\}$ of three users are shown in time domain. For asynchronous transmissions, the arrival times at the BS of the users' signals are not aligned. A symbol from a user overlaps with two adjacent symbols from each of the other two users. In order to carry out IC, the information of two adjacent symbols of other users must be exploited for a reference user.

For example, in Fig. 1.2 (b), assuming that the 2^{nd} user is the reference user its time offset is larger than the 1^{st} user's but smaller than the 3^{rd} user's. This makes the sth symbol of the 2^{nd} user partially overlap with the sth and $(s+1)$th symbols of the 1^{st} user and with the $(s-1)$th and sth symbols of the 3^{rd} user. However, Conv-SIC technique used at NOMA only exploits information from the sth symbol of the co-channel users [20, 39, 43]. This means only partial information

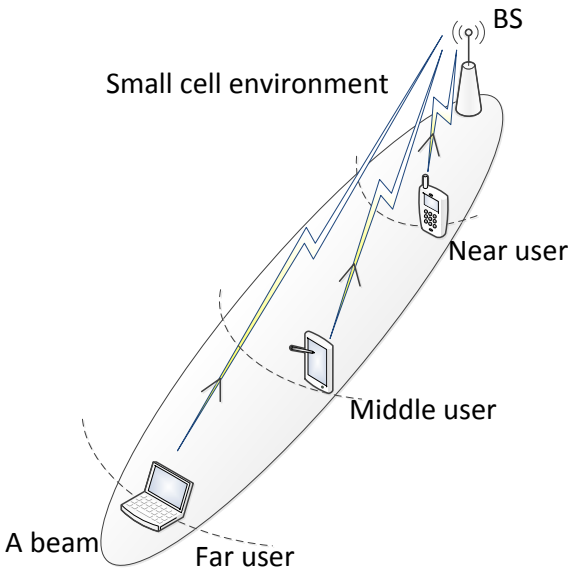

(a) Uplink NOMA system.

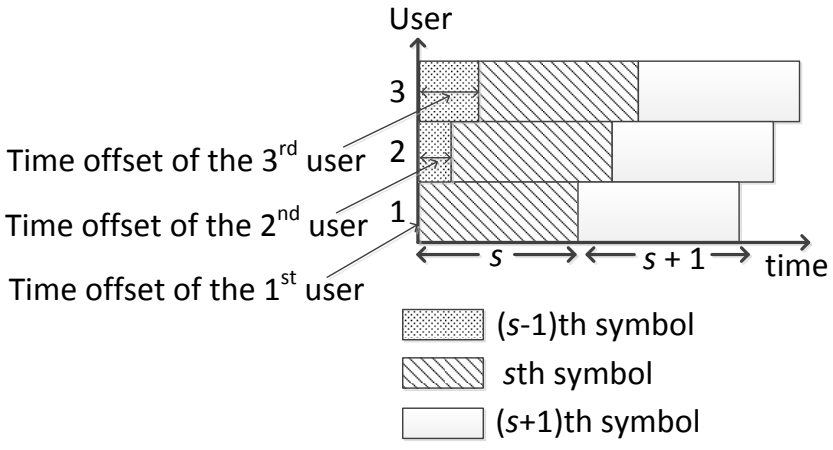

(b) Received signal structure at time domain.

Figure 1.2: Illustration of uplink NOMA system and received signal structure.

of the interference is available to SIC and there is strong residual interference from neighbouring symbol, $\{s-1, s+1\}$, of the co-channel users, which significantly degrade the system performance. Therefore, there is need for a novel IC technique that exploits information of multiple symbols, $\{s-1, s, s+1\}$, of the co-channel users. By suppressing strong interference from these symbols, the novel IC technique can achieve superior performance to Conv-SIC. The received power and time offset differences between NOMA users are the important parameters that determine the strength of the interference from neighbouring symbols of the co-channel users. Thus, the performance gain of the novel IC technique over Conv-SIC depends on these parameters. Therefore, extensive performance analyses with respect to (w.r.t.) these parameters are needed to reveal if it is worth to propose a novel IC technique to address the challenges of NOMA in asynchronous communications.

1.3 Contribution of the Thesis

The objective of this thesis is to study asynchronous NOMA transmissions, address its challenges, and investigate its performance. The contributions of this thesis include:

1. A novel technique called "Triangular SIC (T-SIC)" is proposed to perform asynchronous SIC, which uses multiple symbols from each interfering user to carry out IC. With the multiple symbol information from each interfering user the SIC performance can be improved substantially.

2. Bit error rate (BER) analysis is presented for the T-SIC and Conv-SIC techniques when iterative signal processing is employed at the receiver. The required power ratio of users and the modulation level are studied. The relationship among the number of iterations, detection method (including hard-decision and soft-decision), modulation level and time offset difference among users is investigated. The requirement of an asynchronous SIC technique at

NOMA uplink transmissions is validated by comparing performance of T-SIC and Conv-SIC.

3. Theoretical capacity analysis is given, where performance comparison between NOMA and OFDMA is presented. The effects of the power ratio and time offset difference of users on the capacity performance are presented. It is shown that the proposed T-SIC based NOMA technology significantly outperforms OFDMA and Conv-SIC based NOMA.

4. It is shown that, in the NOMA system users are required to have large received power ratio to satisfy BER requirements and the required received power ratio increases with increasing the modulation level. Also, employing iterative IC provides significant performance gain in NOMA and the number of required iterations depend on the modulation level and detection method. With hard-decision it is sufficient to have two iterations. With soft-decision, for low modulation level, it is enough to have two iterations, whereas for high modulation level, a relatively higher number of iterations is desirable. Further, at asynchronous NOMA transmissions, users' BER and capacity performances strongly depend on the relative time offset between interfering users, besides the received power ratio.

1.4 Structure of the Thesis

This thesis is organized into six Chapters and an Appendix, as follows:

In Chapter 1, the motivation and challenges of NOMA in asynchronous communications are discussed. The main contributions of the thesis to address these challenges are then summarized. Also the structure of the thesis is given.

In Chapter 2, theoretical basis of the SC-SIC, uplink channel capacity, and iterative SIC for NOMA communications are presented. Moreover, the state-of-the-art literature on the NOMA communications is surveyed.

In Chapter 3, the system model is introduced including the received signal structure and iterative signal processing at the receiver.

In Chapter 4, the concept of T-SIC technique is introduced and its performance analyses are given. BER performance analysis of the T-SIC and Conv-SIC techniques are given for iterative symbol detection and IC processing at the receiver. Capacity performance analysis are given to compare the spectral efficiency of NOMA and OFDMA.

In Chapter 5, representative numerical results are shown to evaluate the performance of proposed T-SIC based NOMA technology, compared to Conv-SIC based NOMA and OFDMA. Important performance metrics – BER and capacity – of the users, as well as the sum capacity of the subcarrier are considered for performance comparison.

In Chapter 6, the summary and conclusions of the thesis are given and interesting future research directions are discussed.

In Appendix A, the analysis to obtain the mean square error of detection at a given (e.g. lth) iteration of the signal processing is presented.

The list of related publications to this research is provided on pages v-vi of this thesis. Publications 1 and 3 researches on the performance of uplink NOMA transmissions with a novel asynchronous IC technique. Their findings are discussed throughout the thesis. Publications 2, 6 and 7 researches on the concept of frequency sharing in wireless networks to improve the fairness among users. Results of these publications are discussed in Chapter 2.1. Publications 4 and 10 researches on resource allocation aspects in wireless networks. Learnings of these publications are used at the BER and capacity performance analyses in Chapters 4.2 and 4.3. Publication 5 discusses the new trends in networking platforms (e.g. user-centric and cooperative networking) and the shortage of the current wireless networks in fulfilling the requirements for these evolving trends. The outcomes of this publication are discussed in Chapters 1.1 and 2.4. Publications 8 and 9 researches on scheduling policies that aim to maximize the achievable system throughput while achieving fairness among users. Learnings from these publications are used at discussions in

Chapters 2.1 and 2.3 and capacity performance analysis in Chapter 4.3.2.

Chapter 2

Background Theory and Literature Review

Contents

2.1 Superposition Coding with Successive Interference Cancellation 23

2.2 Uplink Channel Capacity 27

2.3 Iterative Succesive Interference Cancellation 30

2.4 Literature Review 33

2.1 Superposition Coding with Successive Interference Cancellation

SC is a coding technique that performs multiplexing of symbols in power domain [44], where a symbol is an output from a multi-level symbol mapper, such as quadrature amplitude modulation (QAM) [14] or SCM [39]. Multiplexing of symbols in power domain make it possible to extend the capacity of a communications system without expanding the bandwidth. At the receiver, in one channel, different power level of symbols are required to successfully detect each superimposed symbol with

high probability. An illustration of SC for a two-user system is provided in Fig. 2.1, where a 4-QAM symbol of the 2nd user is superimposed to a 4-QAM symbol of the 1st user.

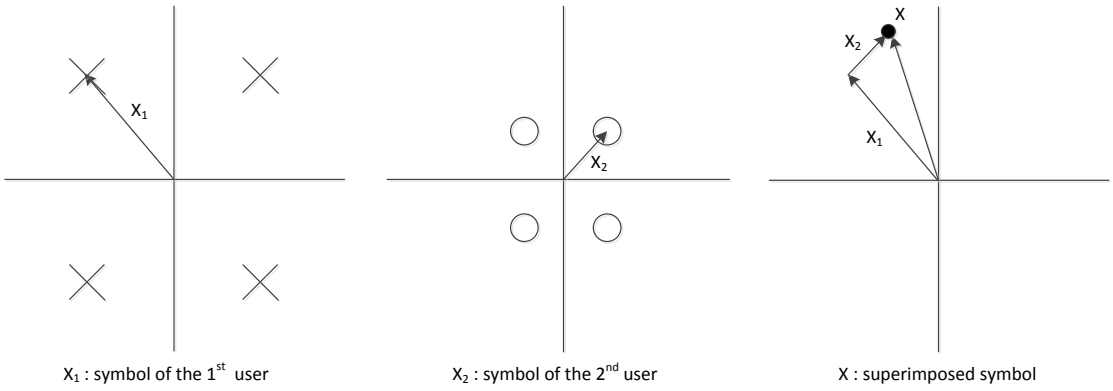

Figure 2.1: SC of two 4-QAM symbols [45].

For uplink transmission, i.e. multiple access channel, the concurrent transmissions from multiple geographically distributed users over the same channel with power control is equivalent to SC. A simple demonstration of this equivalence is as follows. Assuming two geographically distributed users with fixed transmission power, where the 1st user is the near user and 2nd user is the far user. Also, the received signal is distorted by additive white Gaussian noise (AWGN). As both users concurrently transmitting their symbols, i.e. X_1 for the 1st user and X_2 for the 2nd user, over the same channel a superimposed signal $X = X_1h_1 + X_2h_2 + N$ is received at the BS receiver over that channel, where h_k represents the frequency response of the kth user and can be viewed as the weight for SC and N represents noise. Since the 1st user is geographically closer to the BS than the 2nd user its symbol will have higher power level at the superposition at the receiver. This is equivalent to SC illustrated in Fig. 2.1. Note that the difference in users' received power level can also be a result of the transmission power control (if applied). Also the effect of noise at the receiver antenna is similar to the SC and multiple access channel.

As illustrated in Fig. 2.1, SC utilizes the near-far effect at wireless communications [46–48] to convey data of multiple users over the same channel simultaneously.

At orthogonal multiple access (OMA) systems, near-far effect may significantly degrade the achievable performance of the system, especially when very strict fairness is required among users. The notion of fairness considered in this thesis is not to allow users with statistically better channel condition (i.e. near users) to seize system resources at the expense of other users with less favorable channel condition (i.e. far users). In other words, not to allow far users to starve while maximizing the achievable system performance by frequently allocating resources to near users. At OMA systems, in order to provide the fairness (for example proportional fairness [49]) or guarantee the service level agreements for all users [50, 51], no matter how weak the signal of a relative far user is, the user may be served, i.e. allocated with resources according to the fairness constraint. Under this situation, the spectral efficiency over the resources allocated to the far user will be relative low due to the user's poor channel condition [52], which will cause the degredation of the total system performance. However when SC is employed, system performance can be kept high while achieving fairness among users since multiple users can concurrently transmit over the same channel. Concurrent transmissions by SC prevents a user to solitarily occupy the channel in expense of the other users. When SC is employed, a far user can access to the channel together with a near user. While the near users' transmission keeps system performance high, the far users still have the chance to tranmsit their symbols frequently and, given proper interference management, achieve high sum throughput over a time period.

Further, by SC the difference in signal strength of users can be utilized, while the weak signal of the far user can achieve a low spectral efficiency to that user, it also limits the co-channel interference to other users (i.e. near user). Thus, near user can still achieve a high spectral efficiency. These two contrary effects at SC systems prevent the overall system performance to degrade, unlike the case of OMA. Further, SC does not require spectrum spreading [53, 54] (i.e. spreading code) to realize multiplexing of users. By using only error correction coding [55–57], it has been shown that SC (combined with SIC) is the capacity achieving multiple access technique ([58], Chapter 14). These advantages of SC made it a favorable technique

for NOMA.

At the receiver, symbol of each user is detected from the received superimposed signal starting with the user which has the strongest SNR, in a descending order of users' SNR. While proceeding through symbol detection for each user, it is crucial to suppress the signal of earlier detected users. At NOMA, users have largely different received signal strengths, and the signal from users with strong SNR can significantly distort the signal from users with relatively weak SNR if they are not suppressed. The capacity of NOMA system without IC is shown to be much worse than OMA and NOMA with IC systems ([59], Chapter 14.6). Therefore to achieve high performance, it is crucial to adopt a proper IC technique at the NOMA receiver. SIC [60, 61] and parallel IC (PIC) [62, 63] are the two major schemes to implement IC in multi-user systems. It has been shown that when users have unequal received signal strengths SIC outperforms PIC [64]. PIC detects symbols of all users simultaneously and exploit the detected information for IC parallelly to all users. Unequal received signal strengths cause weak users' detection to be in low accuracy and degrade the IC performance. But SIC, employing detection and IC processing in a descending order of users' SNR, can benefit from unequal received signal strengths, since the detection accurracy will be higher as the signal to be detected is much stronger than the interference plus noise signals. Therefore SIC is the preferable IC technique for NOMA, and at the rest of this thesis SC-SIC is considered as the scheme for realizing NOMA communications.

The SIC algorithm reconstructs detected signals by using their CSI, and subtracts them from the received superimposed signal. This suppresses co-channel interference from strong signals for relatively weak signals, and make it possible to successfully detect symbol of all users with high probability. An illustration of SC-SIC detection is provided in Fig. 2.2, where the symbol of the 1^{st} user is detected first, removed from the received superimposed signal and then the symbol of the 2^{nd} user is detected.

At the above example, illustrated with Figs. 2.1 and 2.2, both users successfully transmitted two bits over the same channel. The concept of SC-SIC can be extended to more users by multiplexing more symbols, so called adding layers to the con-

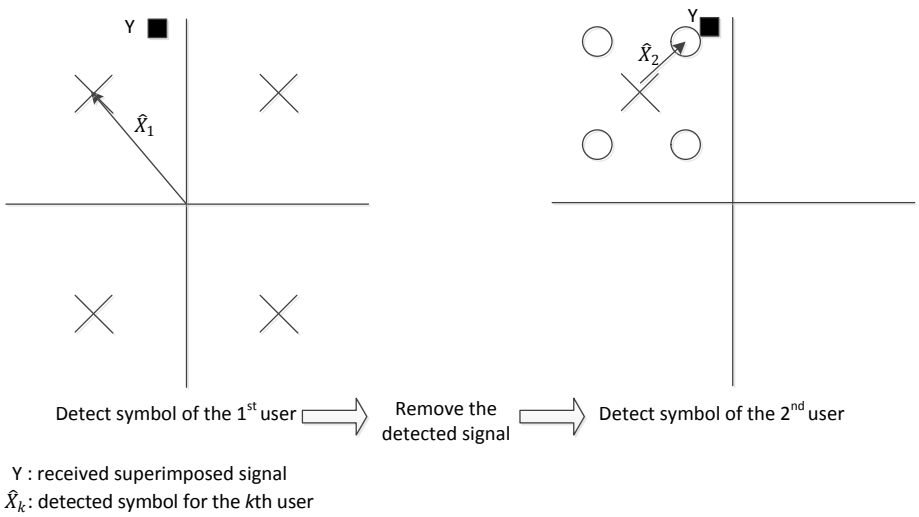

Figure 2.2: SC-SIC detection of two 4-QAM symbols [45].

stellation. It is important to notice that, SC-SIC can achieve data-rate to multiple users simultaneously without the need to expand the bandwidth. This is favorable to increase the channel capacity.

2.2 Uplink Channel Capacity

In wireless communications the channel is defined in terms of the bandwidth and time. The capacity of a channel specify the maximum data rate that can be transmitted over the wireless channel with asymptotically small error probability, assuming no constraints on delay and complexity of the transmitter and receiver ([59], Chapter 4). In multiuser systems, the channel need to be divided among multiple users. Wireless multiple access divides the channel among users and can be realized in two ways – OMA that a subchannel is allocated only to one user and NOMA that a subchannel is allocated to more than one user at the same time. Because the channel can be divided to different users in an infinite number of different ways, multiuser channel capacity is defined by a rate region [65]. This region provides all user rates that can be simultaneously supported by the channel with arbitrarily

small error probability.

Capacity region for a simple case of NOMA is given as follows. Suppose two users are communicating to a BS in the uplink direction and let p_k denotes the average received power for the kth user. It is assumed that all transmitters and the receiver have a single antenna, and the received superimposed signal is distorted by AWGN with double-sided power spectral density $N_0/2$. Let R_k denotes the rate of the kth user. The two-user NOMA uplink capacity region is the closed convex hull of all vectors (R_1, R_2) that satisfy the constraints ([58], Chapter 14.1),

$$R_k \leq B \cdot \log_2 \left(1 + \frac{p_k}{N_0 \cdot B}\right), k = 1, 2, \tag{2.1}$$

$$R_1 + R_2 \leq B \cdot \log_2 \left(1 + \frac{p_1 + p_2}{N_0 \cdot B}\right), \tag{2.2}$$

where B is the bandwidth of the channel. The first constraint, by (2.1), is the capacity associated with each individual user and the second constraint, by (2.2), is the capacity associated with received power equal to the sum of received powers from all users. Then, for $K \geq 2$, where K denote the total number of users in the system, the capacity region is extended to,

$$C_{\text{NOMA}} = \left\{ (R_1, \cdots, R_K) : \sum_{k \in \mathbb{S}} R_k \leq B \cdot \log_2 \left(1 + \frac{\sum_{k \in \mathbb{S}} p_k}{N_0 \cdot B}\right) \forall \mathbb{S} \subset \{1, 2, \cdots, K\} \right\}, \tag{2.3}$$

where $\mathbb{S}$ represent the set of users accessing the channel.

An illustration of the NOMA capacity region for $K = 2$ is provided in Fig. 2.3, where C_k and C_k^* are given by

$$C_k = B \cdot \log_2 \left(1 + \frac{p_k}{N_0 \cdot B}\right), k = 1, 2, \tag{2.4}$$

$$C_1^* = B \cdot \log_2 \left(1 + \frac{p_1}{N_0 \cdot B + p_2}\right), \tag{2.5}$$

$$C_2^* = B \cdot \log_2 \left(1 + \frac{p_2}{N_0 \cdot B + p_1}\right). \tag{2.6}$$

At the figure, the point $(C_1, 0)$ represents the scenario when the 1$^{\text{st}}$ user is transmitting at its maximum rate and the 2$^{\text{nd}}$ user is not transmitting, so called single-user

channel capacity. The vice versa scenario is represented by the point $(0, C_2)$. Points (C_1^*, C_2) and (C_1, C_2^*) represent the scenarios that both users simultaneously transmitting over the channel and the SIC is used at the detection. Specifically, at the first point, the data of the 1st user is detected in the first place, where the 2nd user's signal appear as additional noise. Then subtracting the 1st user's signal from the received signal, the 2nd user can communicate with its maximum rate. That is, NOMA has an interesting property that while one user can achieve its single-user capacity, one or more other users can get a non-zero rate. At the second point, the vice versa scenario is represented. The line connecting points (C_1^*, C_2) and (C_1, C_2^*) is achieved by time-sharing (alternating) between the two scenarios of simulatenous transmission.

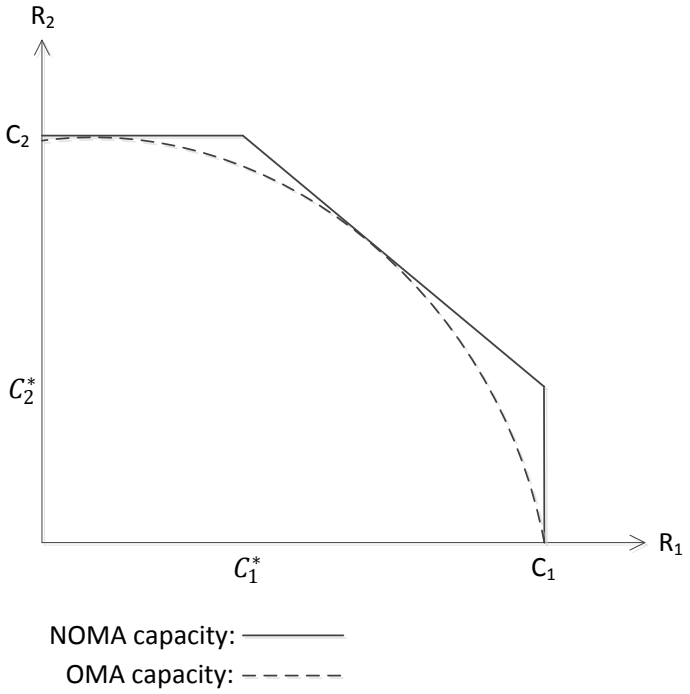

Figure 2.3: Two-user uplink capacity region.

It is important to note that the uplink NOMA capacity region is equivalent to multiple access capacity region. This is due to employing capacity achieving channel codes and SIC at NOMA to separate users' data [20]. With the help of

capacity achieving channel codes, the symbol detection have asymptotically small error probability for the specified data rate by the capacity region. Then, at SIC the interference from a priori detected symbols of co-channel users can be completely suppressed and the uplink NOMA capacity region is equivalent to multiple access capacity region ([59], Chapter 14.6).

The capacity region of OMA for $K = 2$ is also shown in Fig. 2.3. Note that OMA techniques, frequency-division multiple access (FDMA) [66] and time-division multiple access with variable power [67] result in the same capacity region ([59], Chapter 14.6). Suppose FDMA is employed and let B_1 and B_2 denote the bandwidth allocated to the 1^{st} and 2^{nd} users, respectively. Then the capacity region is given by,

$$C_{\text{OMA}} = \bigcup_{\{B_1,B_2:B_1+B_2=B\}} \left(R_1 = B_1 \cdot \log_2 \left(1 + \frac{p_1}{N_0 \cdot B_1} \right), R_2 = B_2 \cdot \log_2 \left(1 + \frac{p_2}{N_0 \cdot B_2} \right) \right), \tag{2.7}$$

where $\bigcup$ is the union of sets operator. It is shown in Chapter 14.3 in [58] that the OMA capacity region touches to the NOMA capacity region at one point. This point is when the sum-rate $R_1 + R_2$ is maximized. It is also shown that to maximize the sum-rate B_1 and B_2 must be proportional to the average received power of users, p_1 and p_2. In wireless networks, users can have largely different channel statistics and working at the point that maximize the sum-rate can be unfair [68, 69]. Since the user with statistically better channel may get a much higher rate at the expense of other users. In such case, to provide fairness the system should operate at points other than the point that maximize the sum-rate. It is shown in Fig. 2.3 that at those points NOMA dominates OMA and is the optimal multiple access technique.

2.3 Iterative Succesive Interference Cancellation

The performance of SIC depends on the accuracy of the interference information [39]. Employing multiple iterations of symbol detection which is based on exploiting a priori estimate obtained from the previous iteration can improve the accuracy of the interference information. In this manner, SIC and symbol detec-

tion performances should improve and users should be exposed to less interference as the number of iterations increases, assuming a priori information obtained from the previous iteration is accurate enough. However if a priori estimate is not accurate enough, iterative SIC has so called error propagation problem [70, 71], where an inaccurately estimated symbol can increase the interference to other symbols and cause built-up of more symbols in error as the number of iterations increases. Another problem of iterative SIC is the increase of the processing delay as the number of iterations increases [72]. Thus for delay sensitive applications [73] the maximum number of iterations can not be too large.

An illustration of iterative SIC for a system with $K = 2$ is provided in Fig. 2.4, where it is assumed that the 1^{st} user has stronger signal than the 2^{nd} user. At the 1^{st} iteration, the symbol of the 1^{st} user is detected first. Since, for the 1^{st} user, there is no a priori information of the interference available at this iteration, the symbol is detected without IC. Before detecting symbol of the 2^{nd} user, SIC reconstructs the 1^{st} user's signal by multiplying the result of this detection with the CSI of the 1^{st} user and subtracts the reconstructed signal from the received superimposed signal. This suppresses the interference to the 2^{nd} user. After IC is performed, the symbol of the 2^{nd} user is detected. Detecting symbol of the two users complete the 1^{st} iteration. At the 2^{nd} iteration, a priori information of the interference is available for the 1^{st} user and SIC can suppress the signal of the 2^{nd} user before detecting the 1^{st} user's symbol for the second time. This will increase the accuracy of the second detection. By having a more accurate detection for the 1^{st} user, SIC can suppress more interference before detecting the 2^{nd} user's symbol for the second time and that detection's accuracy will also improve. Detecting symbol of the two users for the second time complete the 2^{nd} iteration. At further iterations, the signal processing is similar to the 2^{nd} iteration, but accuracy of the interference information is higher. Thus employing more iterations can further improve system performance. However, the gain of additional iteration becomes insignificant as the number of iterations become large [74, 75]. When the maximum specified number of iterations are completed, detection result for the symbol of each user at the latest iteration is

output and signal processing proceeds in time to process next symbol of users.

It is clear from the above discussion that, employing iterative SIC at the receiver can provide significant performance gain to NOMA, and it is important to carefully set the maximum number of iterations that can provide most of the performance gain without causing long processing delay. Thus, iterative SIC is adopted at the receiver and the appropriate number of iterations is studied in this thesis.

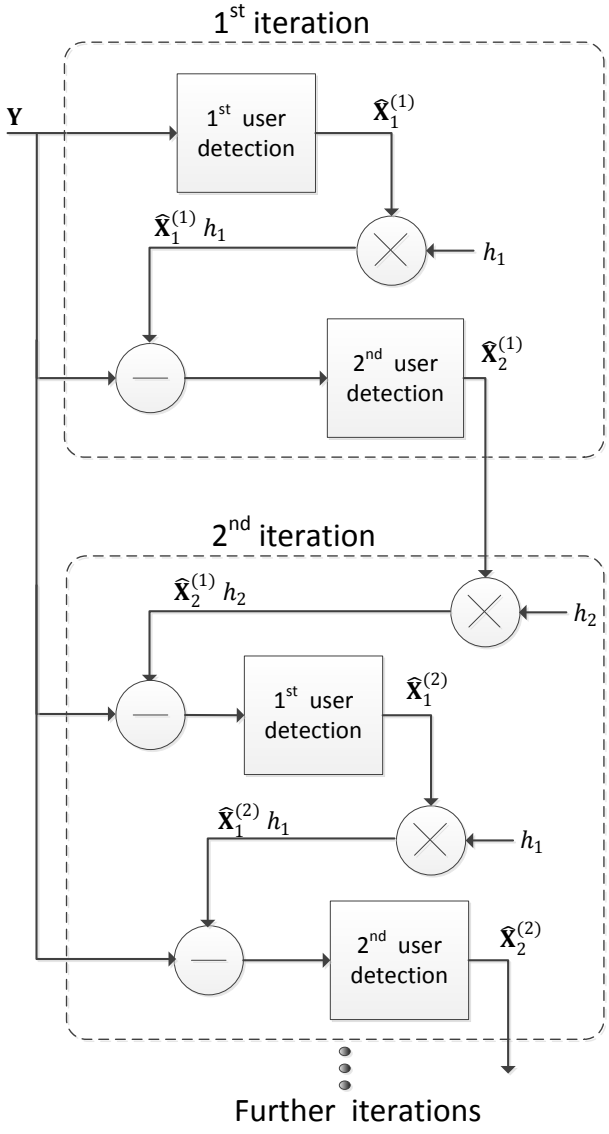

Figure 2.4: Iterative SIC for two-user system.

2.4 Literature Review

OFDMA is widely adopted as the multiple access technique in current wireless communication systems [76–79], since it can provide concurrent interference-free transmission to multiple users that are in orthogonal subcarriers. Although this approach can eleminate interference among concurrent transmissions in orthogonal subcarriers, it does not generally achieve the highest possible data-rate for a given error probability ([58], Chapter 14). Thus, the requirement for higher spectral efficiency [80] and expected improvement of receiver processing capabilities [81] made NOMA a candidate technology for future wireless communications [19, 20]. Experimentations for downlink transmissions with real-hardware testbed showed up to 61%, and real-time simulator for very dense urban area (actual model of Shinjuku, Tokyo) showed up to 51%, of throughput gain of NOMA over OFDMA [82]. The promising concept and experimental results made NOMA a study item in Release 13 of the 3rd generation partnership project standardization [83]. Thereby, the NOMA concept becomes an increasingly popular research topic in the recent years and for the future.

While the theoretical studies and experimental results motivate the use of NOMA, there are many challenges that need to be addressed before its practical realization at future wireless networks. The major challenges can be listed as follows. The first challenge is to find out if the performance gain of NOMA in terms of the achievable data rate over that of OFDMA's is significant enough to worth being implement in future wireless communications. Performance comparisons at interesting networking scenarios (e.g. multi-cell uplink transmissions and MIMO technology) need to be done for validation. Accordingly, the second challenge is to develop adequate radio resource management (RRM) [84] and user scheduling methods for NOMA transmissions to reveal the true (maximum achievable) performance of NOMA. At NOMA, high peak-to-average power ratio (PAPR) problem [85] may rise at the downlink transmission due to superimposing multiple users' signals and uplink transmission due to a user being allocated with a large number of subcarriers (as a result of allowing multiple users to access a subcarrier concurrently). Therefore, the third challenge is how to

overcome this high PAPR problem of NOMA. Since the iterative SIC can provide significant performance gain to NOMA communications. The fourth challenge is to study adequate communication techniques (e.g. signaling and coding techniques) for NOMA when iterative signal processing is employed. And the fifth challenge is to reveal the performance of NOMA when combined with other popular performance improving techniques, such as cooperative transmissions and error-control schemes. The literature on NOMA provide researches that address these challenges. However, the effects of asynchronous transmission on NOMA has not been studied yet. Since the asynchronism causes crucial disturbances to the received signal at NOMA. The literature on NOMA is not accurate for asynchronous transmission. Therefore, revisiting aforementioned challenges in asynchronous NOMA transmissions are crucial and remain as open challenges to be addresed. Also the signal processing complexity of NOMA receiver is another important open challenge. The work of this thesis addresses the open challenge of studying asynchronous NOMA transmissions, proposing a novel IC technique for it, and investigating its performance. Some interesting challenges left for future work are developing RRM and user scheduling methods for asynchronous NOMA transmissions, and investigating asynchronous NOMA transmissions with non-orthogonal waveforms [86].

[13] and [87] addressed the first challenge and provided system-level performance comparisons between NOMA and OFDMA based cellular downlink transmissions, where [13] considered single-antenna transmitter and receivers, and [87] extended performance comparison to MIMO technology with random beamforming [88]. It is shown that NOMA improves both the overall cell throughput and cell-edge user throughput performances over OFDMA. Moreover, at [87] it is observed that the performance of NOMA without MIMO is similar to that of OFDMA with 2x2 random beam-forming, which suggested that NOMA has similar effect of spatial multiplexing with random beam-forming.

[11,17,19,38,40] addressed the second challenge. [19] and [17] proposed transmission power control methods for NOMA in the cellular uplink and compared system-level performance with OFDMA. [19] considered a single-cell environment and [17]

extended the performance investigation to a multi-cell environment with the presence of inter-cell interference [89]. The results suggested that NOMA outperforms OFDMA at uplink communications. Also [17] showed that at NOMA uplink transmissions superimposing multiple users' symbol may increase inter-cell interference and, in the case of excessive total transmit power within the cell, the overall cell throughput and cell-edge user throughput may degrade. Therefore transmission power control is important for NOMA. Further, [11] showed that at NOMA both the choice of users' data rate and allocation of transmission power are critical to meet outage probability requirements. The results demonstrated that given appropriate data rate and power allocations are done for users the NOMA outage performance can outperform OMA's. Otherwise the outage probability will always be one.

[38] proposed a scheduling method for NOMA that aims to maximize the system throughput while achieveing fairness among users. For the performance evaluation, imperfect IC is taken into account and comparison between NOMA and OFDMA is given. Results showed that even with imperfect IC, the NOMA provides gain in the overall cell throughput and cell-edge user throughput over OFDMA. [40] studied the optimal number of users to be scheduled (i.e. SCed) on a subcarrier, and concluded that at optimality there is a high probability that only a few (two to three) users are SCed on a subcarrier.

[90] and [91] addressed the third challenge and studied the PAPR problem of NOMA at high-rate downlink transmissions. To reduce the PAPR of transmitted signal the peak-clipping method [92] is considered. Peak-clipping causes non-linear distortion to the transmitted signal and high BER [93] at conventional systems, such as OFDMA with QAM signaling technique. However, [91] showed that NOMA signaling technique based on superposition of multiple weighted signals, called as SCM, is the optimal among all signaling techniques to minimize the residual clipping noise power. SCM is optimal since superposition of multiple signals result in an approximately Gaussian signal [20], which helps compensation of the residual noise and estimation of the original (un-clipped) signal at the receiver.

[20,39,94] addressed the fourth challenge and studied communication techniques

for NOMA when iterative signal processing is employed. [39] studied signaling techniques for the iterative MMSE detection [95] at NOMA and proved that SCM maximizes the output SINR in the linear MMSE estimates during iterative detection. [20] and [94] researched on coding techniques. [20] designed practical channel codes for iterative SIC, where it is expected to be able to eleminate the residual interference due to imperfect IC as well as differentiate symbols of superimposed users. [94] provided capacity and BER performance comparisons of single-code SCM and multi-code SCM. The results showed that multi-code SCM can achieve superior capacity to single-code SCM.

[96] and [41] addressed the fifth challenge and introduced NOMA concept to current popular performance improving techniques. [96] introduced NOMA to hybrid automatic repeat request scheme [97], where a new packet to be transmitted is superimposed with one or more packet(s) that is/are to be re-transmitted, and then the superimposed packet is transmitted in a single transmission period. The results showed significant improvement at the link-level throughput. [41] applied NOMA to cooperative transmissions and showed that cooperative NOMA can achieve the maximum diversity gain for all users at a cooperative transmission. It was also shown that, cooperative NOMA improves the outage probability with respect to non-cooperative NOMA and OMA schemes.

Despite interesing literature on NOMA technology, so far the researches only consider time-synchronous transmissions. However, synchronous transmission is impractical for uplink transmissions since users are geographically distributed and the mobile environment is dynamic. Asynchronism in the received signal causes crucial disturbances to the SC-SIC and performances of symbol detection and IC are significantly degraded if these disturbances are not properly addressed [98]. Further, it is not straightforward to extend asynchronous communication techniques proposed for OFDMA [99–101] to SC-SIC. This is because asynchronism has different effects on OFDMA and SC-SIC. For OFDMA, asynchronous arriving signals can destroy orthogonality among subcarriers and cause inter carrier interference [102]. However, in SC-SIC there is multiple access interference (MAI) [103]. Thus, employing

communication techniques developed for asynchronous OFDMA at SC-SIC systems will not be an efficient solution. Therefore, there are need for novel communication techniques that address asynchronous NOMA (SC-SIC) transmissions and extensive performance analyses to validate the developed techniques.

Chapter 3

System Model

Contents

3.1 Uplink NOMA system and Received Signal Structure . 38

3.2 Iterative Signal Processing at the Receiver 40

3.1 Uplink NOMA system and Received Signal Structure

In this thesis, an OFDM based uplink NOMA system is investigated with a BS serving a number of geographically distributed users, as shown in Fig. 1.2 (a). It is assumed there are n subcarriers in the system. Each subcarrier is shared by K NOMA users within a small cell environment. It is envisioned that NOMA is used in conjuction with beamforming technology in the small cell environment, where there are a small number of users (e.g. $K < 10$) within each beam [13]. Due to different distances and the dynamic channels from the users to the BS, asynchronous transmissions are assumed among users. Future small cells are expected to operate with very short duration symbols (e.g. symbol duration in nanoseconds) to assist achieve extra-high data rates. Therefore, despite the timing offset is considered among users' symbol, it is assumed that the timing offset is not so high to destroy

the orthogonality of subcarriers. So that, the subcarriers preserve their orthogonality in the received signal and the following analyses focused on *one subcarrier*. Received signal structure in one subcarrier is illustrated in Fig. 3.1, where four adjacent OFDM symbols of three users are shown in time domain. For asynchronous transmissions, the arrival times at the BS of the users' signals are not aligned. A symbol from one user overlaps with two adjacent symbols from each of the other two users. In order to carry out IC, the information of two adjacent symbols of other users must be exploited for the reference user (which is denoted as the k^*th user in the rest of the thesis).

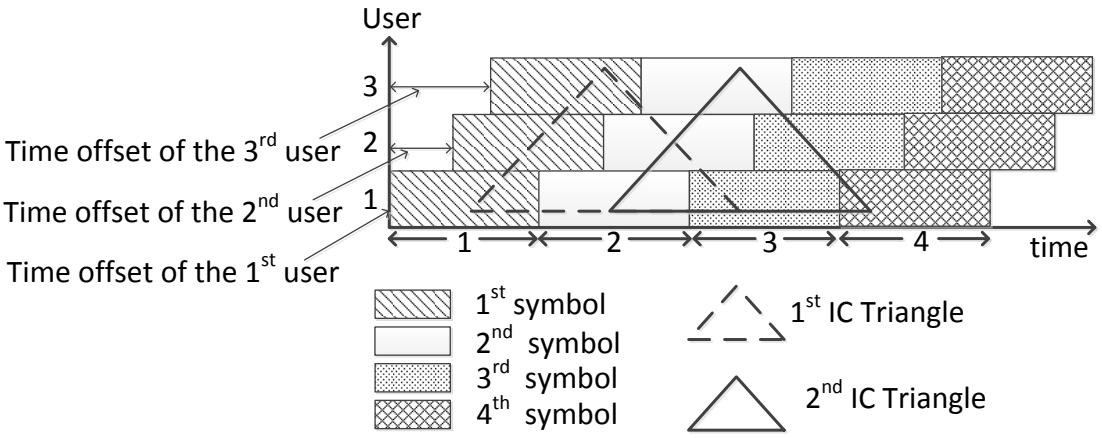

Figure 3.1: Received signal structure at time domain.

$X_k[s]$ denotes the sth symbol of the kth user, which is a complex symbol and output from a multi-level symbol mapper, such as QAM [14] or SCM [39]. $p_k^{\text{tx}}[s]$ is the transmission power allocated to $X_k[s]$ for power domain multiplexing of users' signals. In this thesis the same level of power is applied for all symbols during a scheduling period. Therefore the symbol index "s" is dropped out and p_k^{tx} is used to denote the transmission power. Then, the signal transmitted from the kth user at the sth symbol is represented by $X_k[s] \cdot \sqrt{p_k^{\text{tx}}}$.

In one symbol period, the frequency response on one subcarrier is considered to be flat and depend on path loss, flat fading and phase, and is given by $h_k[s] = \sqrt{(d_k)^{-\lambda}}\alpha_k[s]e^{j\theta_k[s]}$, where $(d_k)^{-\lambda/2}$ is the path loss with the distance d_k between

the BS and the kth user and propagation exponent λ, and $\alpha_k[s]$ denotes magnitude of fading for the sth symbol of the kth user and is assumed to follow Rayleigh distribution independently and identically (i.i.d.) for different users, with $\mathrm{E}[\alpha_k^2[s]] = 1$, where $\mathrm{E}[\cdot]$ is the statistical expectation. It is also assumed that the received signal for the sth symbol of the kth user has random phase $\theta_k[s]$, uniformly distributed over $[0, 2\pi]$. The channel coherence time is assumed to be much larger than the symbol time and $h_k[s]$ is fixed for block of symbols, during a scheduling period. Therefore index "s" is omitted and h_k is used to denote the CSI. Also, AWGN with double-side power spectral density (PSD), N_0, is assumed on the receiver side.

3.2 Iterative Signal Processing at the Receiver

At the BS receiver, iterative signal processing with a maximum L iterations is carried out to improve system performance. At each iteration $l\,(1 \leq l \leq L)$ of the signal processing, symbol detection is applied for each user in descending SNR order to estimate symbols of K users. For one user, co-channel users are sources of interferences which reduce accuracy of symbol detection and cause high BER. Hence the first operation at the receiver is to apply SIC to suppress interference among K users, which requires a priori information (estimate) of symbols from co-channel users. By denoting $\hat{X}_k^{(l)}[s]$ as the estimate of the sth symbol of the kth user at the lth iteration, SIC reconstructs interfering signals by multiplying $\hat{X}_k^{(l)}[s]$ with the CSI of the kth user, h_k. Reconstructed signals are then subtracted from the received signal to suppress the interference. Due to asynchronism, to reconstruct interference accurately for the sth symbol of kth user, the information of symbols $\{s-1, s, s+1\}$ of the co-channel users is required. In our proposed technique, this information is provided through a vector that stores priori estimated symbols of the kth user at the lth iteration, $\hat{\mathbf{X}}_k^{(l)} = \{\hat{X}_k^{(l)}[\varsigma], \varsigma \in \{s, s+1, \cdots, s+K-1\}\}$, $\forall k$, denoted as the "priori symbol vector". Note that the vector contains consecutive symbols up to index $s+K-1$. This is because, in order to achieve low BER performance for all K users,

all the overlapping symbols of a stronger user need to be a priori detected before detecting a symbol of a weak user. For example, in the received signal structure shown in Fig. 3.1 the order of users' SNR is assumed to be 1st user > 2nd user > 3rd user. The 1st symbol of the 3rd user overlaps with two symbols of the 2nd user and these two symbols overlap with three symbols of the 1st user. Therefore in order to achieve low BER for all three users, it is required to detect three consecutive symbols of the 1st user, then two consecutive symbols of the 2nd user and then the symbol of the 3rd user. This is so called the 1st IC Triangle as shown in Fig. 3.1. However, Conv-SIC detects only the 1st symbol of the three users in an iterative manner without constructing IC Triangles.

Let $\mathbf{Y} = \{Y[\varsigma], \varsigma \in \{s, s+1, \cdots, s+K-1\}\}$ denote the vector of the received signal, where $Y[\varsigma]$ is the received signal for the ςth symbol. In Fig. 3.2 (a), the 1st and 2nd iterations of the signal processing for the 1st IC Triangle are illustrated. At the 1st iteration, since the 1st user has the highest SNR, its three consecutive symbols are detected first, with no information available at the priori symbol vector. Then, the two consecutive symbols of the 2nd user is detected with a priori information of the 1st user detected, but no a priori information for the 3rd user. A priori information obtained from the detection of the 1st and 2nd users are used at the detection for the 1st symbol of the 3rd user. As the priori information of the interference is not achieved for detecting 1st and 2nd users' symbols, the results of these detections are in low accuracy. Since the SIC and symbol detection performances depend on the accuracy of $\hat{\mathbf{X}}_k^{(l)}, \forall k$, there is much room for performance improvement. This is done by employing multiple iterations of symbol detection which is based on exploiting a priori estimate obtained from the previous iteration. For example, at the 2nd iteration, the priori information of the 2nd and 3rd users obtained from the 1st iteration are used at the detection for the 1st user and the detection accuracy of the 2nd iteration is considerably improved. Employing more iterations can further improve system performance, but will increase the processing delay. Thus, for delay sensitive applications, L cannot be too large. After L iterations on the 1st IC Triangle, the signal processing advances in time (i.e. shifted by one symbol) to perform

the detection for the next symbol of users, by using the 2nd IC Triangle at Fig. 3.1.

The procedure of iterative processing for the 2nd IC Triangle is illustrated in Fig. 3.2 (b). When performing the IC for the 2nd IC Triangle, the priori information obtained from performing the 1st IC Triangle is exploited as initialization and additional information for the IC. As shown in Fig. 3.1, the 1st and 2nd IC Triangles are overlapped on some symbols, specifically the 2nd and 3rd symbols of the 1st user and the 2nd symbol of the 2nd user. At the 1st iteration of the 2nd IC Triangle, the symbols overlapped by IC Triangles, i.e. 2nd and 3rd symbols, are initialized by values detected the latest at the 1st IC Triangle processing. Then, the order of detection for the 1st iteration of the 2nd IC Triangle is the detection of the 4th symbol of the 1st user, the 3rd symbol of the 2nd user and then the 2nd symbol of the 3rd user. At the 2nd and further detection iterations for the 2nd IC Triangle the estimates of all symbols covered by the 2nd IC Triangle are updated following the similar signal processing to the 2nd iteration of the 1st IC Triangle, with all additional information of interference achieved in the previous IC Triangle. For example, at the 2nd iteration of processing the 2nd IC Triangle, when detecting the 2nd symbol of the 1st user, a priori information of the 1st symbol of the 2nd and 3rd users are adopted from the estimates provided by the 1st IC Triangle processing. Repetitively, processing the following IC Triangles in time sequence is similar to processing the 2nd IC Triangle.

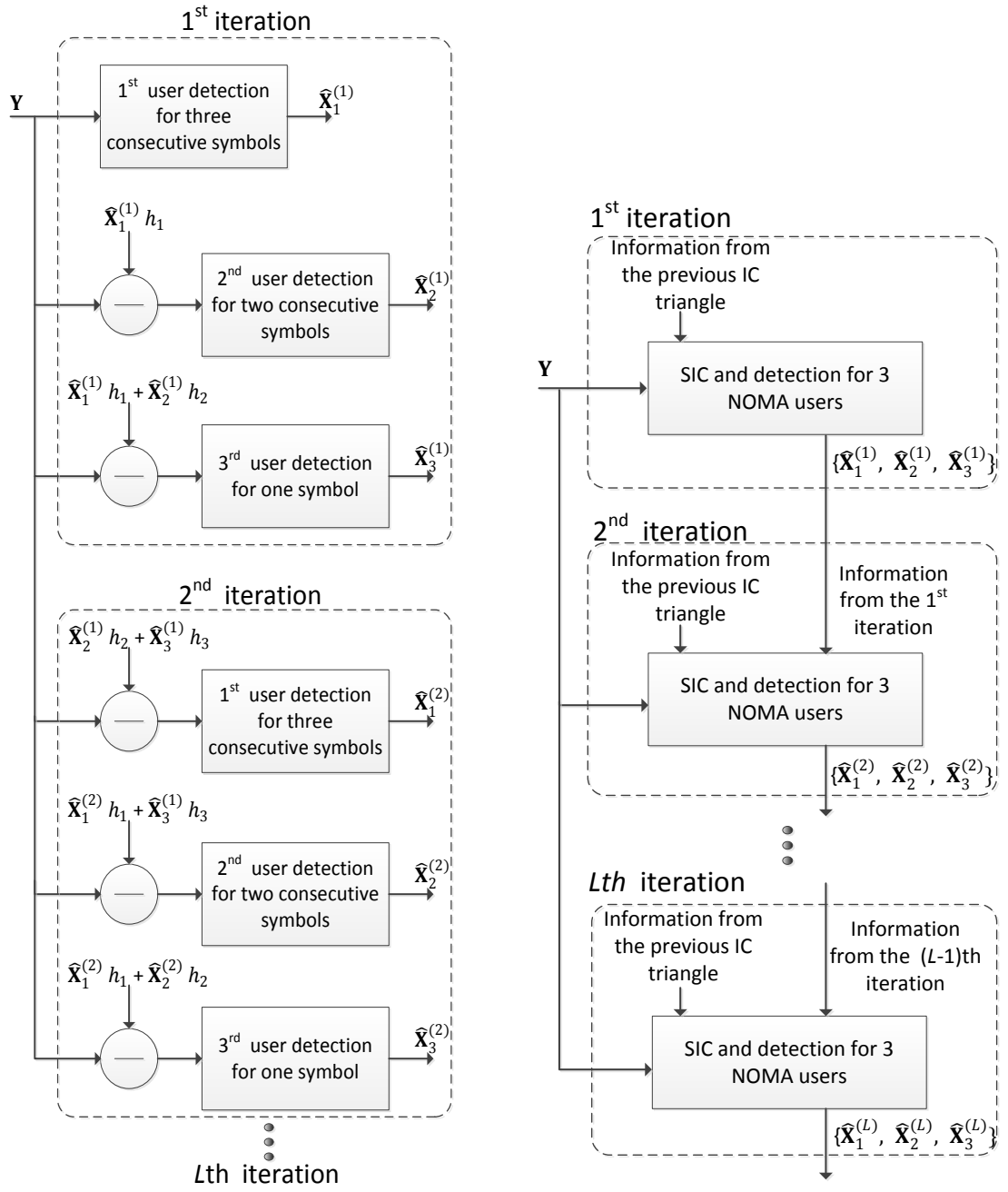

(a) Processing for the 1st IC Triangle. (b) Processing for the 2nd and further IC Triangles.

Figure 3.2: Iterative SIC and symbol detection processing for IC Triangles.

Chapter 4

Triangular Successive Interference Cancellation (T-SIC) and Performance Analyses

Contents

4.1 T-SIC Technique 44

4.2 Received Signal and Average BER Analyses 48

4.3 Shannon Capacity based Performance Comparison . . . 58

4.3.1 NOMA Spectral Efficiency 58

4.3.2 OFDMA Spectral Efficiency 60

4.1 T-SIC Technique

This section will present the approach of the T-SIC technique for IC in asynchronous NOMA transmissions. T-SIC constructs IC Triangles that are used to detect and exploit a priori information of all the symbols (especially from the strong users) that overlap with the symbol to be detected. While constructing IC Triangles it is important to consider relative time offset between users. Let τ_k represent the

time offset of the kth user to a reference time. Fig. 3.1 shows the received signal structure for $K = 3$ with $\tau_1 < \tau_2 < \tau_3$. Taking the 1st user as the reference user, its sth symbol overlap with the $(s-1)$th and sth symbols of the 2nd and 3rd users. Thus, T-SIC uses the time offset information of users to correctly determine the symbols of co-channel users that interfere with the symbol to be detected. Then, it searches the priori symbol vector to obtain the latest estimates for these interfering symbols, and uses this information to reconstruct and subtract (i.e. IC) the interfering signals from the received signal.

The procedure of T-SIC to construct and iteratively process IC Triangles is demonstrated by the flowchart in Fig. 4.1, based on the scenario in Fig. 3.1 and a total number of S symbols are transmitted during a scheduling period. Suppose the 1st iteration takes place on the 1st IC Triangle. The 1st, 2nd and 3rd steps are proceeded to detect the 1st, 2nd and 3rd symbol of the 1st user, respectively, since the 1st user has the highest SNR. As $\tau_1 < \tau_2 < \tau_3$, T-SIC determines that for the sth symbol of the 1st user, the $(s-1)$th and sth symbols of the 2nd and 3rd users are interferes. At this iteration, the priori symbol vector do not contain information of these symbols so that it is not possible to suppress interference from these symbols before the detecion. Detected symbols of the 1st user are forwarded to the priori symbol vector.

The 4th and 5th steps are to detect the 1st and 2nd symbol of the 2nd user. Comparing time offset of users, T-SIC determines that for the sth symbol of the 2nd user, the sth and $(s+1)$th symbols of the 1st user and the $(s-1)$th and sth symbols of the 3rd user are interferes. T-SIC searches the priori symbol vector for their estimates. Information of the 1st user's symbols is available but the 3rd user's is not. The interference from the stronger user is suppressed before the detection (even at the 1st iteration). Then, the detected symbols of the 2nd user are forwarded to the priori symbol vector.

The 6th step is to detect the 1st symbol of the 3rd user. T-SIC determines that for the sth symbol of the 3rd user, the $(s-1)$th and sth symbols of the 1st and 2nd users are interfering. Information of all these symbols is available at the priori

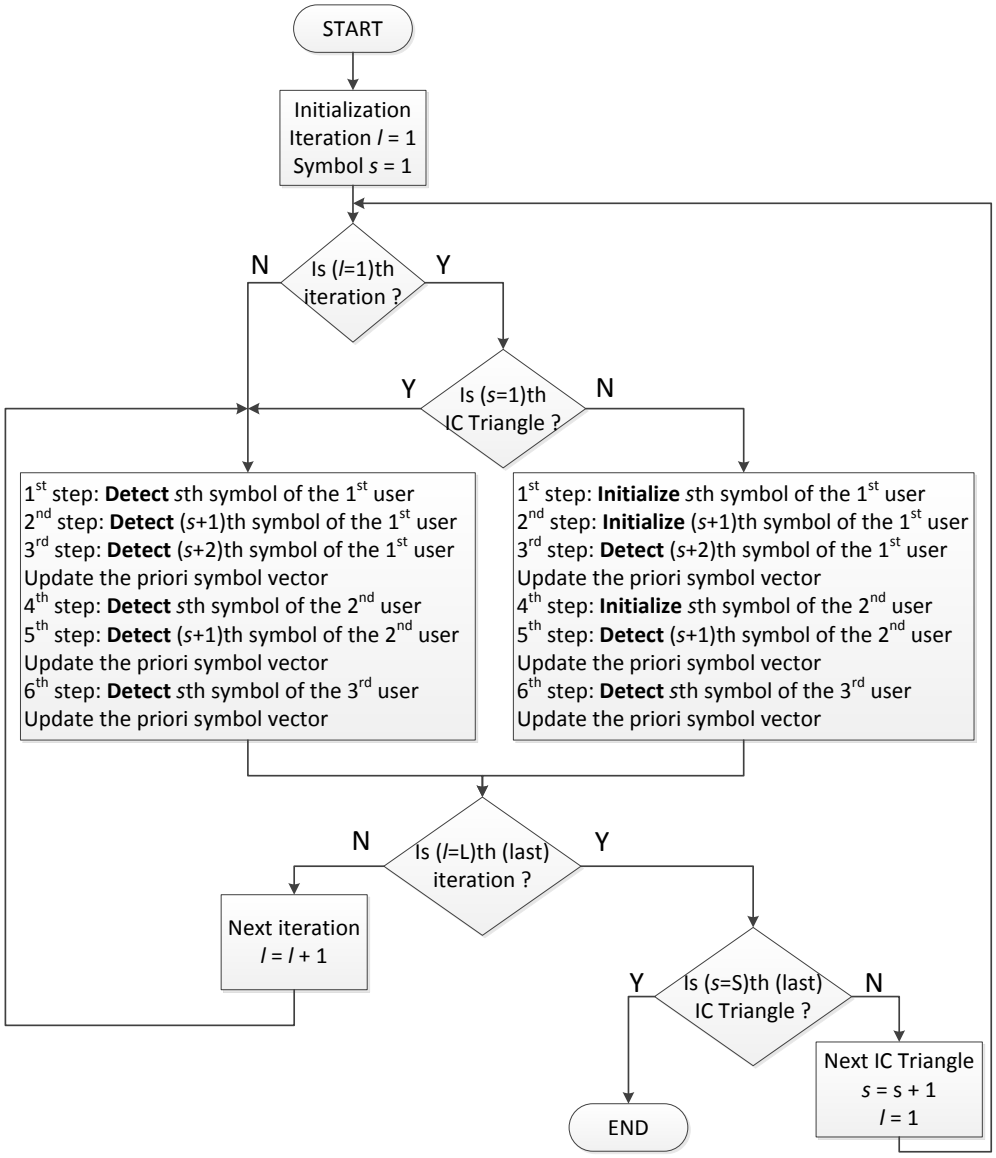

Figure 4.1: Flowchart of T-SIC algorithm.

symbol vector and used by T-SIC to suppress interference for the 3rd user. Detected symbol of the 3rd user is forwarded to the priori symbol vector and the 1st iteration is completed.

Then, at the 2nd iteration above six steps are repeated but with the updated information from the 1st iteration now available at the priori symbol vector. For example, at the 1st step, a priori information of the symbols of the 2nd and 3rd users is available; at the 4th step a priori information of the symbols of the 1st and 3rd users is available; and so on. That is, the complete interference information for the 1st symbol of all users is available. The processing for further iterations, $l > 2$, is similar to the 2nd iteration, but with updated (more accurate) information from the latest iteration available at the priori symbol vector.

In Fig. 4.2, symbols marked with numbers 1-6 illustrates the constructed 1st IC Triangle, where from small to big numbers on the symbols show the order of detection. After completing L iterations on the 1st IC Triangle, the information bits for the 1st symbol of users are output, and the processing advances in time by shifting the IC Triangle by one symbol to the 2nd IC Triangle. The 2nd IC Triangle is illustrated by the symbols marked with $\{2, 3, 5, 7, 8, 9\}$. At the 1st iteration on the 2nd IC Triangle, a priori information (latest) obtained from the 1st IC Triangle is used to initialize values of the common symbols to both IC Triangles, i.e. symbols $\{2, 3, 5\}$, and only the other symbols marked with $\{7, 8, 9\}$ are respectively detected. Then, at the lth ($l \geq 2$) iteration, the values of all the symbols included under the 2nd IC Triangle are updated (detected) by exploiting both the information provided from the 1st IC Triangle symbols, i.e. $\{4, 6\}$, and the most recent iteration of the 2nd IC Triangle. The processing for the 3rd and later IC Triangle is similar to the 2nd IC Triangle's.

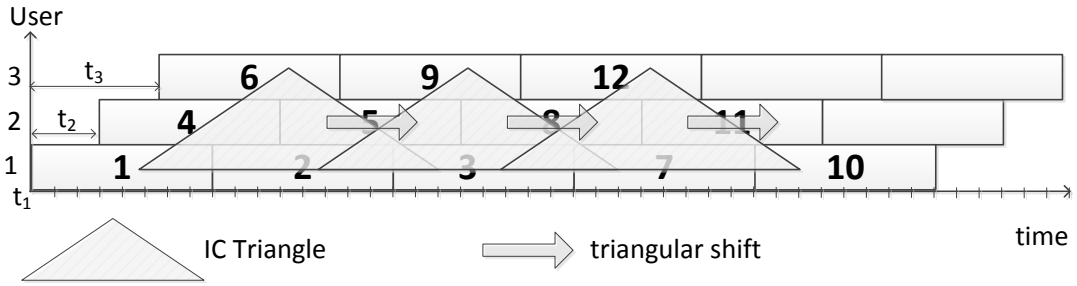

Figure 4.2: T-SIC received signal structure.

4.2 Received Signal and Average BER Analyses

To further present the procedure and performance of T-SIC, quantitative analyses of the received signal and average BER performance are provided in the following. Let the sth symbol of the k^*th user be the desired symbol to be detected. At the BS receiver, the received signal for the k^*th user at the sth symbol is given by

$$Y_{k^*}[s] = X_{k^*}[s] \cdot \sqrt{p_{k^*}} \cdot \alpha_{k^*} + \eta_{k^*}[s] + N. \tag{4.1}$$

On the right hand side (RHS) of (4.1), the first term is the desired signal and $p_{k^*} = p_{k^*}^{\text{tx}} \cdot d_{k^*}^{-\lambda/2}$ represents the average received power of the signal of the k^*th user. $N = \sqrt{N_0} \cdot e^{j\theta_{k^*,N}}$ is complex AWGN, where N_0 is the PSD and $e^{j\theta_{k^*,N}}$ represents the phase mismatch of the noise to the k^*th user's signal. $\eta_{k^*}[s]$ represents the total interference to the desired signal, given by

$$\eta_{k^*}[s] = \sum_{\substack{k \in \Omega \\ k \neq k^*}} \sum_{\varsigma=s-1}^{s+1} \eta_{k^*,k}[s, \varsigma], \tag{4.2}$$

where Ω is the set of users accessing the subcarrier and $\eta_{k^*,k}[s, \varsigma]$ is the interference from the $\varsigma \in \{(s-1), s, (s+1)\}$th symbol of the kth user to the desired symbol, given by

$$\eta_{k^*,k}[s, \varsigma] = \Delta_{k^*,k}[s, \varsigma] \cdot X_k[\varsigma] \cdot \sqrt{p_k} \cdot \alpha_k \cdot e^{j\theta_{k^*,k}}, \tag{4.3}$$

where $e^{j\theta_{k^*,k}}$ represents the phase mismatch of the kth user's signal to the k^*th user and $\Delta_{k^*,k}[s, \varsigma]$ represents percentage of the symbol time that the ςth symbol of the

kth user overlaps with the desired symbol, given by

$$\Delta_{k^*,k}[s,\varsigma] = \frac{1}{T}\max\Bigg\{0, \Big(\delta(\varsigma - s)\cdot T - |\tau_{k^*} - \tau_k|\Big) \\ , \Big((1-\delta(\varsigma - s))\cdot(\tau_{k^*} - \tau_k)\cdot(\varsigma - s)\Big)\Bigg\}, \tag{4.4}$$

where T is a symbol period. $\delta(\cdot)$ is the Dirac delta function. $\delta(\varsigma - s) = 1$ if $\varsigma = s$ and otherwise zero.

Referring to the iterative SIC and detection structure of T-SIC, shown at Fig. 3.2, at the lth iteration the reconstructed interference signal from the ςth symbol of the kth user is given by,

$$\hat{\eta}^{(l)}_{k^*,k}[s,\varsigma] = \Delta_{k^*,k}[s,\varsigma]\cdot\hat{X}^{(\mathfrak{L})}_k[\varsigma]\cdot\sqrt{p_k}\cdot\alpha_k\cdot e^{j\theta_{k^*,k}}, \tag{4.5}$$

where $\mathfrak{L} \in \{l-1, l\}$ is the latest version of estimate available at the priori symbol vector for the ςth symbol of the kth user. For interferers with higher SNR, i.e. $k < k^*$, $\mathfrak{L} = l$ since symbols of these stronger interferers are most recently detected at the lth iteration before the k^*th user, but for interferers with smaller SNR, i.e. $k > k^*$, $\mathfrak{L} = l-1$ since symbols of these weaker interferers are detected after the k^*th user and only symbols at the $(l-1)$th iteration are estimated.

Then, subtracting the reconstructed interference of all the overlapping symbols of the interferers, the interference cancelled (ICed) signal for the desired symbol can be expressed in terms of the desired signal and residual interference plus noise and given by

$$\tilde{Y}^{(l)}_{k^*}[s] = Y_{k^*}[s] - \sum_{\substack{k\in\Omega \\ k\neq k^*}}\sum_{\varsigma=s-1}^{s+1}\hat{\eta}^{(l)}_{k^*,k}[s,\varsigma] = X_{k^*}[s]\cdot\sqrt{p_{k^*}}\cdot\alpha_{k^*} + \tilde{\eta}^{(l)}_{k^*}[s] + N, \tag{4.6}$$

where $\tilde{\eta}^{(l)}_{k^*}[s]$ represents the residual interference at the lth iteration to the desired symbol, given by

$$\tilde{\eta}^{(l)}_{k^*}[s] = \sum_{\substack{k\in\Omega \\ k\neq k^*}}\sum_{\varsigma=s-1}^{s+1}\Delta_{k^*,k}[s,\varsigma]\cdot\Big(X_k[\varsigma] - \hat{X}^{(\mathfrak{L})}_k[\varsigma]\Big)\cdot\sqrt{p_k}\cdot\alpha_k\cdot e^{j\theta_{k^*,k}}. \tag{4.7}$$

It is clear from (4.7) that the magnitude of residual interference at the lth iteration depends on the accuracy of the most recent detection of interferers' symbols.

The ICed signal, according to (4.6), is the decision parameter at the lth iteration's symbol detection and with hard-decision the data of the desired symbol is recovered by the minimum distance criteria, given by

$$\hat{X}_{k^*}^{(l)}[s] = \underset{m_i \in \mathfrak{M}, \forall i}{\arg\min} \left| \tilde{Y}_{k^*}^{(l)}[s] - m_i \right|^2 \tag{4.8}$$

where $|\cdot|$ is the modulus operator and arg min denotes the argument of the minimum. For QAM, m_i is the ith constellation point of the constellation

$$\mathfrak{M} = \left\{ m_i = (2i_I - 1 - \sqrt{M}) + j(2i_Q - 1 - \sqrt{M}), i_I, i_Q \in \{1, 2, \cdots, \sqrt{M}\} \right\}, \tag{4.9}$$

where M is the modulation level.

The error statistics at this detection is obtained as follows. The residual interference and noise at the ICed signal distort the desired signal and can cause detection errors. Based on (4.7), the magnitude of residual interference depends on the accuracy of detection at the $\mathfrak{L}$th iteration for symbols of the interferers (see term $(X_k[\varsigma] - \hat{X}_k^{(\mathfrak{L})}[\varsigma])$ at (4.7)). Therefore, the error statistics at the lth iteration are conditioned on the detection accuracy of symbols of the interferers at the $(l-1)$th (for weaker interferers) and lth (for stronger interferers) iterations. To obtain these conditional statistics, let $\mathrm{e}_k^{(\mathfrak{L})}[\varsigma] = (X_k[\varsigma] \neq \hat{X}_k^{(\mathfrak{L})}[\varsigma])$ denote the event that at the latest iteration the symbol of the interferer was detected in error and $\mathrm{c}_k^{(\mathfrak{L})}[\varsigma] = (X_k[\varsigma] = \hat{X}_k^{(\mathfrak{L})}[\varsigma])$ denote the event that at the latest iteration the symbol of the interferer was correctly detected. Also, let $\mathrm{z}_k^{(\mathfrak{L})}[\varsigma] \in \{\mathrm{e}_k^{(\mathfrak{L})}[\varsigma], \mathrm{c}_k^{(\mathfrak{L})}[\varsigma]\}$ indicate the status of the latest detection for the symbol of the interferer, i.e. in error or correct, and $\mathbf{z}^{(\mathfrak{L})} = \{\mathrm{z}_k^{(\mathfrak{L})}[\varsigma], \forall k, \forall \varsigma\}$ be the vector form of the latest indicator parameters.

Then, from (4.7), at the lth iteration the variance of the residual interference to the desired symbol is given by,

$$\begin{aligned} \mathrm{Var}(\tilde{\eta}_{k^*}^{(l)}[s] \,\big|\, \mathbf{z}^{(\mathfrak{L})}, \boldsymbol{\Delta}_{k^*}[s]) &= E\left[(\tilde{\eta}_{k^*}^{(l)}[s] \,\big|\, \mathbf{z}^{(\mathfrak{L})}, \boldsymbol{\Delta}_{k^*}[s])^2 \right] \\ &= \sum_{\substack{k \in \Omega \\ k \neq k^*}} \sum_{\varsigma = s-1}^{s+1} \Delta_{k^*,k}[s, \varsigma] \left(\mathrm{D}_k^{(\mathfrak{L})}[\varsigma] \,\big|\, \mathrm{z}_k^{(\mathfrak{L})}[\varsigma] \right) \frac{p_k}{2} \end{aligned} \tag{4.10}$$

where $(A \,\big|\, B)$ represents A conditioned on B and $\boldsymbol{\Delta}_{k^*}[s] = \{\Delta_{k^*,k}[s, \varsigma], \forall k, \forall \varsigma\}$ is the vector of interferers' time offset to the desired user. The distribution of the time offset

between users is assumed to be uniform distribution $\mathrm{U}[\tau_{min}, \tau_{max}]$, where τ_{min} and τ_{max} are the minimum and maximum time offset, respectively. $\left(\mathrm{D}_k^{(\mathfrak{L})}[\varsigma] \,\middle|\, \mathrm{z}_k^{(\mathfrak{L})}[\varsigma]\right) = E[(X_k[\varsigma] - \hat{X}_k^{(\mathfrak{L})}[\varsigma])^2]$ represents the mean square error (MSE) of the detection at the $\mathfrak{L}$th iteration for the ςth symbol of the kth user. As shown by the analysis at Appendix A, i.e. is given by

$$\left(\mathrm{D}_k^{(\mathfrak{L})}[\varsigma] \,\middle|\, \mathrm{z}_k^{(\mathfrak{L})}[\varsigma]\right) = \begin{cases} 1, & \text{for } \mathfrak{L} = 0, \text{i.e. no priori detection was done for the symbol} \\ {}^{6}/_{(M-1)}, & \text{for } \mathfrak{L} \geq 1 \text{ and } \mathrm{z}_k^{(\mathfrak{L})}[\varsigma] = \mathrm{e}_k^{(\mathfrak{L})}[\varsigma], \text{i.e. priori detection was in error} \\ 0, & \text{for } \mathfrak{L} \geq 1 \text{ and } \mathrm{z}_k^{(\mathfrak{L})}[\varsigma] = \mathrm{c}_k^{(\mathfrak{L})}[\varsigma], \text{i.e. priori detection was correct.} \end{cases} \tag{4.11}$$

Based on (4.6), at the lth iteration the SINR for the desired symbol is given by

$$\left(\tilde{\gamma}_{k^*}^{(l)}[s] \,\middle|\, \mathbf{z}^{(\mathfrak{L})}, \alpha_{k^*}^2, \mathbf{\Delta}_{k^*}[s]\right) = \frac{p_{k^*} \cdot \alpha_{k^*}^2}{\mathrm{Var}(\tilde{\eta}_{k^*}^{(l)}[s] \,|\, \mathbf{z}^{(\mathfrak{L})}, \mathbf{\Delta}_{k^*}[s]) + \mathrm{Var}(N)}, \tag{4.12}$$

where $\mathrm{Var}(N) = N_0/2$ is the variance of the noise. The desired symbol is detected in error when the power of residual interference plus noise exceeds half of the distance between two nearest constellation points. Since the distance between constellation points depend on the received power of the desired user, the error statistics can be represented in terms of the SINR as follows. The conditional error probability at the lth iteration for the desired symbol is given by

$$\mathrm{P}(\mathrm{e}_{k^*}^{(l)}[s] \,|\, \mathbf{z}^{(\mathfrak{L})}, \alpha_{k^*}^2, \mathbf{\Delta}_{k^*}[s]) = 1 - \left(1 - \mathrm{P}\left(\mathrm{Var}(\tilde{\eta}_{k^*}^{(l)}[s] \,|\, \mathbf{z}^{(\mathfrak{L})}, \mathbf{\Delta}_{k^*}[s]) + \mathrm{Var}(N) > \mathrm{de}_{k^*}\right)\right)^2, \tag{4.13}$$

where $\mathrm{P}\left(A \,\middle|\, B\right)$ is conditional probability of A given B. de_{k^*} is half of the distance between two nearest constellation points for the desired user, given by ([59], Chapter 6.1.4) $\mathrm{de}_{k^*} = \sqrt{{}^{3 \cdot p_{k^*} \cdot \alpha_{k^*}^2}/_{2 \cdot (M-1)}}$, and $\mathrm{P}\big(\mathrm{Var}(\tilde{\eta}_{k^*}^{(l)}[s] \,\big|\, \mathbf{z}^{(\mathfrak{L})}, \mathbf{\Delta}_{k^*}[s]) + \mathrm{Var}(N) > \mathrm{de}_{k^*}\big)$ is the error probability for one branch of QAM. Note that at (4.13), it is assumed that conditional parameters $\mathbf{z}^{(\mathfrak{L})}, \alpha_{k^*}^2, \mathbf{\Delta}_{k^*}[s]$ are independent of each other and the error probability can be averaged over them one by one. The distribution of the power of

residual interference plus noise is required to find out the error probability for one branch of QAM. Based on (4.10), it is clear that there are two symbols from each co-channel user that interfers the desired symbol. Transmitted symbols independently and identically follow discrete uniform distribution over the constellation points. It is shown in Chapter 4.9 in [104] that the convolution of i.i.d. uniform random variables (r.v.s) converge to the Gaussian distribution very fast. Already for four convoluted r.v.s, i.e. for two asynchronous interferers, the difference between the Gaussian distribution and the exact distribution is negligible ([104], Chapter 4.9). The probability density function (pdf) of Gaussian distribution and convolution of two to five i.i.d. uniform r.v.s [105] are shown in Fig. 4.3 to illustrate the accuracy of Gaussian distribution approximation. The figure validates very fast convergence to Gaussian distribution. Therefore for the case of $K > 1$ the residual interference can be approximated to be Gaussian distributed, with increasing accurracy as K increases. Also, the distribution of the power of residual interference plus noise follows Gaussian distribution with zero mean and variance $\mathrm{Var}(\tilde{\eta}_{k^*}^{(l)}[s] \,|\, \mathbf{z}^{(\mathfrak{L})}, \mathbf{\Delta}_{k^*}[s]) + \mathrm{Var}(N)$. Then, one obtains ([59], Chapter 6.1.4)

$$\mathrm{P}\left(\mathrm{Var}\big(\tilde{\eta}_{k^*}^{(l)}[s] \,\big|\, \mathbf{z}^{(\mathfrak{L})}, \mathbf{\Delta}_{k^*}[s]\big) + \mathrm{Var}(N) > \mathrm{de}_{k^*}\right) = \mathrm{Q}\left(\sqrt{\frac{3 \cdot \left(\tilde{\gamma}_{k^*}^{(l)}[s] \,|\, \mathbf{z}^{(\mathfrak{L})}, \alpha_{k^*}^2, \mathbf{\Delta}_{k^*}[s]\right)}{2 \cdot (M-1)}}\right) \tag{4.14}$$

where $\mathrm{Q}(\cdot)$ is the Q function. Substituting (4.14) into (4.13) the conditional error probability is obtained as

$$\mathrm{P}(\mathrm{e}_{k^*}^{(l)}[s] \,|\, \mathbf{z}^{(\mathfrak{L})}, \alpha_{k^*}^2, \mathbf{\Delta}_{k^*}[s]) = 1 - \left(1 - \mathrm{Q}\left(\sqrt{\frac{3 \cdot \left(\tilde{\gamma}_{k^*}^{(l)}[s] \,|\, \mathbf{z}^{(\mathfrak{L})}, \alpha_{k^*}^2, \mathbf{\Delta}_{k^*}[s]\right)}{2 \cdot (M-1)}}\right)\right)^2 . \tag{4.15}$$

Then $\mathrm{P}(\mathrm{e}_{k^*}^{(l)}[s])$ denotes the error probability and $\mathrm{P}(\mathrm{c}_{k^*}^{(l)}[s]) = (1 - \mathrm{P}(\mathrm{e}_{k^*}^{(l)}[s]))$ is the probability of correct detection. In order to obtain $\mathrm{P}(\mathrm{e}_{k^*}^{(l)}[s])$, we first derive the conditional probability in (4.15) further over the permutations of $\mathbf{z}^{(\mathfrak{L})}$. Then a conditional error probability can be obtained as

$$\mathrm{P}(\mathrm{e}_{k^*}^{(l)}[s] \,|\, \alpha_{k^*}^2, \mathbf{\Delta}_{k^*}[s]) = \sum_{i=1}^{2^{2(K-1)}} \mathrm{P}(\mathrm{e}_{k^*}^{(l)}[s] \,|\, {}_i\mathrm{P}_{\mathbf{z}^{(\mathfrak{L})}}, \alpha_{k^*}^2, \mathbf{\Delta}_{k^*}[s]) \prod_{\substack{k \in \Omega, \varsigma \in \{s-1, s, s+1\} \\ k \neq k^*}} \mathrm{Pr}_{i,k}^{(\mathfrak{L})}[\varsigma]. \tag{4.16}$$

where ${}_i\mathrm{P}_{\mathbf{z}^{(\mathfrak{L})}}$ denote the ith permutation of $\mathbf{z}^{(\mathfrak{L})}$, $1 \leq i \leq 2^{2(K-1)}$. $\mathrm{Pr}_{i,k}^{(\mathfrak{L})}[\varsigma]$ is the probability of the detection status, i.e. being in error or correct, of the latest detection $\mathfrak{L}$, i.e. $\mathfrak{L} = l$ for stronger interferers and $\mathfrak{L} = (l-1)$ for weaker interferers, for the ςth symbol of the kth (interfering) user, considered at the ith permutation of $\mathbf{z}^{(\mathfrak{L})}$. Specifically, at the ith permutation of $\mathbf{z}^{(\mathfrak{L})}$ in case the status of the latest detection of the ςth symbol of the kth user is considered to be a correct detection $\mathrm{Pr}_{i,k}^{(\mathfrak{L})}[\varsigma] = 1 - \mathrm{P}(\mathrm{e}_k^{(\mathfrak{L})}[\varsigma])$. Otherwise, $\mathrm{Pr}_{i,k}^{(\mathfrak{L})}[\varsigma] = \mathrm{P}(\mathrm{e}_k^{(\mathfrak{L})}[\varsigma])$. Thus, it is seen from (4.16) that the error probability of the desired symbol at the lth iteration depends on the error probabilities of interferers' symbols at the most recent detection (current and previous) iteration. Then, $\mathrm{P}(\mathrm{e}_{k^*}^{(l)}[s])$ is obtained by averaging (4.16) over $\alpha_{k^*}^2$ and $\mathbf{\Delta}_{k^*}[s]$, given by

$$\mathrm{P}(\mathrm{e}_{k^*}^{(l)}[s]) = \frac{1}{\tau_{max} - \tau_{min}} \int_{\tau_{min}}^{\tau_{max}} \int_0^{\infty} \mathrm{P}(\mathrm{e}_{k^*}^{(l)}[s] \,\big|\, a, \mathbf{\Delta}) \cdot e^{-a} \, \mathrm{d}a \, \mathrm{d}\mathbf{\Delta}. \tag{4.17}$$

where $a = \alpha_{k^*}^2$ and $\mathbf{\Delta}$ represents $\mathbf{\Delta}_{k^*}[s]$. Then, assuming the symbol energy is divided equally among all bits and the Gray coding is used for mapping bits to symbols, the average BER performance is given by ([59], Chapter 6.1.1),

$$\mathrm{P}_{\mathrm{bit},k^*}^{(l)}[s] = \mathrm{P}(\mathrm{e}_{k^*}^{(l)}[s]) / \log_2(M). \tag{4.18}$$

A demonstration to obtain $\mathrm{P}(\mathrm{e}_{k^*}^{(l)}[s])$ for T-SIC technique is provided as follows. For easy understanding, suppose $K = 2$ and T-SIC is applied to the 1st IC Triangle (see Fig. 3.1 for case $K = 2$).

The 1st iteration

The 1st step is to detect the 1st symbol of the 1st user. Since in this step there is no a priori detection done for the 1st symbol of the 2nd user (i.e. the interfering symbol), (4.10)-(4.15) are conditioned on $\mathbf{z}^{(0)}$. Then based on (4.11), $\left(\mathrm{D}_2^{(0)}[1] \,\middle|\, \mathfrak{L} = 0\right) = 1$. Note that to avoid notational abundance we show $\mathfrak{L} = 0$ as the conditional parameter at (4.11), instead of $\mathrm{z}_2^{(0)}[1]$ since the MSE will always be equal to one when there is no a priori detection done for the interfering symbol. And then substituting the

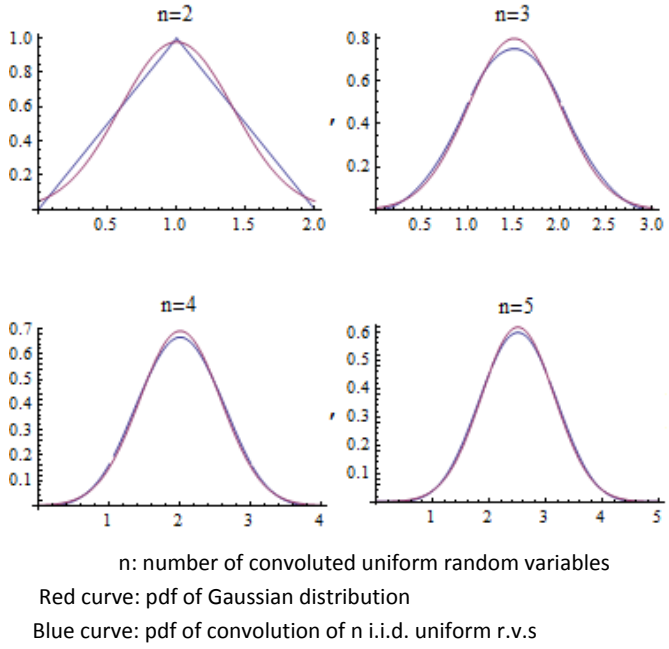

Figure 4.3: Comparison of pdf of Gaussian distribution and convolution of i.i.d. uniform r.v.s.

MSE into (4.10), the variance of residual interference is

$$\mathrm{Var}(\tilde{\eta}_1^{(1)}[1] \,\big|\, \mathfrak{L}=0, \boldsymbol{\Delta}_1[1]) = \Delta_{1,2}[1,1]\cdot p_2/2. \tag{4.19}$$

Substituting (4.19) into (4.12) and (4.12) into (4.15), the conditional error probability is

$$\mathrm{P}(\mathrm{e}_1^{(1)}[1] \,\big|\, \alpha_1^2, \boldsymbol{\Delta}_1[1]) = 1 - \left(1 - \mathrm{Q}\left(\sqrt{\frac{3\cdot p_1\cdot \alpha_1^2}{(M-1)\cdot(\Delta_{1,2}[1,1]\cdot p_2 + N_0)}}\right)\right)^2. \tag{4.20}$$

Note that at (4.20) there is no need to condition on $\mathbf{z}^{(0)}$ since MSE will always be equal to one for $\mathfrak{L}=0$. Then, substituting (4.20) into (4.17) we obtain $\mathrm{P}(\mathrm{e}_1^{(1)}[1])$.

The 2nd step is to detect the 2nd symbol of the 1st user. Similar to the 1st step, the interfering symbols are not a priori detected. Therefore based on (4.11), $\left(\mathrm{D}_2^{(0)}[1] \,\big|\, \mathfrak{L}=0\right) = 1$ and $\left(\mathrm{D}_2^{(0)}[2] \,\big|\, \mathfrak{L}=0\right) = 1$, and substituting them into (4.10), the variance of residual interference is

$$\mathrm{Var}(\tilde{\eta}_1^{(1)}[2] \,\big|\, \{\mathfrak{L}=0, \mathfrak{L}=0\}, \boldsymbol{\Delta}_1[2]) = (\Delta_{1,2}[2,1] + \Delta_{1,2}[2,2])\cdot p_2/2. \tag{4.21}$$

Substituting (4.21) into (4.12) and (4.12) into (4.15), the conditional error probability is

$$\mathrm{P}(\mathrm{e}_1^{(1)}[2] \,|\, \alpha_1^2, \boldsymbol{\Delta}_1[2]) = 1 - \left(1 - \mathrm{Q}\left(\sqrt{\frac{3 \cdot p_1 \cdot \alpha_1^2}{(M-1) \cdot ((\Delta_{1,2}[2,1] + \Delta_{1,2}[2,2]) \cdot p_2 + N_0)}}\right)\right)^2 . \quad (4.22)$$

Then, substituting (4.22) into (4.17) we obtain $\mathrm{P}(\mathrm{e}_1^{(1)}[2])$.

The 3rd step is to detect the 1st symbol of the 2nd user. At previous steps of this iteration the interfering symbols, i.e. the 1st and 2nd symbols of the 1th user, are detected. Therefore $\mathrm{P}(\mathrm{e}_2^{(1)}[1])$ is conditioned on the permutation of these latest detection results. Then, let $\{\mathrm{e}_1^{(1)}[1], \mathrm{e}_1^{(1)}[2]\}$ be the 1st permutation that detection results of both symbols of the 1st user was in error. This permutation occurs with probability $(\mathrm{P}(\mathrm{e}_1^{(1)}[1]) \cdot \mathrm{P}(\mathrm{e}_1^{(1)}[2]))$. Then based on (4.11), $\left(\mathrm{D}_1^{(1)}[1] \,|\, \mathrm{e}_1^{(1)}[1]\right) = ({}^{6}/_{(M-1)})$ and $\left(\mathrm{D}_1^{(1)}[2] \,|\, \mathrm{e}_1^{(1)}[2]\right) = ({}^{6}/_{(M-1)})$ and substituting them into (4.10), the variance of residual interference is

$$\mathrm{Var}(\tilde{\eta}_2^{(1)}[1] \,|\, \{\mathrm{e}_1^{(1)}[1], \mathrm{e}_1^{(1)}[2]\}, \boldsymbol{\Delta}_2[1]) = (\Delta_{2,1}[1,1] + \Delta_{2,1}[1,2]) \cdot ({}^{6}/_{(M-1)}) \cdot p_1/2. \quad (4.23)$$

Substituting (4.23) into (4.12) and (4.12) into (4.15) we obtain $\mathrm{P}(\mathrm{e}_2^{(1)}[1] \,|\, \{\mathrm{e}_1^{(1)}[1], \mathrm{e}_1^{(1)}[2]\}, \alpha_2^2, \boldsymbol{\Delta}_2[1])$. Then, let $\{\mathrm{e}_1^{(1)}[1], \mathrm{c}_1^{(1)}[2]\}$ be the 2nd permutation that detection result for the 1st symbol was in error but the 2nd symbol was correct for the 1st user. This permutation occurs with probability $(\mathrm{P}(\mathrm{e}_1^{(1)}[1]) \cdot (1 - \mathrm{P}(\mathrm{e}_1^{(1)}[2])))$. In this case $\left(\mathrm{D}_1^{(1)}[1] \,|\, \mathrm{e}_1^{(1)}[1]\right) = ({}^{6}/_{(M-1)})$ and $\left(\mathrm{D}_1^{(1)}[2] \,|\, \mathrm{c}_1^{(1)}[2]\right) = 0$ and substituting them into (4.10), the variance of residual interference is

$$\mathrm{Var}(\tilde{\eta}_2^{(1)}[1] \,|\, \{\mathrm{e}_1^{(1)}[1], \mathrm{c}_1^{(1)}[2]\}, \boldsymbol{\Delta}_2[1]) = \Delta_{2,1}[1,1] \cdot ({}^{6}/_{(M-1)}) \cdot p_1/2. \quad (4.24)$$

Substituting (4.24) into (4.12) and (4.12) into (4.15) we obtain $\mathrm{P}(\mathrm{e}_2^{(1)}[1] \,|\, \{\mathrm{e}_1^{(1)}[1], \mathrm{c}_1^{(1)}[2]\}, \alpha_2^2, \boldsymbol{\Delta}_2[1])$. Let the 3rd permutation be $\{\mathrm{c}_1^{(1)}[1], \mathrm{e}_1^{(1)}[2]\}$ which occurs with probability $((1-\mathrm{P}(\mathrm{e}_1^{(1)}[1])) \cdot \mathrm{P}(\mathrm{e}_1^{(1)}[2]))$ and the 4th permutation be $\{\mathrm{c}_1^{(1)}[1], \mathrm{c}_1^{(1)}[2]\}$ which occurs with probability $((1 - \mathrm{P}(\mathrm{e}_1^{(1)}[1])) \cdot (1 - \mathrm{P}(\mathrm{e}_1^{(1)}[2])))$. Then, $\mathrm{P}(\mathrm{e}_2^{(1)}[1] \,|\, \{\mathrm{c}_1^{(1)}[1], \mathrm{e}_1^{(1)}[2]\}, \alpha_2^2, \boldsymbol{\Delta}_2[1])$ and $\mathrm{P}(\mathrm{e}_2^{(1)}[1] \,|\, \{\mathrm{c}_1^{(1)}[1], \mathrm{c}_1^{(1)}[2]\}, \alpha_2^2, \boldsymbol{\Delta}_2[1])$ are obtained in

the similar way as the previous permutations. Once the conditional error probability for each permutation is obtained, the error probability that is averaged over the permutations is obtained by

$$\begin{aligned}\mathrm{P}(\mathrm{e}_2^{(1)}[1] \,|\, \alpha_2^2, \boldsymbol{\Delta}_2[1]) = &\Big(\mathrm{P}(\mathrm{e}_2^{(1)}[1] \,|\, \{\mathrm{e}_1^{(1)}[1], \mathrm{e}_1^{(1)}[2]\}, \alpha_2^2, \boldsymbol{\Delta}_2[1]) \cdot \mathrm{P}(\mathrm{e}_1^{(1)}[1]) \cdot \mathrm{P}(\mathrm{e}_1^{(1)}[2])\Big) \\ &+ \Big(\mathrm{P}(\mathrm{e}_2^{(1)}[1] \,|\, \{\mathrm{e}_1^{(1)}[1], \mathrm{c}_1^{(1)}[2]\}, \alpha_2^2, \boldsymbol{\Delta}_2[1]) \cdot \mathrm{P}(\mathrm{e}_1^{(1)}[1]) \cdot (1 - \mathrm{P}(\mathrm{e}_1^{(1)}[2]))\Big) \\ &+ \Big(\mathrm{P}(\mathrm{e}_2^{(1)}[1] \,|\, \{\mathrm{c}_1^{(1)}[1], \mathrm{e}_1^{(1)}[2]\}, \alpha_2^2, \boldsymbol{\Delta}_2[1]) \cdot (1 - \mathrm{P}(\mathrm{e}_1^{(1)}[1])) \cdot \mathrm{P}(\mathrm{e}_1^{(1)}[2])\Big) \\ &+ \Big(\mathrm{P}(\mathrm{e}_2^{(1)}[1] \,|\, \{\mathrm{c}_1^{(1)}[1], \mathrm{c}_1^{(1)}[2]\}, \alpha_2^2, \boldsymbol{\Delta}_2[1]) \cdot (1 - \mathrm{P}(\mathrm{e}_1^{(1)}[1])) \cdot (1 - \mathrm{P}(\mathrm{e}_1^{(1)}[2]))\Big).\end{aligned} \tag{4.25}$$

Then, substituting (4.25) into (4.17) we obtain $\mathrm{P}(\mathrm{e}_2^{(1)}[1])$.

The 2nd iteration

The 1st step is to detect the 1st symbol of the 1st user. Since the 1st symbol of the 2nd user was detected at the 1st iteration, $\mathrm{P}(\mathrm{e}_1^{(2)}[1])$ is conditioned on the permutation of that detection result. Then, let the 1st permutation be $\{\mathrm{e}_2^{(1)}[1]\}$, which occurs with probability $\mathrm{P}(\mathrm{e}_2^{(1)}[1])$. From (4.11), $\Big(\mathrm{D}_2^{(1)}[1] \,|\, \mathrm{e}_2^{(1)}[1]\Big) = ({}^{6}/_{(M-1)})$ and substitute it into (4.10), the variance of residual interference is

$$\mathrm{Var}(\tilde{\eta}_1^{(2)}[1] \,|\, \mathrm{e}_2^{(1)}[1], \boldsymbol{\Delta}_1[1]) = \Delta_{1,2}[1,1] \cdot ({}^{6}/_{(M-1)}) \cdot p_2/2. \tag{4.26}$$

Substituting (4.26) into (4.12) and (4.12) into (4.15) we obtain $P(\mathrm{e}_1^{(2)}[1] \,|\, \mathrm{e}_2^{(1)}[1], \alpha_1^2, \boldsymbol{\Delta}_1[1])$. Then, the 2nd permutation is $\{\mathrm{c}_2^{(1)}[1]\}$, which occurs with probability $(1 - \mathrm{P}(\mathrm{e}_2^{(1)}[1]))$. From (4.11), $\Big(\mathrm{D}_2^{(1)}[1] \,|\, \mathrm{c}_2^{(1)}[1]\Big) = 0$ and from (4.10), $\mathrm{Var}(\tilde{\eta}_1^{(2)}[1] \,|\, \mathrm{c}_2^{(1)}[1], \boldsymbol{\Delta}_1[1]) = 0$. Then by substituting $\mathrm{Var}(\tilde{\eta}_1^{(2)}[1] \,|\, \mathrm{c}_2^{(1)}[1], \boldsymbol{\Delta}_1[1])$ into (4.12) and (4.12) into (4.15) we obtain $\mathrm{P}(\mathrm{e}_1^{(2)}[1] \,|\, \mathrm{c}_2^{(1)}[1], \alpha_1^2, \boldsymbol{\Delta}_1[1])$. The error probability that is averaged w.r.t. the permutations is given by

$$\begin{aligned}\mathrm{P}(\mathrm{e}_1^{(2)}[1] \,|\, \alpha_1^2, \boldsymbol{\Delta}_1[1]) = &\Big(\mathrm{P}(\mathrm{e}_1^{(2)}[1] \,|\, \mathrm{e}_2^{(1)}[1], \alpha_1^2, \boldsymbol{\Delta}_1[1]) \cdot \mathrm{P}(\mathrm{e}_2^{(1)}[1])\Big) \\ &+ \Big(\mathrm{P}(\mathrm{e}_1^{(2)}[1] \,|\, \mathrm{c}_2^{(1)}[1], \alpha_1^2, \boldsymbol{\Delta}_1[1]) \cdot (1 - \mathrm{P}(\mathrm{e}_2^{(1)}[1]))\Big).\end{aligned} \tag{4.27}$$

Then, substituting (4.27) into (4.17) we obtain $\mathrm{P}(\mathrm{e}_1^{(2)}[1])$.

The 2nd step is to detect the 2nd symbol of the 1st user. From the interfering symbols, only the 1st symbol of the 2nd user was a priori detected at the previous iteration. Therefore $\mathrm{P}(\mathrm{e}_1^{(2)}[2])$ is conditioned on the permutations w.r.t. only the detection result for the 1st symbol of the 2nd user. Then let the 1st permutation be $\{\mathrm{e}_2^{(1)}[1]\}$, which occurs with the probability $\mathrm{P}(\mathrm{e}_2^{(1)}[1])$. From (4.11), $\left(\mathrm{D}_2^{(1)}[1] \,\middle|\, \mathrm{e}_2^{(1)}[1]\right) = ({}^{6}/_{(M-1)})$ and $\left(\mathrm{D}_2^{(0)}[2] \,\middle|\, \mathfrak{L}=0\right) = 1$ and substituting them into (4.10), the variance of residual interference is

$$\mathrm{Var}(\tilde{\eta}_1^{(2)}[2] \,|\, \{\mathrm{e}_1^{(1)}, \mathfrak{L}=0\}, \boldsymbol{\Delta}_1[2]) = \Delta_{1,2}[2,1]\cdot({}^{6}/_{(M-1)})\cdot p_2/2 + \Delta_{1,2}[2,2]\cdot p_2/2. \quad (4.28)$$

Substituting (4.28) into (4.12) and (4.12) into (4.15) we obtain $\mathrm{P}(\mathrm{e}_1^{(2)}[2] \,|\, \{\mathrm{e}_1^{(1)}, \mathfrak{L}=0\}, \alpha_1^2, \boldsymbol{\Delta}_1[2])$. Then the 2nd permutation is $\{\mathrm{c}_2^{(1)}[1]\}$, which occurs with the probability $(1-\mathrm{P}(\mathrm{e}_2^{(1)}[1]))$. From (4.11), $\left(\mathrm{D}_2^{(1)}[1] \,\middle|\, \mathrm{c}_2^{(1)}[1]\right) = 0$ and $\left(\mathrm{D}_2^{(0)}[2] \,\middle|\, \mathfrak{L}=0\right) = 1$ and substituting them into (4.10), the variance of residual interference is

$$\mathrm{Var}(\tilde{\eta}_1^{(2)}[2] \,|\, \{\mathrm{c}_1^{(1)}, \mathfrak{L}=0\}, \boldsymbol{\Delta}_1[2]) = \Delta_{1,2}[2,2]\cdot p_2/2. \quad (4.29)$$

Substituting (4.29) into (4.12) and (4.12) into (4.15) we obtain $\mathrm{P}(\mathrm{e}_1^{(2)}[2] \,|\, \{\mathrm{c}_1^{(1)}, \mathfrak{L}=0\}, \alpha_1^2, \boldsymbol{\Delta}_1[2])$. Then the error probability that is averaged w.r.t the permutations is given by

$$\begin{aligned}\mathrm{P}(\mathrm{e}_1^{(2)}[2] \,|\, \alpha_1^2, \boldsymbol{\Delta}_1[2]) = &\left(\mathrm{P}(\mathrm{e}_1^{(2)}[2] \,|\, \{\mathrm{e}_1^{(1)}, \mathfrak{L}=0\}, \alpha_1^2, \boldsymbol{\Delta}_1[2])\cdot \mathrm{P}(\mathrm{e}_2^{(1)}[1])\right) \\ &+ \left(\mathrm{P}(\mathrm{e}_1^{(2)}[2] \,|\, \{\mathrm{c}_1^{(1)}, \mathfrak{L}=0\}, \alpha_1^2, \boldsymbol{\Delta}_1[2])\cdot(1-\mathrm{P}(\mathrm{e}_2^{(1)}[1]))\right). \quad (4.30)\end{aligned}$$

Then, substituting (4.30) into (4.17) we obtain $\mathrm{P}(\mathrm{e}_1^{(2)}[2])$.

The 3rd step is to detect the 1st symbol of the 2nd user. $\mathrm{P}(\mathrm{e}_2^{(2)}[1])$ is obtained by following similar calculations at the 3rd step of the 1st iteration but using the most recent information, i.e. by substituting $\mathrm{P}(\mathrm{e}_1^{(1)}[1])$ and $\mathrm{P}(\mathrm{e}_1^{(1)}[2])$ with $\mathrm{P}(\mathrm{e}_1^{(2)}[1])$ and $\mathrm{P}(\mathrm{e}_1^{(2)}[2])$.

The error statistics for further iterations are obtained in the similar way to calculations provided at the 2nd iteration. And obtaining BER performance for T-SIC is straightforward by substituting $\mathrm{P}(\mathrm{e}_{k^*}^{(l)}[s])$ obtained by above calculations into (4.18). For Conv-SIC, BER performance is obtained by following above calculations only for detecting sth symbol of users and setting $\left(\mathrm{D}_k^{(0)}[\varsigma] \,\middle|\, \mathfrak{L}=0\right) = 1$ for adjacent symbols $\varsigma \in \{(s-1),(s+1)\}$ of interferers, since no a priori information is available for them.

4.3 Shannon Capacity based Performance Comparison

In this section theoretical analysis is provided to compare capacity between Conv-SIC and T-SIC based NOMA systems. Also an uplink OFDMA system is considered for comparison. The theoretical analysis of SC-SIC based NOMA systems is based on so called "onion pealing" or "stripping aided detection" [90], where it is assumed that the interference from a priori detected symbols is perfectly cancelled. Thus, a single iteration of signal processing is applied on the sth IC Triangle. Also through the theoretical analysis, it is considered that transmitted signals and the residual interference signal are Gaussian signals (Equation (2) in [20]). As performance metrics, the spectral efficiency, that is the number of bits transmitted per symbol with arbitrarily small error probability, and the output SINR of system are investigated.

4.3.1 NOMA Spectral Efficiency

Given the ICed signal by (4.6), the theoretical model of the desired symbol in terms of the desired signal and interference plus noise is given by

$$\tilde{Y}_{k^*}^{\mathrm{Th}}[s] = X_{k^*}[s] \cdot \sqrt{p_{k^*}} \cdot \alpha_{k^*} + \tilde{\eta}_{k^*}^{\mathrm{Th}}[s] + N, \tag{4.31}$$

where superscript "Th" represents the theoretical signal model and $\tilde{\eta}_{k^*}^{\mathrm{Th}}[s]$ is the theoretical residual interference to the desired symbol, given by

$$\begin{aligned}\tilde{\eta}_{k^*}^{\mathrm{Th}}[s] = &\sum_{\substack{k\in\Omega\\ k<k^*}} \sum_{\varsigma=s-1}^{s+1} (1 - I_{\mathrm{asyn}}) \cdot \Delta_{k^*,k}[s,\varsigma] \cdot \big(1 - \delta(\varsigma - s)\big) \cdot \big|X_k[\varsigma] - X_k[s]\big| \cdot \sqrt{p_k} \cdot \alpha_k \cdot e^{j\theta_{k^*,k}} \\ &+ \sum_{\substack{k\in\Omega\\ k>k^*}} \sum_{\varsigma=s-1}^{s+1} \Big(1 - \delta\big((\varsigma - s) + 1 + (1 - I_{\mathrm{asyn}})\big)\Big) \cdot \Delta_{k^*,k}[s,\varsigma] \cdot X_k[\varsigma] \cdot \sqrt{p_k} \cdot \alpha_k \cdot e^{j\theta_{k^*,k}}.\end{aligned} \tag{4.32}$$

where I_{asyn} is the indicator parameter that shows if employed SIC technique uses a priori information from adjacent symbols $\{(s-1),(s+1)\}$ of interferers, given by $I_{\mathrm{asyn}} \in \{0,1\}$, $I_{\mathrm{asyn}} = 1$ for T-SIC and $I_{\mathrm{asyn}} = 0$ for Conv-SIC. On the RHS of

(4.32), the first term shows that T-SIC technique completely removes interference from stronger users. But, in case of Conv-SIC technique there is residual interference from adjacent symbols $\{(s-1),(s+1)\}$ of stronger users. Residual interference is due to using inaccurate information of the sth symbol to suppress these signals. The second term on the RHS of (4.32) shows that the T-SIC technique removes interference from the $(s-1)$th symbol of weaker users which are late interferers, i.e. interferers whose time offset is larger than the desired user's.

From (4.31), the SINR of the desired symbol at the NOMA system is given by

$$\gamma_{k^*}^{\mathfrak{N}}[s] = \frac{p_{k^*} \cdot \alpha_{k^*}^2}{\mathrm{Var}(\tilde{\eta}_{k^*}^{\mathrm{Th}}[s]) + \mathrm{Var}(N)}, \tag{4.33}$$

where superscript "$\mathfrak{N}$" denotes NOMA-based system and $\mathrm{Var}(\tilde{\eta}_{k^*}^{\mathrm{Th}}[s])$ is the variance of theoretical residual interference to the desired symbol, given by

$$\begin{aligned}\mathrm{Var}(\tilde{\eta}_{k^*}^{\mathrm{Th}}[s]) = &\sum_{\substack{k\in\Omega\\ k<k^*}} \sum_{\varsigma=s-1}^{s+1} (1-I_{\mathrm{asyn}}) \cdot \Delta_{k^*,k}[s,\varsigma] \cdot \big(1-\delta(\varsigma-s)\big) \cdot p_k \\ &+ \sum_{\substack{k\in\Omega\\ k>k^*}} \sum_{\varsigma=s-1}^{s+1} \Big(1-\delta\big((\varsigma-s)+1+(1-I_{\mathrm{asyn}})\big)\Big) \cdot \Delta_{k^*,k}[s,\varsigma] \cdot p_k/2. \end{aligned} \tag{4.34}$$

Based on (4.34), for T-SIC the variance is caused only by the sth and $(s+1)$th symbols of the weaker users. But for Conv-SIC, the variance is caused by adjacent symbols $\{(s-1),(s+1)\}$ of stronger users and all overlapping symbols of weaker users. Thus, T-SIC significantly reduces the variance of the residual interference, compared to Conv-SIC.

The spectral efficiency for the desired symbol is given by

$$\zeta_{k^*}^{\mathfrak{N}}[s] = \int_0^\infty \log_2(1+\gamma) \cdot f_\gamma^{\mathfrak{N}}(\gamma)\, \mathrm{d}\gamma, \tag{4.35}$$

where $\gamma = \gamma_{k^*}^{\mathfrak{N}}[s]$ represents the instantaneous SINR for the desired symbol and $f_\gamma^{\mathfrak{N}}(\gamma)$ represents pdf of γ. Defining

$$\mathfrak{c}_{k^*} = \frac{p_{k^*}}{\mathrm{Var}(\tilde{\eta}_{k^*}^{\mathrm{Th}}[s]) + Var(N)}, \tag{4.36}$$

substituting (4.36) into (4.33), $\gamma = \mathfrak{c}_{k^*} \cdot \alpha_{k^*}^2$. Since $\alpha_{k^*}^2$ follows exponential distribution with unit mean, γ follows an exponential distribution with mean equal to $\mathfrak{c}_{k^*}$, given

by

$$f_{\gamma}^{\mathfrak{N}}(\gamma) = \left({}^{1}/_{\mathfrak{c}_{k^*}}\right) \cdot e^{-\frac{\gamma}{\mathfrak{c}_{k^*}}}. \tag{4.37}$$

Replacing $f_{\gamma}^{\mathfrak{N}}(\gamma)$ in (4.35) by (4.37), the spectral efficiency of the desired symbol at the NOMA system can then be obtained.

4.3.2 OFDMA Spectral Efficiency

In OFDMA-based systems, users contend to access a subcarrier. Proportional fairness (PF) is a popular metric for contention-based access at wireless cellular networks. It maximizes average throughput of users while prevent users from starving. This paper considers PF scheduler (PFS) for allocation of subcarriers to users in order to guarantee a fair data rate is achieved by each user that is proportional to its transmission distance. Let $\Pr_{\text{access}}(k)$ denote the probability of the subcarrier to be allocated to the kth user and α^2_{access} denote the squared magnitude of channel fading for the user accessing the subcarrier. It has been shown that with i.i.d. fading channel users, PFS provides the same opportunity for being allocated with a subcarrier to users regardless of their location (i.e. average channel condition) [106]. Therefore, with K users contending for the subcarrier, $\Pr_{\text{access}}(k) = 1/K$, $\forall k$. Further, the subcarrier allocation only depends on the fading of the channel and the user with the best channel condition will be allocated for transmission over the subcarrier, i.e. user that wins the contention is $k^* = \arg\max_{k\in\Omega}\{\alpha_k^2\}$ and $\alpha^2_{\text{access}} = \max_{k\in\Omega}\{\alpha_k^2\}$, where arg max denotes the argument of maximum. Let the superscript "$\mathfrak{O}$" represent OFDMA-based system and $\gamma_{k^*}^{\mathfrak{O}}[s]$ denote the instantaneous SNR for the sth symbol of the k^*th user when allocated with the subcarrier, given by

$$\gamma_{k^*}^{\mathfrak{O}}[s] = \mathfrak{c} \cdot \alpha^2_{\text{access}}, \tag{4.38}$$

where $\mathfrak{c} = \left({}^{p_{k^*}}/_{\text{Var}(N)}\right)$. The pdf of $\gamma_{k^*}^{\mathfrak{O}}[s]$ is given by,

$$f_{\gamma}^{\mathfrak{O}}(\gamma) = \frac{K}{\mathfrak{c}}\left(1 - e^{-\frac{\gamma}{\mathfrak{c}}}\right)^{K-1} e^{-\frac{\gamma}{\mathfrak{c}}}. \tag{4.39}$$

(4.39) is from the order statistics of maximum of K i.i.d. exponentially distributed r.v.s ([107], Chapter 8.1). Then, by considering the percentage of time the k^*th user

can access the channel and $f_{\gamma}^{\mathfrak{O}}(\gamma)$, the spectral efficiency for the sth symbol of the k^*th user is given by

$$\zeta_{k^*}^{\mathfrak{O}}[s] = \frac{1}{K} \int_0^{\infty} \log_2(1+\gamma) \cdot f_{\gamma}^{\mathfrak{O}}(\gamma)\, \mathrm{d}\gamma. \tag{4.40}$$

Comparing SINR expression of NOMA, given by (4.33), to OFDMA, given by (4.38), there is $\mathrm{Var}(\tilde{\eta}_{k^*}^{\mathrm{Th}}[s])$ contributing as an additional noise term that degrade SINR performance of a NOMA user compared to an OFDMA user. The impact of SINR loss on spectral efficiency is in *logarithmic scale*. However, by comparing spectral efficiency expression of NOMA, given by (4.35), to OFDMA, given by (4.40), it is clear that NOMA has frequency reuse gain of $(1/K)^{-1}$ times at *linear scale*. The rate of increase of *linear scale* is superior to *logarithmic scale*. Thus, for acceptable amount of residual interference, NOMA can provide much higher spectral efficiency than OFDMA. Extensive numerical results are provided in the next Chapter to investigate capacity performance of NOMA and OFDMA systems w.r.t. various received power ratio and time offset of users.

Chapter 5

Numerical Results

Contents

5.1 BER Results **62**

5.2 Capacity Results **73**

In this Chapter, representative numerical results are provided for evaluating BER and capacity performances of the proposed T-SIC based NOMA technology, compared to Conv-SIC based NOMA and OFDMA. The results obtained from theoretical analyses and systematic simulations are both illustrated in a multiuser uplink OFDM system.

5.1 BER Results

In this section, the analytical BER performance presented in Chapter 4.2 is compared with simulation results for the scheme based on hard-decision and the scheme employing MMSE equalization and soft-decision.

Figs. 5.1 - 5.4 show the BER performance of T-SIC and Conv-SIC techniques w.r.t. different modulation levels and iterative signal processing with $L = 3$ iterations. QAM levels are chosen to investigate the performance at various scenarios from low, $\{4, 16\}$, to high order, $\{64, 256\}$, modulation. Two users are considered to

share a subcarrier at a NOMA based system. Average received power and time offset of users are varied to investigate the performance. The ratio of the average received power of the 1st user to that of the 2nd user, called received power ratio, is changed from 0 to 40 dB to consider the cases where two users have different power levels, e.g. users at a similar to largely seperated distances to the BS.

In Figs. 5.1 and 5.2, the time offset difference of users are assumed to be uniformly distributed between $[1 - 50]\%$ of the symbol time to obtain average BER performance. Fig. 5.1 shows the comparison of BER at the 3rd iteration for the analysis and systematic simulations, when 16-QAM and hard-decision are employed. It can be seen from the figure that the analysis and systematic simulations have good agreement for both T-SIC and Conv-SIC techniques.

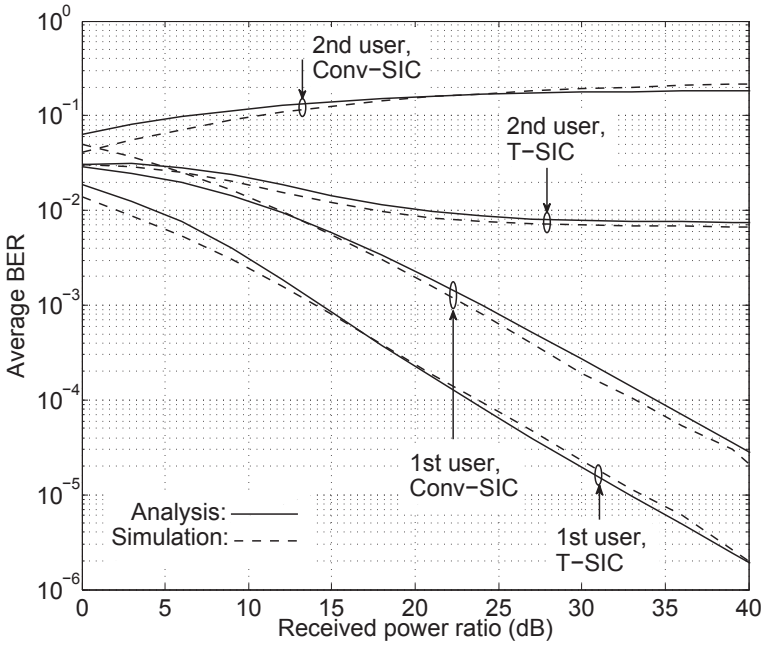

Figure 5.1: Analysis versus simulation BER results at the 3rd iteration. 16-QAM, 2nd user's average received SNR=25dB.

Figs. 5.2 (a)-(d) compare the BER results obtained from the analyis of T-SIC and Conv-SIC, where hard-decision and $\{4, 16, 64, 256\}$-QAM are taken, respectively. It can be seen that when Conv-SIC is employed, only the strong user can achieve low BER but the 2nd user suffers from high BER and cannot have reliable communication

even with the lowest modulation. This is due to strong interference from the adjacent symbol of the 1st user. For reliable communications, a NOMA system needs to satisfy BER constraints of all users. It is seen that, by suppressing the interference from all overlapping symbols of the co-channel user, T-SIC technique can provide low BER to both users for all considered modulation levels when received power ratio of users becomes large. Thus for reliable NOMA communications, it is crucial to handle the asynchronous overlapping symbols, and users need to have large received power ratio. When the power ratio between users increases, the 1st user's signal become much stronger than the 2nd user's signal and many of the 1st user's symbol estimates are correct with high probability. SIC can suppress interference from these correctly estimated symbols and many of the 2nd user's symbols can be correctly estimated with high probability. It can be also seen that as the modulation level increases, the received power ratio required to achieve a given BER increases as well. In order to achieve BER $\leq 10^{-3}$ for the 1st user and BER $\leq 10^{-2}$ for the 2nd user, 4-QAM requires 15 dB but 256-QAM requires 28 dB received power ratio between users. This is because energy per bit required for a given BER is high when the modulation level is high, and the 1st user's signal should be much more stronger than the 2nd user's.

Another important observation from Figs. 5.2 (a)-(d) is the performance gain by iterative signal processing when hard-decision is employed. Figs. 5.2 (a) and (b) show that for low level modulation, there is not significant performance gain after the 2nd iteration. And in Figs. 5.2 (c) and (d) for high modulation level, the 3rd iteration provides approximately 2 dB gain when the received power ratio between users is small, but as the received power ratio between users increases the gain of the 3rd iteration decreases. Thus, when hard-decision is employed it is enough to have two iterations to obtain most of the performance gain when the received power ratio of users is relatively large, e.g. larger than 20 dB.

Figs. 5.3 and 5.4 show BER performance obtained from systematic simulations of T-SIC technique, when MMSE equalization and soft-decision are employed. Time offset (TO) difference of users, called level of asynchronism, is used as a system

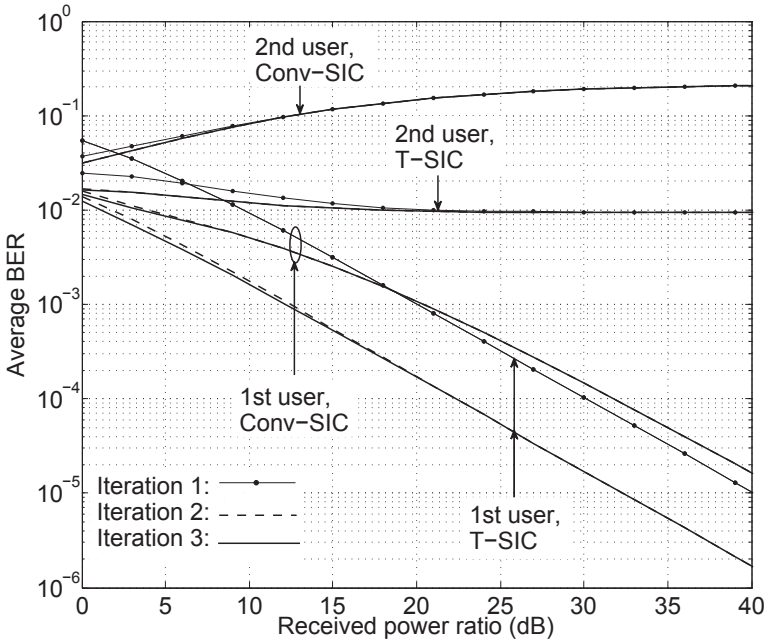

(a) 4-QAM. 2nd user's average received SNR=17dB.

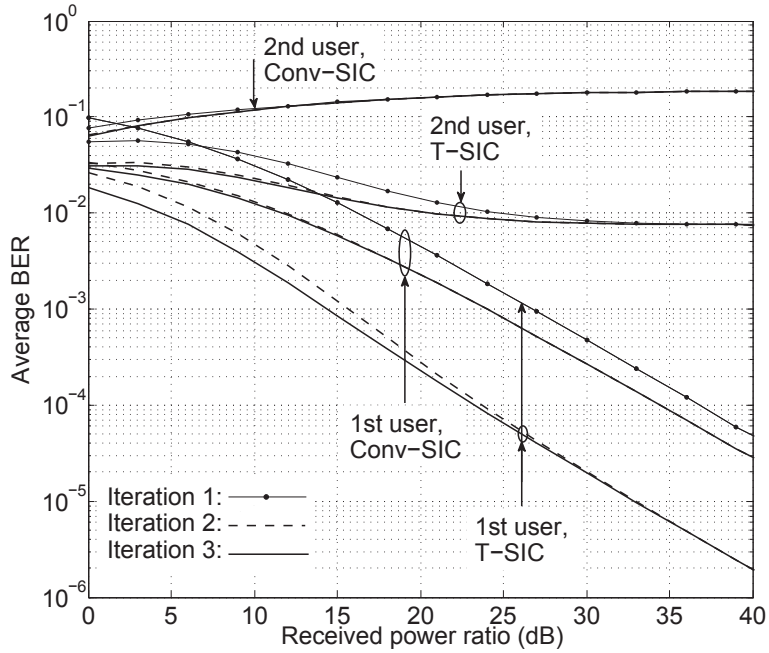

(b) 16-QAM. 2nd user's average received SNR=25dB.

Figure 5.2: Average BER performance.

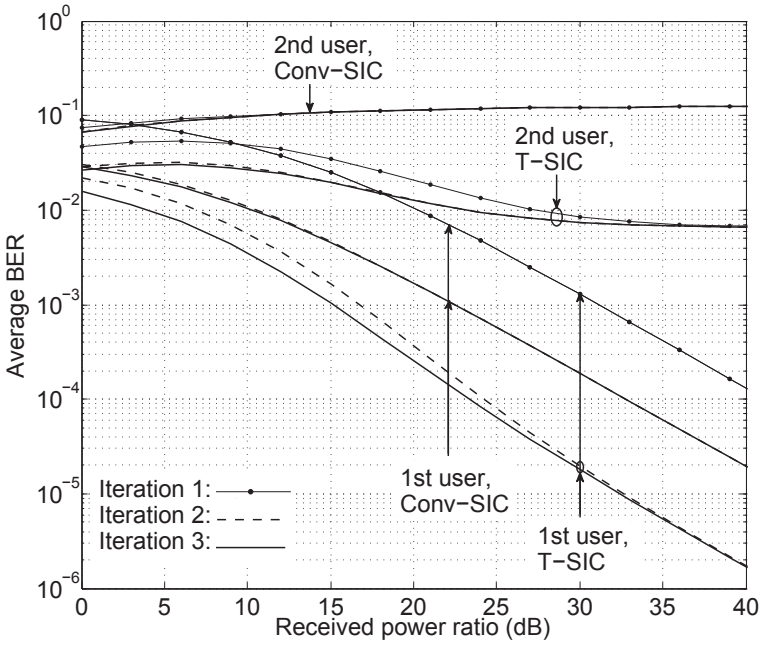

(c) 64-QAM. 2nd user's average received SNR=30dB.

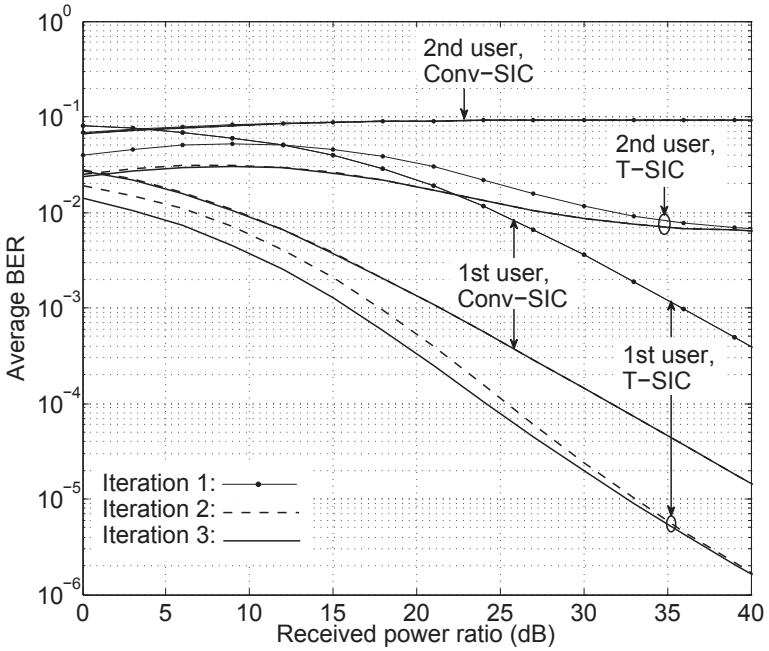

(d) 256-QAM. 2nd user's average received SNR=35dB.

Figure 5.2: Average BER performance.

parameter to investigate the relationship to BER performance. TO is defined as percentage of the symbol time. For example, TO = 10% means the TO of the users are different by 10% of the symbol time. Two scenarios of TO between users are considered – little asynchronism, TO = 10%, illustrated in Fig. 5.3 and high asynchronism, TO = 35%, illustrated in Fig. 5.4.

From Figs. 5.3 and 5.4, it can be seen that when asynchronism is higher the iterative signal processing provides higher performance gain and a lower BER is experienced. This is explained as follows. Referring to the received signal structure in Fig. 3.1 for the two-user case; with the increase of asynchronism from 10% to 35%, at the 1st IC Triangle there is larger portion of the 1st symbol of the 1st user that is interference free from the 2nd user. This results in a more accurate detection of the symbol. Therefore more interference can be suppressed when detecting the 1st symbol of the 2nd user and this detection is more accurate as well. Performing multiple iterations on the 1st IC Triangle also improves the accuracy of detection of other symbols. When the processing is shifted to the $(s \geq 2)$th IC Triangle, the sth symbol of the 1st user is initialized to a more accurate value and also its overlapping with the $(s-1)$th symbol of the 2nd user is larger, which is in high accuracy. These result in symbols of the $(s \geq 2)$th IC Triangle to have more accurate detection. In summary, large asynchronism leads to a start with more accurate detection and then better performances of the subsequent SIC and detection, which results in BER improvement for both users.

The other effect seen from Figs. 5.4 (a)-(d) is the performance gain by iterative signal processing when soft-decision and MMSE equalization are employed. It is seen from Figs. 5.4 (a) and (b) that when a low modulation level is used, most of the gain is obtained at first two iterations. Specifically, in Fig. 5.4 (b) the 2nd iteration provides about 16 dB gain over the 1st iteration, but the 3rd iteration provides less than 1 dB gain over the 2nd iteration. This relationship between the number of iterations and performance gain is similar to the hard-decision case shown in Fig. 5.2 (b), since soft-decision has small performance gain when the modulation level is low. On the other hand when the modulation level increases the gain provided by

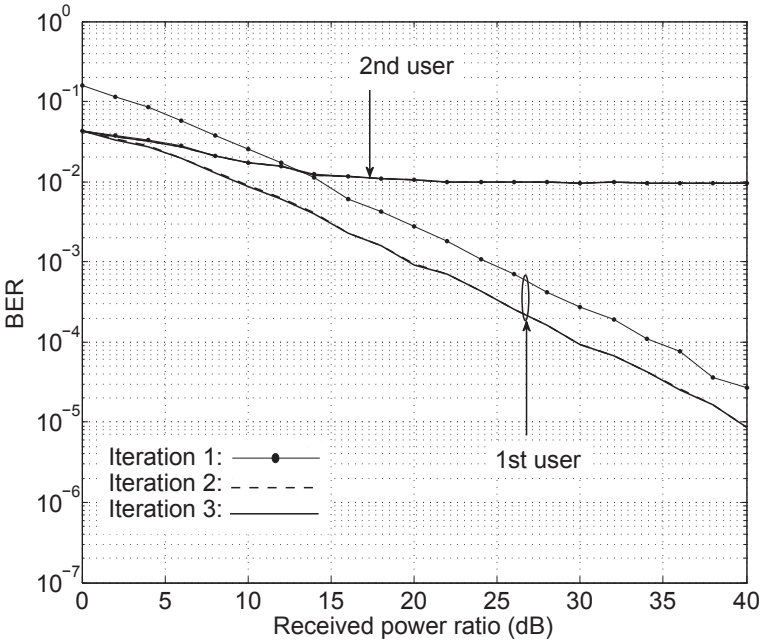

(a) 4-QAM. 2nd user's average received SNR=17dB.

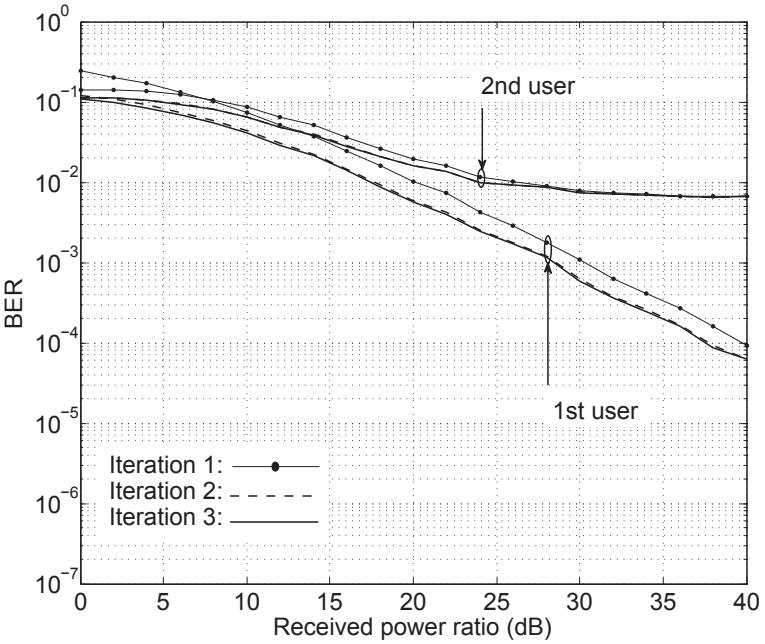

(b) 16-QAM. 2nd user's average received SNR=25dB.

Figure 5.3: BER performance for TO =10%.

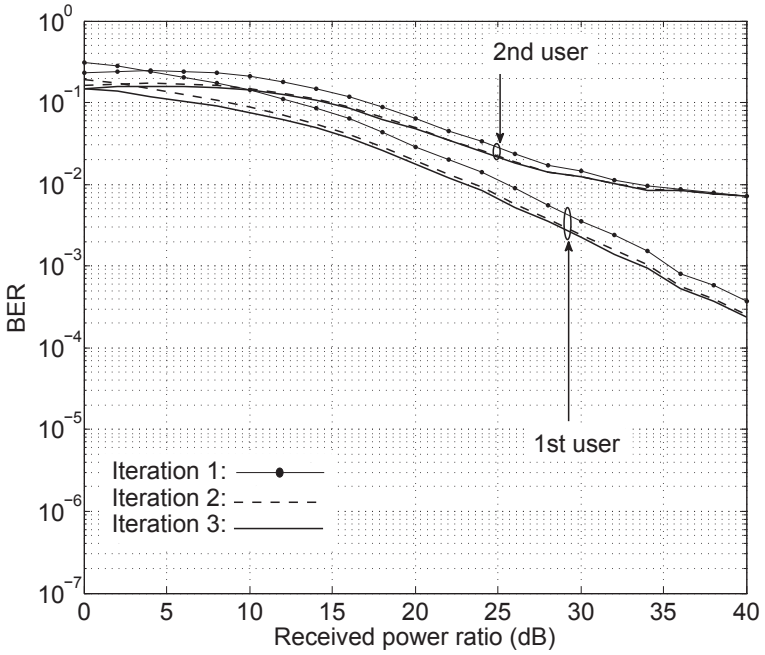

(c) 64-QAM. 2nd user's average received SNR=30dB.

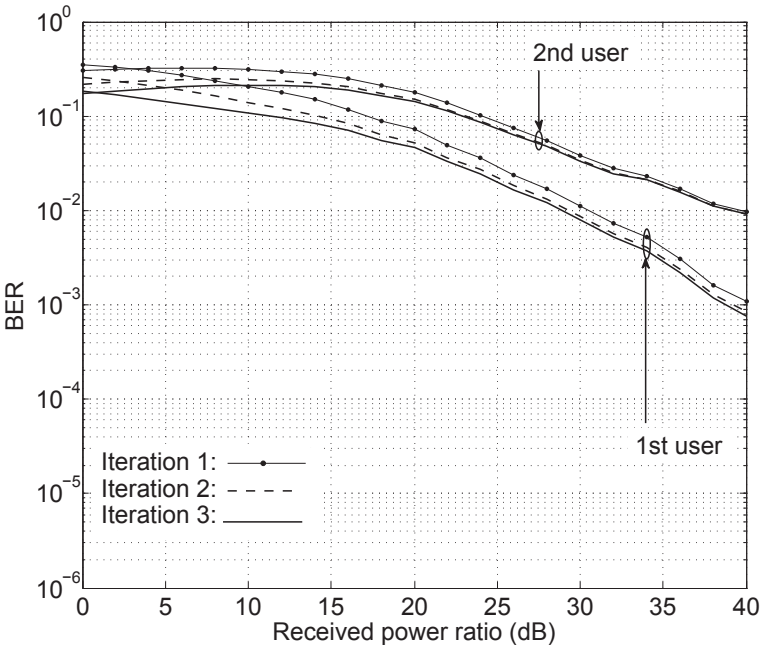

(d) 256-QAM. 2nd user's average received SNR=35dB.

Figure 5.3: BER performance for TO =10%.

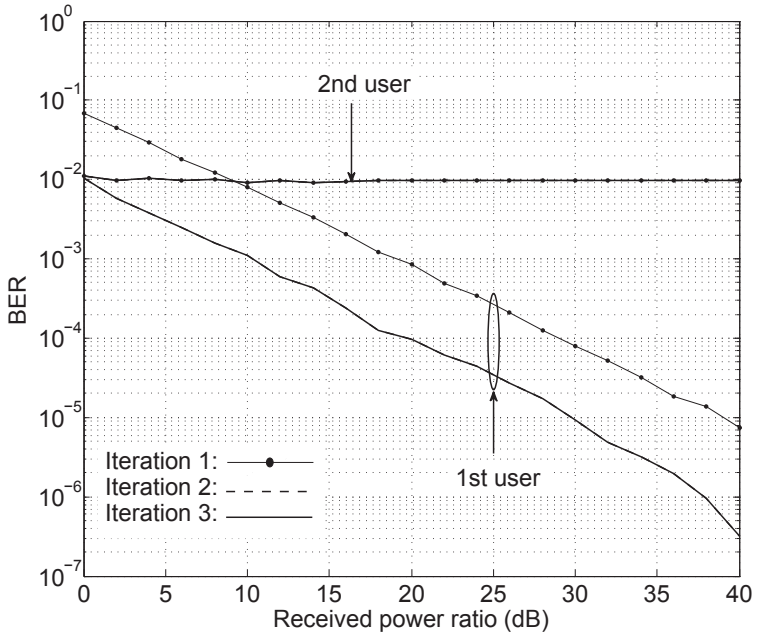

(a) 4-QAM. 2nd user's average received SNR=17dB.

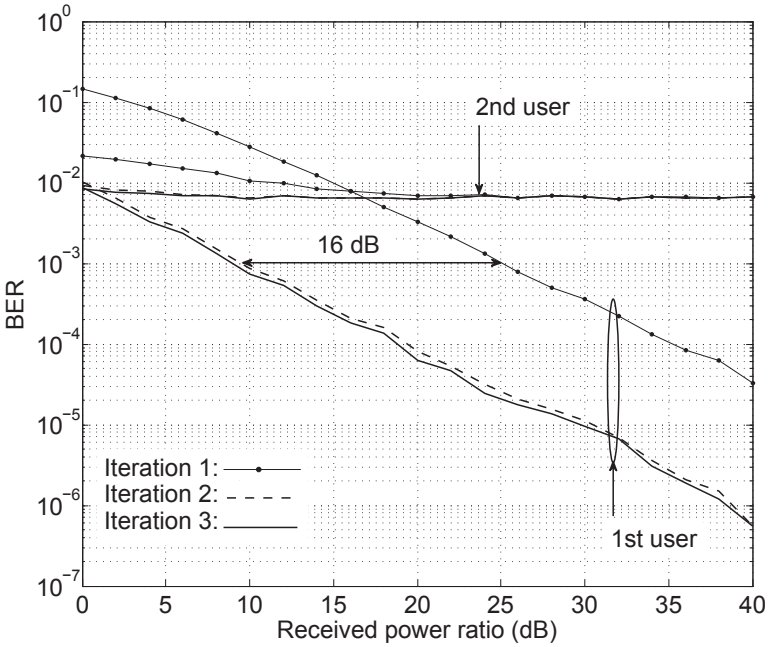

(b) 16-QAM. 2nd user's average received SNR=25dB.

Figure 5.4: BER performance for TO =35%.

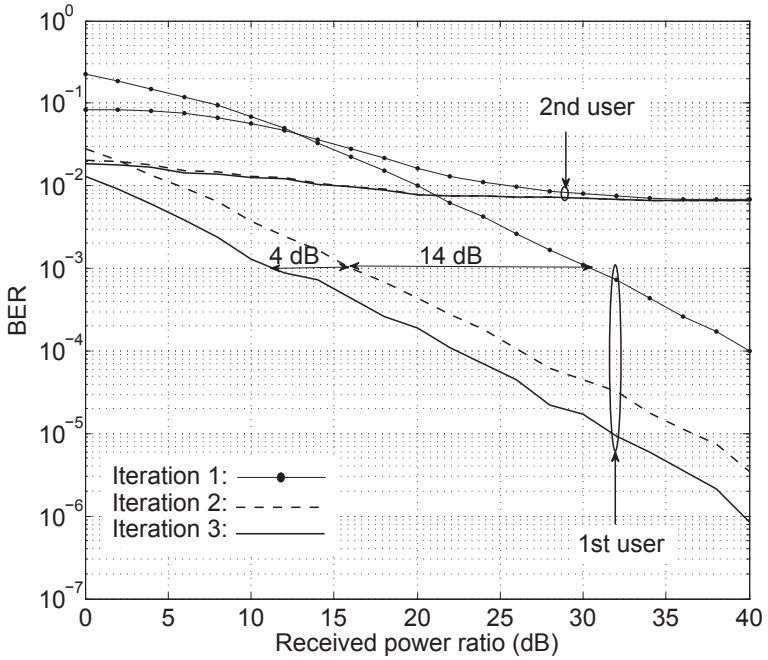

(c) 64-QAM. 2nd user's average received SNR=30dB.

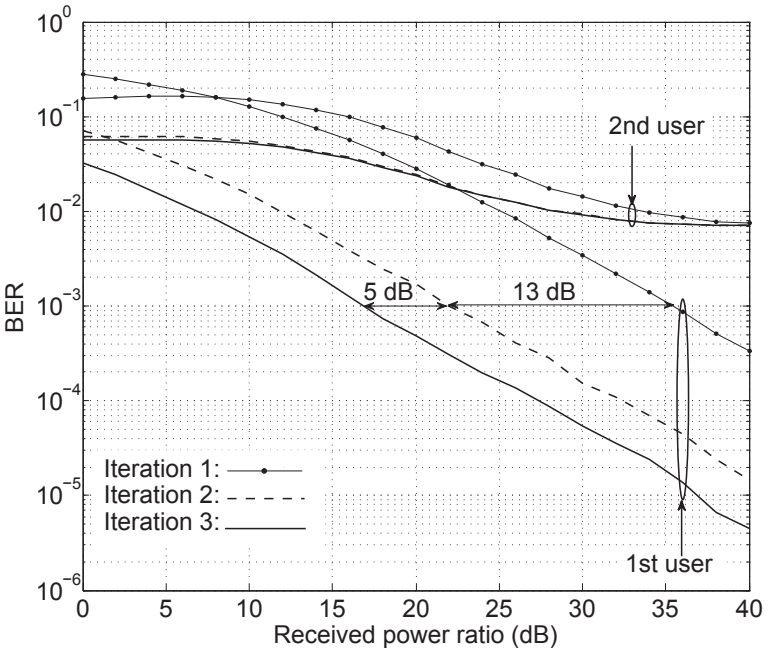

(d) 256-QAM. 2nd user's average received SNR=35dB.

Figure 5.4: BER performance for TO =35%.

the 3rd iteration increases, as seen in Figs. 5.4 (c) and (d). For 256-QAM in Fig. 5.4 (d), the 2nd iteration provides about 13 dB gain over the 1st iteration and the 3rd iteration provides about 5 dB gain over the 2nd iteration. Thus, soft-detection provides more gain as the modulation level increases and can benefit from a number of iterations that is larger than two.

Fig. 5.5 shows the effect of varying transmit SNR of the users on the BER performance when the power ratio between two users is fixed. The BER performance of T-SIC at the 3rd iteration for three different power ratios – 15, 25 and 35 dB for small, medium and large power ratio cases– are shown in the figure. Assuming $\lambda = 3$ for the small cell environment, the power ratios correspond to having the path loss for about 3, 7 and 15 meters distance between the two users. Also, the distance between the BS and the 1st user (near user) is assumed to be 5 meters corresponding to about 21 dB path loss. The transmit SNR of the two users are assumed to be equal and varied from $60 - 100$ dB to investigate the effect on BER performance. It is seen from the figure that, when the power ratio is 15 dB both users' BER performance reaches an interference-limited floor at about 75 dB transmit SNR and any further increase in the transmit SNR does not improve the users' BER performance. This is due to the relatively high interference among the co-channel users and the interference dominates the BER performance rather than the noise at this region. In other words, the BER performance becomes interference-limited rather than noise-limited. By increasing the power ratio between the two users, it is seen that the interference-limited floor occur at lower BER values; such as for 25 dB power ratio the floor goes down to about 10^{-3} and 10^{-5} for the 2nd and 1st users. The interference-limited floor for 35 dB power ratio does not occur within the 100 dB transmit SNR range and the system can achieve BER less than 10^{-3} and 10^{-6} for the 2nd and 1st users. Therefore, in order to achieve desired BER constraint of users, it is important to consider the power ratio between users (i.e. interference-limited BER region), as well as the noise-limit.

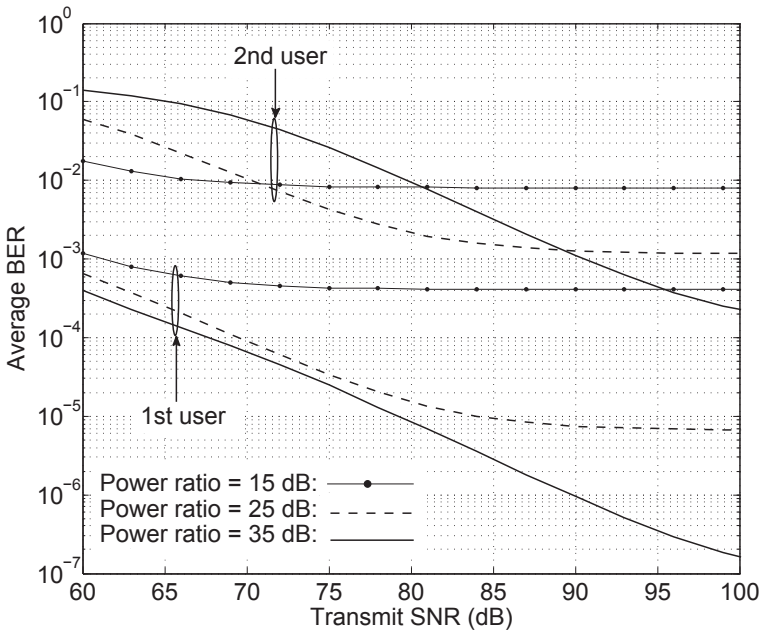

Figure 5.5: Average BER performance at the 3rd iteration versus transmit SNR. 16 QAM.

5.2 Capacity Results

In this section the capacity performance is numerically evaluated based on analysis in Section 4.3. Three users accessing a subcarrier for uplink transmissions is considered. Transmit SNR of users is set to be 50 dB, where the variance of noise is normalized to be unity. Received SNR and time offset of users are varied to investigate performance. Combinations of considered average received SNR of users are shown in Table 5.1. The combinations are choosen to represent various scenarios of users at a similar to largely seperated distance(s) to the BS. Time offset triplets (ToT $= (\tau_1, \tau_2, \tau_3)$) are used to represent the time offset of three users, where scenarios of little and high asynchronism among users are considered.

Fig. 5.6 shows the ratio of residual MAI to transmit power for the desired symbol, called ratio of MAI to transmit power, given by $|\text{MAI}/p_{k^*}| = \text{Var}(\tilde{\eta}_{k^*}^{\text{Th}}[s])/p_{k^*}$, where $\text{Var}(\tilde{\eta}_{k^*}^{\text{Th}}[s])$ is given by (4.34), when Conv-SIC and T-SIC techniques are employed. Figs. 5.6 (a) and (b) illustrates the performance for the cases of little asynchronism,

Scenario ID	Avg. received SNR (dB)			Power ratio (dB)
	1^{st} user	2^{nd} user	3^{rd} user	
A	40	40	40	0
B	40	37	34	3
C	40	34	28	6
D	40	31	22	9
E	40	28	16	12
F	40	25	10	15

Table 5.1: Average received SNR of users.

ToT = $(0\%, 5\%, 10\%)$, and high asynchronism, ToT = $(0\%, 35\%, 50\%)$, respectively. For T-SIC it is seen that $|\text{MAI}/p_{k^*}|$ decreases as the power ratio of users increases, since interfering signals are getting weaker. This output result shows that by superimposing users from different distances and/or adjusting transmission power of users, $|\text{MAI}/p_{k^*}|$ can be controlled. However for Conv-SIC the 2^{nd} and 3^{rd} users meet a high interference floor due to the residual interference from the adjacent symbol of the stronger users. Note that the value of interference floor depends on the time offset. With little asynchronism, in Fig. 5.6 (a), the interference floor is much lower than high asynchronism, in Fig. 5.6 (b). This is because as the asynchronism increases the overlapping with (i.e. interference from) adjacent symbol of stronger users increases, see $\Delta_{k^*,k}[s, \varsigma]$ term at (4.34). It is also seen that, for the 1^{st} user T-SIC provides much significant performance gain over Conv-SIC at high asynchronism, compared to the performance gain at little asynchronism. This is because the overlapping with the $(s-1)$th symbol of weaker interferers increases. In summary, it is seen from Fig. 5.6 that, at asynchronous NOMA transmissions $|\text{MAI}/p_{k^*}|$ performance do not only depend on the power ratio of users, as in synchronous NOMA transmissions, but also it strongly depend on the time offset of users.

Fig. 5.7 shows spectral efficiency performance of users, given by (4.35), when Conv-SIC and T-SIC techniques are employed. Average received SNR of users are

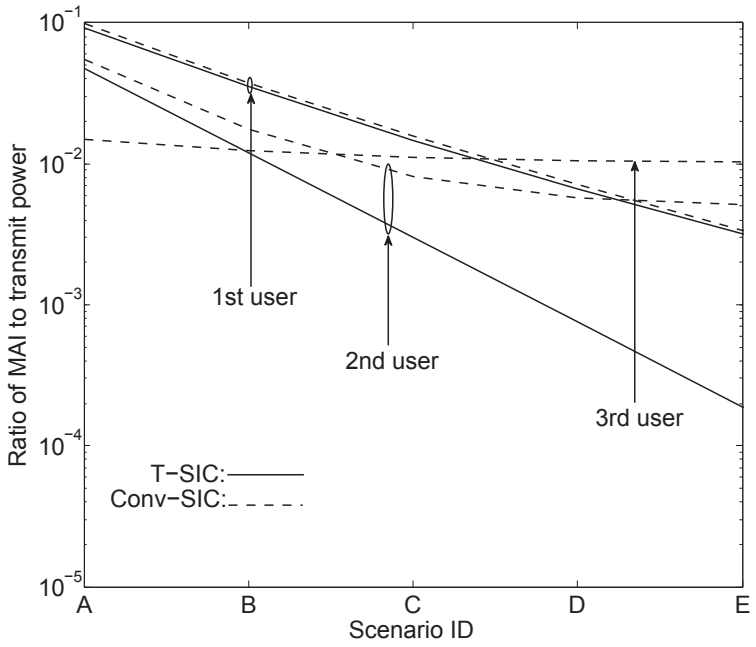

(a) Little asynchronism, ToT = $(0\%, 5\%, 10\%)$.

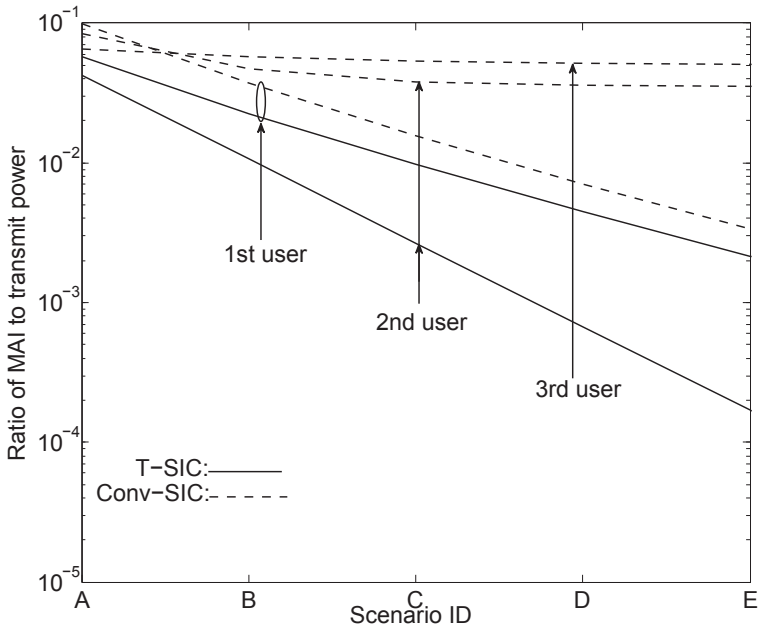

(b) High asynchronism, ToT = $(0\%, 35\%, 50\%)$.

Figure 5.6: $|\mathrm{MAI}/p_{k^*}|$ versus different average received SNR ratios (see Table 5.1).

assumed to be 30 dB for the 1st user, 18 dB for the 2nd user and 6 dB for the 3rd user. That is, the power ratio between the 1st user and the 2nd user or the 2nd user and the 3rd user is 12 dB. Time offset between users are represented by the x-axis of Fig. 5.7. That is, for the x-axis value equal to 10, the time offset difference between the 1st user and the 2nd user or the 2nd user and the 3rd user is 10% of the symbol time. It is seen from the figure that the spectral efficiency of the 1st user increases with increasing asynchronism, when T-SIC is used, since more interference is suppressed from the $(s-1)$th symbol of the 2nd and 3rd users. However, Conv-SIC does not exploit this a priori information and has worse performance than T-SIC, where the performance difference increase with increasing asynchronism. Spectral efficiency of the 2nd user is increasing slightly with increasing asynchronism, when T-SIC is employed, since more interference from the $(s-1)$th symbol of the 3rd user is suppressed. When Conv-SIC is employed, spectral efficiency of the 2nd user decreases rapidly as asynchronism increases. This is due to interference from the 1st user getting stronger. Spectral efficiency of the 3rd user is fixed at approx. 2 bits/symbol, when T-SIC is employed. But when Conv-SIC is employed the 3rd user is not able to have any successful data transmission. These observations show that spectral efficiency performance of NOMA users depends on the time offset of users. Therefore, performance analysis cannot be accurate without considering the time offset of users. Also it is seen that if asynchronism is not handled at NOMA uplink transmissions, only the strongest user can communicate its data and other users need to be turned off.

Fig. 5.8 shows sum spectral efficiency of a subcarrier when OFDMA and NOMA with Conv-SIC and T-SIC techniques are considered for multiple access. Sum spectral efficiency of a subcarrier is given by $\zeta = \sum_{k\in\Omega} \zeta_k$, where ζ_k is given by (4.40) and (4.35) for OFDMA and NOMA, respectively. Several scenarios from little asynchronism, ToT $= (0\%, 5\%, 10\%)$, to high asynchronism, ToT $= (0\%, 35\%, 50\%)$, with different power ratio of users, given by Table 5.1, are considered. It is seen from Fig. 5.8 that performance of OFDMA decreases linearly as average power ratio increases. This is because the 2nd and 3rd users achieve less bits/symbol due to smaller

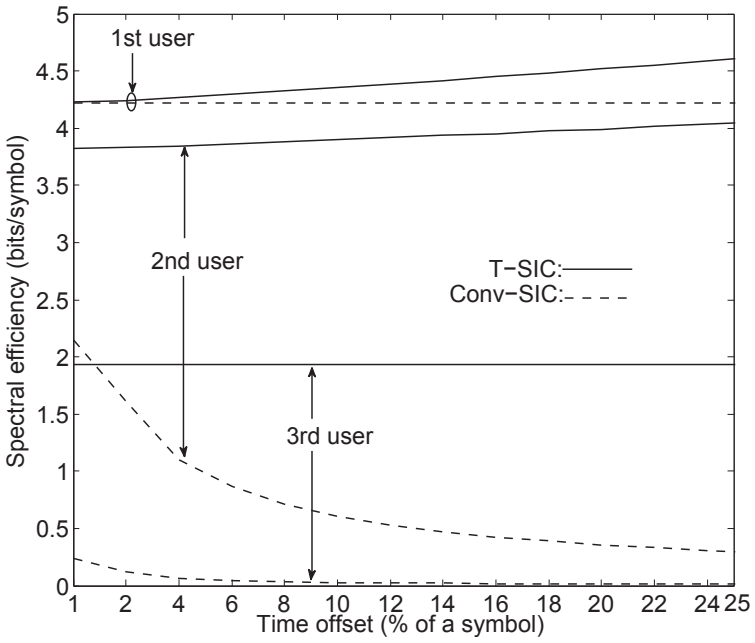

Figure 5.7: Spectral efficiency versus different levels of asynchronism of users.

average SNR. When Conv-SIC is employed for NOMA its performance is worse than the OFDMA even with little asynchronism, for all considered power ratios. This is because of strong interference among SCed users. When the power ratio increases, the performance gradually improves, but still significantly worse than OFDMA. On the contrary when T-SIC is employed, NOMA has superior performance to OFDMA for all the considered scenarios. The performance gain over OFDMA increases with increasing the power ratio. This is because NOMA allows all users to access a subcarrier concurrently. While the 2^{nd} and 3^{rd} users' reduced average received SNR reduces their achievable bits/symbol, it also reduces co-channel interference to other users (as illustrated by Fig. 5.6) so that other users' achievable bits/symbol is increased. These two contrary effect prevent sum spectral efficiency of a subcarrier to degrade, unlike the case of OFDMA. Therefore NOMA can benefit from near-far effect in wireless communications. Further, performance gain over OFDMA increases with increasing asynchronism since T-SIC can suppress more interference. In summary, NOMA has performance gain over OFDMA when asynchronism is properly addressed.

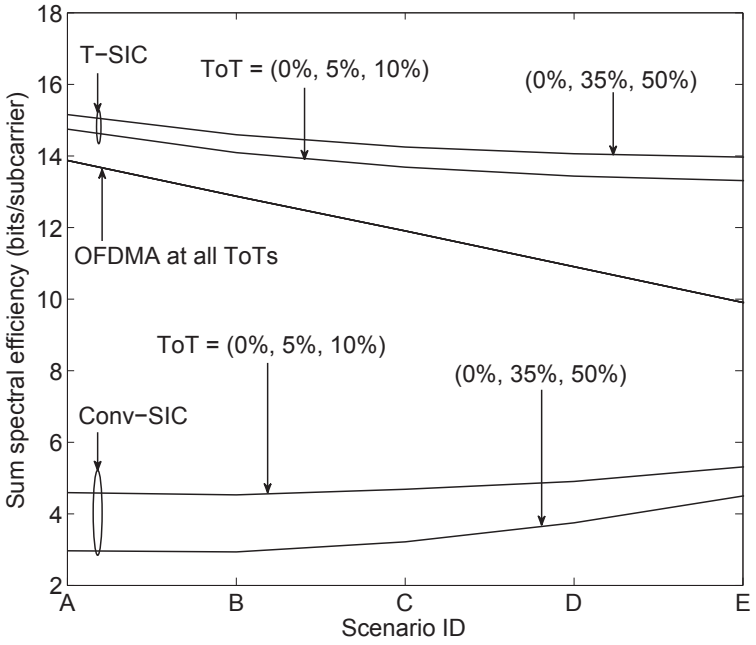

Figure 5.8: Sum spectral efficiency verus different user power ratios (see Table 5.1).

Fig. 5.9 shows the spectral efficiency performance of users when their average channel condition are largely different, see scenarios D-F in Table 5.1. When users' channel condition are largely different it is important for a multiple access technology to preserve the fairness among users in terms of not degrading performance of far users too much to cause them to starve. The figure shows performance of OFDMA and NOMA with T-SIC. It is seen from the figure that, when NOMA with T-SIC is employed the performance of far users (i.e. the 2^{nd} and 3^{rd} users) are significantly better than that of OFDMA's. Specifically, when NOMA with T-SIC is employed the far users' spectral efficiency are not less than 3 bits/symbol at considered scenarios. However, when OFDMA is employed the worst user's spectral efficiency degrades down to about 1.3 bits/symbol. Therefore, referring to Figs. 5.8 and 5.9 it is seen that NOMA with T-SIC can provide superior sum spectral efficiency than OFDMA while preserving fairness among users.

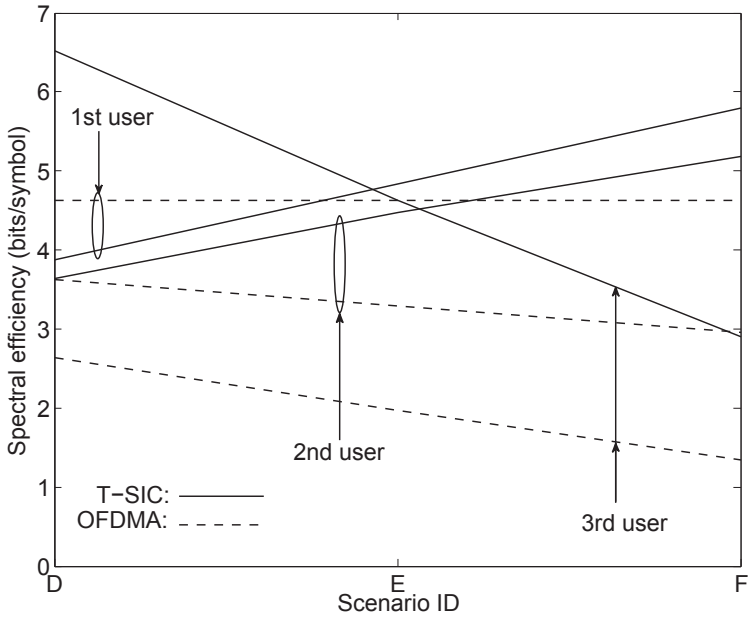

Figure 5.9: Spectral efficiency when users' average channel conditions are largely different (see Table 5.1).

Chapter 6

Conclusions and Future Research

Contents

6.1 Summary and Conclusions 80

6.2 Future Research Directions 81

6.1 Summary and Conclusions

NOMA can overcome a major problem of OMA based techniques that is not to allow frequency reuse within one cell, and is an advantageous technique for uplink transmission in future wireless communications. By considering the effect of asynchronism on NOMA communications, a novel SIC technique called T-SIC was proposed that can benefit from frequency reuse as well as the near-far effect. The BER and capacity performances of the NOMA with Conv-SIC and T-SIC techniques were investigated. Also the capacity of NOMA and OFDMA were compared. The following conclusions are drawn.

1. In the NOMA system, SCed users are required to have large received power ratio to satisfy BER requirements. And the required received power ratio increases with increasing the modulation level.

2. In the NOMA uplink transmissions, the proposed T-SIC technique with iterative signal processing provides significant BER performance improvement.

3. At iterative signal processing for NOMA, the number of iterations to obtain most of the gain at BER performance depend on the modulation level and detection method. With hard-decision it is sufficient to have two iterations. With soft-decision, for low modulation level, it is enough to have two iterations, whereas for high modulation level, a relatively higher number of iterations is desirable.

4. Unlike synchronous communications, at uplink transmissions, users' BER and capacity performances strongly depend on the relative time offset between interfering users, besides the received power ratio. If asynchronism is not considered, when the time offset difference between users increases, the interference increases and performance degrades. But when asynchronism is properly addressed and interference is suppressed by the T-SIC, performance can be improved significantly.

5. With the developed T-SIC techique, by adjusting users' average received power, $|\mathrm{MAI}/p_{k^*}|$ and related performances – capacity and BER – of users can be controlled.

6. At uplink communications, NOMA with the proposed T-SIC technique significantly outperforms OFDMA due to frequency reuse.

6.2 Future Research Directions

The research presented by this thesis showed that NOMA is an advantageous technology for future wireless communications. Yet, for the practical realization of the NOMA still much research effort is needed to develop advanced NOMA signal processing techniques. Following are a number of interesting research directions that the research of this thesis can be extended:

- **Extended T-SIC.** The received signal structure presented in Fig. 3.1 showed that symbols of SCed users overlaps with two adjacent symbols of other users in time domain. This may introduce correlation among detection of users' symbols in time domain and so detecting symbols of users' in groups, i.e. in a time window, may improve detection performance. Therefore it can be interesting to propose and investigate an "Extended T-SIC" algorithm that extends the IC Triangles to cover a larger group, i.e. a window, of symbols and apply the iterative processing to the window of symbols, as illustrated in Fig. 6.1. It is required to compare the performances of "non-extended T-SIC" and "Extended T-SIC" to find out if it is worth to extend IC Triangles. Moreover, finding the minimum size of the window that may provide significant performance gain over "non-extended T-SIC" can be beneficial to find out the optimal window size that keeps the detection latency as low as possible.

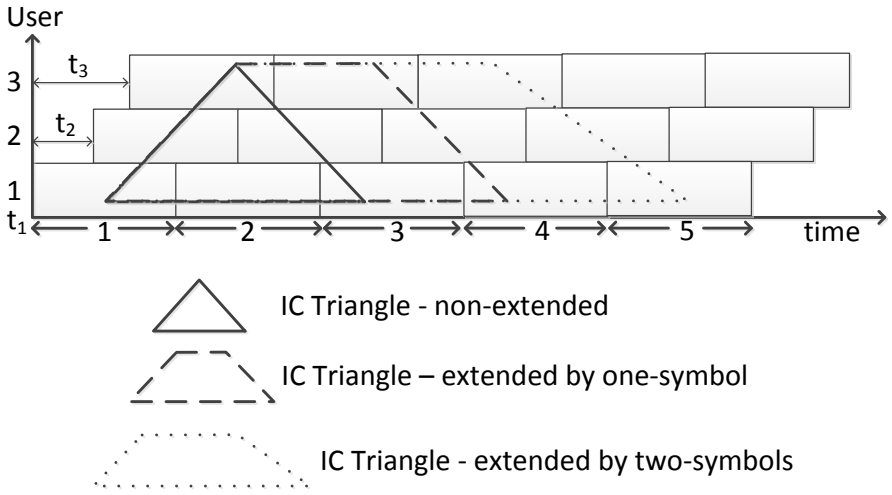

Figure 6.1: Extended T-SIC concept.

- **User scheduling and RRM for NOMA uplink transmissions.** The presented research showed that in NOMA uplink the performance of users strongly depends on the relative time offset among co-channel users, besides the received power ratio. Therefore, users' time offset can be used as one of the important parameters at user scheduling and RRM algorithms, i.e. "time-offset

aware" frequency, transmission power, and modulation level, allocation can be studied.

- **Investigation of NOMA uplink transmissions with non-orthogonal waveforms.** OFDM is a widely adopted multiplexing technique for multi-carrier (MC) wireless communications systems. However, requirements for the 5G and beyond wireless networks present challenges for OFDM [108]. GFDM [36] is a flexible multiplexing technique for MC systems that can overcome challenges of OFDM and proposed for the air interface of 5G networks. Therefore, it will be interesting to research and develop the performance of asynchronous NOMA transmissions at GFDM based systems. Further, the research can be extended to other waveforms, such as universal filtered multi-carrier [109] and bi-orthogonal frequency division multiplexing [110].

The output of this thesis and future research contribute to the state-of-the-art on uplink communications, and can be used by industry to design, optimize and investigate performance of future communication systems.

Appendix A

The Mean Square Error of Detection at the lth iteration

Given (4.10), $\left(\mathrm{D}_k^{(\mathfrak{L})}[\varsigma] \,\middle|\, \mathrm{z}_k^{(\mathfrak{L})}[\varsigma]\right) = E[(X_k[\varsigma] - \hat{X}_k^{(\mathfrak{L})}[\varsigma])^2]$ represents the MSE of the detection at the $\mathfrak{L}$th iteration for the ςth symbol of the kth user. For $\mathfrak{L} = 0$, there was no a priori detection done for the symbol yet, so $\mathrm{D}_k^{(0)}[\varsigma] = 1$. For $\mathfrak{L} \geq 1$, a priori detection was done for the symbol. With probability $(1 - \mathrm{Pe}_k^{(\mathfrak{L})}[\varsigma])$ the detection was correct so $\left(\mathrm{D}_k^{(\mathfrak{L})}[\varsigma] \,\middle|\, X_k[\varsigma] = \hat{X}_k^{(\mathfrak{L})}[\varsigma]\right) = 0$; with probability $\mathrm{Pe}_k^{(\mathfrak{L})}[\varsigma]$ the detection was in error and $\left(\mathrm{D}_k^{(\mathfrak{L})}[\varsigma] \,\middle|\, X_k[\varsigma] \neq \hat{X}_k^{(\mathfrak{L})}[\varsigma]\right)$ is obtained as follows. Let $\mathrm{P}(m_i \,|\, m_j)$ denote the probability of detecting constellation point m_i, given that constellation m_j is transmitted. For M-QAM constellation $\left(\mathrm{D}_k^{(\mathfrak{L})}[\varsigma] \,\middle|\, X_k[\varsigma] \neq \hat{X}_k^{(\mathfrak{L})}[\varsigma]\right)$ is given by

$$\left(\mathrm{D}_k^{(\mathfrak{L})}[\varsigma] \,\middle|\, X_k[\varsigma] \neq \hat{X}_k^{(\mathfrak{L})}[\varsigma]\right) = \sum_{\substack{i=1 \\ i \neq j}}^{M} (m_j - m_i)^2 \cdot \mathrm{P}(m_i \,|\, m_j). \tag{A.1}$$

With hard-decision, the event with $\mathrm{P}(m_i \,|\, m_j)$ occurs when the power of residual interference plus noise exceeds half of the distance between nearest constellation points and the resultant ICed signal is closest to constellation point m_i. Since the power of residual interference plus noise is Gaussian distributed (as explained in Chapter 4.2) and Gaussian distribution has tail distribution with exponential falloff, the error probability for a constellation point for another point that is not one of its nearest neighbour is much less than that for a nearest neighbour. Thus nearest

neighbour approximation to the detection error is used in this paper ([59], Chapter 5.1). Then, for Gray coded QAM constellation with average unit power,

$$\left(\mathrm{D}_k^{(\mathfrak{L})}[\varsigma] \,\middle|\, X_k[\varsigma] \neq \hat{X}_k^{(\mathfrak{L})}[\varsigma]\right) = (m_i - m_j)^2 = (2 \cdot \mathrm{d}_{\text{unit}})^2 = ({}^{6}/_{(M-1)}) \tag{A.2}$$

where $\mathrm{d}_{\text{unit}} = \sqrt{{}^{3}/_{2(M-1)}}$ is half of the distance between two nearest neighbour constellation points at a constellation with average unit power. Then, the unified expression for all above cases is given by

$$\left(\mathrm{D}_k^{(\mathfrak{L})}[\varsigma] \,\middle|\, \mathrm{z}_k^{(\mathfrak{L})}[\varsigma]\right) = \begin{cases} 1, & \text{for } \mathfrak{L} = 0, \text{i.e. no priori detection was done for the symbol} \\ {}^{6}/_{(M-1)}, & \text{for } \mathfrak{L} \geq 1 \text{ and } \mathrm{z}_k^{(\mathfrak{L})}[\varsigma] = \mathrm{e}_k^{(\mathfrak{L})}[\varsigma], \text{i.e. priori detection was in error} \\ 0, & \text{for } \mathfrak{L} \geq 1 \text{ and } \mathrm{z}_k^{(\mathfrak{L})}[\varsigma] = \mathrm{c}_k^{(\mathfrak{L})}[\varsigma], \text{i.e. priori detection was correct.} \end{cases} \tag{A.3}$$

References

[1] A. Zanella, N. Bui, A. Castellani, L. Vangelista, and M. Zorzi, "Internet of Things for Smart Cities," *IEEE Internet of Things Journal*, vol. 1, pp. 22–32, Feb 2014.

[2] Libelium, "50 sensor applications for a smarter world: get inspired!." http:/www.libelium.com/top_50_iot_sensor_applications_ranking, August 2013. Accessed: 2014-12-01.

[3] J. Stankovic, "Research Directions for the Internet of Things," *IEEE Internet of Things Journal*, vol. 1, pp. 3–9, Feb 2014.

[4] V. Kostakos, T. Ojala, and T. Juntunen, "Traffic in the Smart City: Exploring City-Wide Sensing for Traffic Control Center Augmentation," *IEEE Internet Computing*, vol. 17, pp. 22–29, Nov 2013.

[5] N. Golrezaei, P. Mansourifard, A. Molisch, and A. Dimakis, "Base-Station Assisted Device-to-Device Communications for High-Throughput Wireless Video Networks," *IEEE Transactions on Wireless Communications*, vol. 13, pp. 3665–3676, July 2014.

[6] S. Abdelwahab, B. Hamdaoui, M. Guizani, and A. Rayes, "Enabling Smart Cloud Services Through Remote Sensing: An Internet of Everything Enabler," *IEEE Internet of Things Journal*, vol. 1, pp. 276–288, June 2014.

[7] A. Osseiran, F. Boccardi, V. Braun, K. Kusume, P. Marsch, M. Maternia, O. Queseth, M. Schellmann, H. Schotten, H. Taoka, H. Tullberg, M. Uusitalo, B. Timus, and M. Fallgren, "Scenarios for 5G mobile and wireless communications: the vision of the METIS project," *IEEE Communications Magazine*, vol. 52, pp. 26–35, May 2014.

[8] H. Zhu, "Performance Comparison Between Distributed Antenna and Microcellular Systems," *IEEE Journal on Selected Areas in Communications*, vol. 29, pp. 1151–1163, June 2011.

[9] H. Zhu and J. Wang, "Performance Analysis of Chunk-Based Resource Allocation in Multi-Cell OFDMA Systems," *IEEE Journal on Selected Areas in Communications*, vol. 32, pp. 367–375, February 2014.

[10] H. Osman, H. Zhu, D. Toumpakaris, and J. Wang, "Achievable Rate Evaluation of In-Building Distributed Antenna Systems," *IEEE Transactions on Wireless Communications*, vol. 12, pp. 3510–3521, July 2013.

[11] Z. Ding, Z. Yang, P. Fan, and H. Poor, "On the Performance of Non-Orthogonal Multiple Access in 5G Systems with Randomly Deployed Users," *IEEE Signal Processing Letters*, vol. 21, pp. 1501–1505, Dec 2014.

[12] J. Choi, "Non-Orthogonal Multiple Access in Downlink Coordinated Two-Point Systems," *IEEE Communications Letters*, vol. 18, pp. 313–316, February 2014.

[13] Y. Saito, Y. Kishiyama, A. Benjebbour, T. Nakamura, A. Li, and K. Higuchi, "Non-Orthogonal Multiple Access (NOMA) for Cellular Future Radio Access," in *2013 IEEE 77th Vehicular Technology Conference (VTC Spring)*, pp. 1–5, June 2013.

[14] H. Zhu and J. Wang, "Chunk-Based Resource Allocation in OFDMA Systems Part II: Joint Chunk, Power and Bit Allocation," *IEEE Transactions on Communications*, vol. 60, pp. 499–509, February 2012.

[15] N. Abu-Ali, A. Taha, M. Salah, and H. Hassanein, "Uplink Scheduling in LTE and LTE-Advanced: Tutorial, Survey and Evaluation Framework," *IEEE Communications Surveys and Tutorials*, vol. PP, no. 99, pp. 1–27, 2013.

[16] H. Zhu, "Radio Resource Allocation for OFDMA Systems in High Speed Environments," *IEEE Journal on Selected Areas in Communications*, vol. 30, pp. 748–759, May 2012.

[17] Y. Endo, Y. Kishiyama, and K. Higuchi, "Uplink non-orthogonal access with MMSE-SIC in the presence of inter-cell interference," in *2012 International Symposium on Wireless Communication Systems (ISWCS)*, pp. 261–265, Aug 2012.

[18] H. Zhu and J. Wang, "Chunk-based resource allocation in OFDMA systems - part I: chunk allocation," *IEEE Transactions on Communications*, vol. 57, pp. 2734–2744, September 2009.

[19] M. Al-Imari, P. Xiao, M. Imran, and R. Tafazolli, "Uplink non-orthogonal multiple access for 5G wireless networks," in *2014 11th International Symposium on Wireless Communications Systems (ISWCS)*, pp. 781–785, Aug 2014.

[20] R. Zhang and L. Hanzo, "A Unified Treatment of Superposition Coding Aided Communications: Theory and Practice," *IEEE Communications Surveys and Tutorials*, vol. 13, pp. 503–520, Third 2011.

[21] V. Jungnickel, K. Manolakis, W. Zirwas, B. Panzner, V. Braun, M. Lossow, M. Sternad, R. Apelfroĺjd, and T. Svensson, "The role of small cells, coordinated multipoint, and massive MIMO in 5G," *IEEE Communications Magazine*, vol. 52, pp. 44–51, May 2014.

[22] S. Chen and J. Zhao, "The requirements, challenges, and technologies for 5G of terrestrial mobile telecommunication," *IEEE Communications Magazine*, vol. 52, pp. 36–43, May 2014.

[23] W. H. Chin, Z. Fan, and R. Haines, "Emerging technologies and research challenges for 5G wireless networks," *IEEE Wireless Communications*, vol. 21, pp. 106–112, April 2014.

[24] F. Boccardi, R. Heath, A. Lozano, T. Marzetta, and P. Popovski, "Five disruptive technology directions for 5G," *IEEE Communications Magazine*, vol. 52, pp. 74–80, February 2014.

[25] E. Larsson, O. Edfors, F. Tufvesson, and T. Marzetta, "Massive MIMO for next generation wireless systems," *IEEE Communications Magazine*, vol. 52, pp. 186–195, February 2014.

[26] C. Lim, T. Yoo, B. Clerckx, B. Lee, and B. Shim, "Recent trend of multiuser MIMO in LTE-advanced," *IEEE Communications Magazine*, vol. 51, pp. 127–135, March 2013.

[27] C. Park, Y.-P. Wang, G. Joĺngren, and D. Hammarwall, "Evolution of uplink MIMO for LTE-advanced," *IEEE Communications Magazine*, vol. 49, pp. 112–121, February 2011.

[28] J. Wang, H. Zhu, and N. Gomes, "Distributed Antenna Systems for Mobile Communications in High Speed Trains," *IEEE Journal on Selected Areas in Communications*, vol. 30, pp. 675–683, May 2012.

[29] H. Zhu, "On frequency reuse in cooperative distributed antenna systems," *IEEE Communications Magazine*, vol. 50, pp. 85–89, April 2012.

[30] H. Zhu, S. Karachontzitis, and D. Toumpakaris, "Low-complexity resource allocation and its application to distributed antenna systems," *IEEE Wireless Communications*, vol. 17, pp. 44–50, June 2010.

[31] H. ElSawy, E. Hossain, and D. I. Kim, "HetNets with cognitive small cells: user offloading and distributed channel access techniques," *IEEE Communications Magazine*, vol. 51, pp. 28–36, June 2013.

[32] H. Wang, X. Zhou, and M. Reed, "Coverage and Throughput Analysis with a Non-Uniform Small Cell Deployment," *IEEE Transactions on Wireless Communications*, vol. 13, pp. 2047–2059, April 2014.

[33] M. Shakir, K. Qaraqe, H. Tabassum, M.-S. Alouini, E. Serpedin, and M. Imran, "Green heterogeneous small-cell networks: toward reducing the CO2 emissions of mobile communications industry using uplink power adaptation," *IEEE Communications Magazine*, vol. 51, pp. 52–61, June 2013.

[34] 3rd Generation Partnership Project 2, "Physical layer for ultra mobile broadband (UMB) air interface specification. 3GPP2 C.P0084-001 ." http:/www.3gpp2.org, February 2007.

[35] Q.-D. Ho and T. Le-Ngoc, "Efficient Algorithms for Non-Realtime Video Multicasting in Wireless Networks," in *2009 IEEE International Conference on Communications*, pp. 1–5, June 2009.

[36] G. Fettweis, M. Krondorf, and S. Bittner, "GFDM - Generalized Frequency Division Multiplexing," in *2009 IEEE 69th Vehicular Technology Conference (VTC Spring)*, pp. 1–4, April 2009.

[37] A. Goldsmith, S. Jafar, I. Maric, and S. Srinivasa, "Breaking Spectrum Gridlock With Cognitive Radios: An Information Theoretic Perspective," *Proceedings of the IEEE*, vol. 97, pp. 894–914, May 2009.

[38] J. Schaepperle, "Throughput of a wireless cell using superposition based multiple-access with optimized scheduling," in *2010 IEEE 21st International Symposium on Personal Indoor and Mobile Radio Communications (PIMRC)*, pp. 212–217, Sept 2010.

[39] L. Ping, J. Tong, X. Yuan, and Q. Guo, "Superposition coded modulation and iterative linear MMSE detection," *IEEE Journal on Selected Areas in Communications*, vol. 27, pp. 995–1004, August 2009.

[40] A. Zafar, M. Shaqfeh, M.-S. Alouini, and H. Alnuweiri, "On Multiple Users Scheduling Using Superposition Coding over Rayleigh Fading Channels," *IEEE Communications Letters*, vol. 17, pp. 733–736, April 2013.

[41] Z. Ding, M. Peng, and H. V. Poor, "Cooperative Non-Orthogonal Multiple Access in 5G Systems," *arXiv:1410.5846s*, October 2014.

[42] J. Tate and I. Bate, "A feedback-driven timing synchronisation protocol for cellular sensornets," in *2010 IEEE 7th International Conference on Mobile Adhoc and Sensor Systems (MASS)*, pp. 482–491, Nov 2010.

[43] H. Osada, M. Inamori, and Y. Sanada, "Non-Orthogonal Access Scheme over Multiple Channels with Iterative Interference Cancellation and Fractional Sampling in OFDM Receiver," in *2012 IEEE 75th Vehicular Technology Conference (VTC Spring)*, pp. 1–5, May 2012.

[44] S. Vanka, S. Srinivasa, Z. Gong, P. Vizi, K. Stamatiou, and M. Haenggi, "Superposition Coding Strategies: Design and Experimental Evaluation," *IEEE Transactions on Wireless Communications*, vol. 11, pp. 2628–2639, July 2012.

[45] D. Tse and P. Viswanath, *Fundamentals of Wireless Communication*. New York, NY, USA: Cambridge University Press, 2005.

[46] L. Li and J. Townsend, "Near-Far Resistant Synchronization for UWB Communications," *IEEE Transactions on Wireless Communications*, vol. 10, pp. 519–529, February 2011.

[47] J. Kodithuwakku, N. Letzepis, R. McKilliam, and A. Grant, "Decoder-Assisted Timing Synchronization in Multiuser CDMA Systems," *IEEE Transactions on Communications*, vol. 62, pp. 2061–2071, June 2014.

[48] H. Ju and R. Zhang, "Throughput Maximization in Wireless Powered Communication Networks," *IEEE Transactions on Wireless Communications*, vol. 13, pp. 418–428, January 2014.

[49] H. Haci, H. Zhu, and J. Wang, "Novel scheduling for a mixture of real-time and non-real-time traffic," in *2012 IEEE Global Communications Conference (GLOBECOM)*, pp. 4647–4652, Dec 2012.

[50] A. Vallejo, A. Zaballos, J. Selga, and J. Dalmau, "Next-generation QoS control architectures for distribution smart grid communication networks," *IEEE Communications Magazine*, vol. 50, pp. 128–134, May 2012.

[51] D. Huang, B. He, and C. Miao, "A Survey of Resource Management in Multi-Tier Web Applications," *IEEE Communications Surveys Tutorials*, vol. 16, pp. 1574–1590, Third 2014.

[52] T. Liu, C. Yang, and L.-L. Yang, "A Unified Analysis of Spectral Efficiency for Two-Hop Relay Systems With Different Resource Configurations," *IEEE Transactions on Vehicular Technology*, vol. 62, pp. 3137–3148, Sept 2013.

[53] Y. Wang and J. Coon, "MUI-Reducing Spreading Code Design for BS-CDMA in the Presence of Carrier Frequency Offset," *IEEE Transactions on Vehicular Technology*, vol. 60, pp. 2583–2593, July 2011.

[54] L. Guan, Z. Li, J. Si, and B. Hao, "Analysis of asynchronous frequency hopping multiple-access network performance based on the frequency hopping sequences," *IET Communications*, vol. 9, no. 1, pp. 117–121, 2015.

[55] M. Butt, S. X. Ng, and L. Hanzo, "Self-Concatenated Code Design and its Application in Power-Efficient Cooperative Communications," *IEEE Communications Surveys Tutorials*, vol. 14, pp. 858–883, Third 2012.

[56] Z. Yang, L. Cai, Y. Luo, and J. Pan, "Topology-Aware Modulation and Error-Correction Coding for Cooperative Networks," *IEEE Journal on Selected Areas in Communications*, vol. 30, pp. 379–387, February 2012.

[57] H. Chen, R. Maunder, and L. Hanzo, "A Survey and Tutorial on Low-Complexity Turbo Coding Techniques and a Holistic Hybrid ARQ Design Example," *IEEE Communications Surveys Tutorials*, vol. 15, pp. 1546–1566, Fourth 2013.

[58] T. M. Cover and J. A. Thomas, *Elements of Information Theory.* New York, NY, USA: Wiley-Interscience, 1991.

[59] A. Goldsmith, *Wireless Communications.* New York, NY, USA: Cambridge University Press, 2005.

[60] N. Miridakis and D. Vergados, "A Survey on the Successive Interference Cancellation Performance for Single-Antenna and Multiple-Antenna OFDM Systems," *IEEE Communications Surveys and Tutorials*, vol. 15, pp. 312–335, First 2013.

[61] J. Andrews, "Interference cancellation for cellular systems: a contemporary overview," *IEEE Wireless Communications*, vol. 12, pp. 19–29, April 2005.

[62] P. Salvo Rossi and G. Kraidy, "Iterative Multiuser Detection for Cooperative MIMO Systems over Quasi-Static Fading Channels," *IEEE Transactions on Wireless Communications*, vol. 10, pp. 3638–3643, November 2011.

[63] F. Xinxin, H. Minn, L. Yan, and L. Jinhui, "PIC-based iterative SDR detector for OFDM systems in doubly-selective fading channels," *IEEE Transactions on Wireless Communications*, vol. 9, pp. 86–91, January 2010.

[64] P. Patel and J. Holtzman, "Analysis of a simple successive interference cancellation scheme in a DS/CDMA system," *IEEE Journal on Selected Areas in Communications*, vol. 12, pp. 796–807, Jun 1994.

[65] I. Krikidis, "Analysis and Optimization Issues for Superposition Modulation in Cooperative Networks," *IEEE Transactions on Vehicular Technology*, vol. 58, pp. 4837–4847, Nov 2009.

[66] M. Hua, B. Ren, M. Wang, J. Zou, C. Yang, and T. Liu, "Performance Analysis of OFDMA and SC-FDMA Multiple Access Techniques for Next Generation Wireless Communications," in *2013 IEEE 77th Vehicular Technology Conference (VTC Spring)*, pp. 1–4, June 2013.

[67] H. Inaltekin and S. Hanly, "Optimality of Binary Power Control for the Single Cell Uplink," *IEEE Transactions on Information Theory*, vol. 58, pp. 6484–6498, Oct 2012.

[68] H. Shi, R. Prasad, E. Onur, and I. Niemegeers, "Fairness in Wireless Networks:Issues, Measures and Challenges," *IEEE Communications Surveys Tutorials*, vol. 16, pp. 5–24, First 2014.

[69] A. Gyasi-Agyei and S.-L. Kim, "Comparison of opportunistic scheduling policies in time-slotted amc wireless networks," in *Wireless Pervasive Computing, 2006 1st International Symposium on*, pp. 6 pp.–, Jan 2006.

[70] A. Benjebbour, A. Li, Y. Saito, Y. Kishiyama, A. Harada, and T. Nakamura, "System-level performance of downlink NOMA for future LTE enhancements," in *2013 IEEE Globecom Workshops (GC Wkshps)*, pp. 66–70, Dec 2013.

[71] A. Benjebbour, Y. Saito, Y. Kishiyama, A. Li, A. Harada, and T. Nakamura, "Concept and practical considerations of non-orthogonal multiple access (NOMA) for future radio access," in *2013 International Symposium on Intelligent Signal Processing and Communications Systems (ISPACS)*, pp. 770–774, Nov 2013.

[72] J. Ketonen, M. Juntti, and J. Cavallaro, "Performance - Complexity Comparison of Receivers for a LTE MIMO - OFDM System," *IEEE Transactions on Signal Processing*, vol. 58, pp. 3360–3372, June 2010.

[73] H. Haci and H. Zhu, "Novel scheduling characteristics for mixture of real-time and non-real-time traffic," in *2013 IEEE Wireless Communications and Networking Conference (WCNC)*, pp. 1733–1738, April 2013.

[74] Y. Zhou and T.-S. Ng, "MIMO-OFCDM systems with joint iterative detection and optimal power allocation," *IEEE Transactions on Wireless Communications*, vol. 7, pp. 5504–5516, December 2008.

[75] C.-Y. Tso, J.-M. Wu, and P.-A. Ting, "Iterative Interference Cancellation for STBC-OFDM Systems in Fast Fading Channels," in *2009 IEEE Global Telecommunications Conference*, pp. 1–5, Nov 2009.

[76] M. Salem, A. Adinoyi, M. Rahman, H. Yanikomeroglu, D. Falconer, Y.-D. Kim, E. Kim, and Y.-C. Cheong, "An Overview of Radio Resource Management in Relay-Enhanced OFDMA-Based Networks," *IEEE Communications Surveys and Tutorials*, vol. 12, pp. 422–438, Third 2010.

[77] D. Lopez-Perez, X. Chu, and J. Zhang, "Dynamic Downlink Frequency and Power Allocation in OFDMA Cellular Networks," *IEEE Transactions on Communications*, vol. 60, pp. 2904–2914, October 2012.

[78] T. Novlan, R. Ganti, A. Ghosh, and J. Andrews, "Analytical Evaluation of Fractional Frequency Reuse for OFDMA Cellular Networks," *IEEE Transactions on Wireless Communications*, vol. 10, pp. 4294–4305, December 2011.

[79] A. Hamza, S. Khalifa, H. Hamza, and K. Elsayed, "A Survey on Inter-Cell Interference Coordination Techniques in OFDMA-Based Cellular Networks," *IEEE Communications Surveys and Tutorials*, vol. 15, pp. 1642–1670, Fourth 2013.

[80] G. Wunder, M. Kasparick, S. ten Brink, F. Schaich, T. Wild, I. Gaspar, E. Ohlmer, S. Krone, N. Michailow, A. Navarro, G. Fettweis, D. Ktenas, V. Berg, M. Dryjanski, S. Pietrzyk, and B. Eged, "5GNOW: Challenging the LTE Design Paradigms of Orthogonality and Synchronicity," in *2013 IEEE 77th Vehicular Technology Conference (VTC Spring)*, pp. 1–5, June 2013.

[81] S. Chen and J. Zhao, "The requirements, challenges, and technologies for 5G of terrestrial mobile telecommunication," *IEEE Communications Magazine*, vol. 52, pp. 36–43, May 2014.

[82] NTT DOCOMO, "5G Concept and Technologies." http:5gworkshop.hhi.fraunhofer.de/wp-content/uploads/2014/12/Globecom-2014-

WS-on-5G-New-Air-Interface-NTT-DOCOMO.pdf, December 2014. Accessed: 2015-03-17.

[83] 3rd Generation Partnership Project, "Release 13: RP-141831." http:/www.3gpp.org/release-13, September 2014. Accessed: 2015-03-17.

[84] H. Haci, H. Zhu, and J. Wang, "Resource Allocation in User-Centric Wireless Networks," in *2012 IEEE 75th Vehicular Technology Conference (VTC Spring)*, pp. 1–5, May 2012.

[85] Y. Rahmatallah and S. Mohan, "Peak-To-Average Power Ratio Reduction in OFDM Systems: A Survey And Taxonomy," *IEEE Communications Surveys and Tutorials*, vol. 15, pp. 1567–1592, Fourth 2013.

[86] G. Wunder, P. Jung, M. Kasparick, T. Wild, F. Schaich, Y. Chen, S. Brink, I. Gaspar, N. Michailow, A. Festag, L. Mendes, N. Cassiau, D. Ktenas, M. Dryjanski, S. Pietrzyk, B. Eged, P. Vago, and F. Wiedmann, "5GNOW: non-orthogonal, asynchronous waveforms for future mobile applications," *IEEE Communications Magazine*, vol. 52, pp. 97–105, February 2014.

[87] K. Higuchi and Y. Kishiyama, "Non-Orthogonal Access with Random Beamforming and Intra-Beam SIC for Cellular MIMO Downlink," in *2013 IEEE 78th Vehicular Technology Conference (VTC Fall)*, pp. 1–5, Sept 2013.

[88] M. Sharif and B. Hassibi, "On the capacity of MIMO broadcast channels with partial side information," *IEEE Transactions on Information Theory*, vol. 51, pp. 506–522, Feb 2005.

[89] T. Matsumoto, Y. Hatakawa, and S. Konishi, "Performance analysis of interleave-division multiple access for uplink in multi-cell environment," in *2011 7th International Wireless Communications and Mobile Computing Conference (IWCMC)*, pp. 376–381, July 2011.

[90] J. Tong, L. Ping, and X. Ma, "Superposition Coded Modulation With Peak-Power Limitation," *IEEE Transactions on Information Theory*, vol. 55, pp. 2562–2576, June 2009.

[91] J. Tong, L. Ping, Z. Zhang, and V. Bhargava, "Iterative Soft Compensation for OFDM Systems with Clipping and Superposition Coded Modulation," *IEEE Transactions on Communications*, vol. 58, pp. 2861–2870, October 2010.

[92] K. Bae, J. Andrews, and E. Powers, "Quantifying an iterative clipping and filtering technique for reducing PAR in OFDM," *IEEE Transactions on Wireless Communications*, vol. 9, pp. 1558–1563, May 2010.

[93] N. Miridakis and D. Vergados, "A Survey on the Successive Interference Cancellation Performance for Single-Antenna and Multiple-Antenna OFDM Systems," *IEEE Communications Surveys and Tutorials*, vol. 15, pp. 312–335, First 2013.

[94] J. Tong and L. Ping, "Performance analysis of superposition coded modulation," *Physical Communication*, vol. 3, no. 3, pp. 147–155, 2010.

[95] Q. Guo, D. Huang, S. Nordholm, J. Xi, and L. Ping, "Soft-In Soft-Out Detection Using Partial Gaussian Approximation," *IEEE Access*, vol. 2, pp. 427–436, 2014.

[96] R. Zhang and L. Hanzo, "Superposition-Coding-Aided Multiplexed Hybrid ARQ Scheme for Improved End-to-End Transmission Efficiency," *IEEE Transactions on Vehicular Technology*, vol. 58, pp. 4681–4686, Oct 2009.

[97] H. A. Ngo and L. Hanzo, "Hybrid Automatic-Repeat-reQuest Systems for Cooperative Wireless Communications," *IEEE Communications Surveys and Tutorials*, vol. 16, pp. 25–45, First 2014.

[98] H. Haci and H. Zhu, "Performance of Non-orthogonal Multiple Access with a Novel Interference Cancellation Method," in *2015 IEEE International Conference on Communications (ICC)*, June 2015.

[99] Z. Wang, S. Zhou, J. Catipovic, and P. Willett, "Asynchronous Multiuser Reception for OFDM in Underwater Acoustic Communications," *IEEE Transactions on Wireless Communications*, vol. 12, pp. 1050–1061, March 2013.

[100] K. Hamdi, "Precise interference analysis of OFDMA time-asynchronous wireless ad-hoc networks," *IEEE Transactions on Wireless Communications*, vol. 9, pp. 134–144, January 2010.

[101] K. Raghunath and A. Chockalingam, "SIR analysis and interference cancellation in uplink OFDMA with large carrier frequency/timing offsets," *IEEE Transactions on Wireless Communications*, vol. 8, pp. 2202–2208, May 2009.

[102] H. Wang, R. Song, and S. Leung, "Analysis of Uplink Inter-Carrier-Interference in OFDMA Femtocell Networks," *IEEE Transactions on Vehicular Technology*, vol. PP, no. 99, pp. 1–1, 2014.

[103] F. Zhu, X. Shang, B. Chen, and H. Poor, "On the Capacity of Multiple-Access-Z-Interference Channels," *IEEE Transactions on Information Theory*, vol. 60, pp. 7732–7750, Dec 2014.

[104] A. Reyni, *Probability Theory.* Amsterdam: North-Holland, 1970.

[105] University of Alabama in Huntsville, Virtual Laboratories, "Special Distribution Simulator." http://www.math.uah.edu/stat/applets/SpecialSimulation.html. Accessed: 2015-05-05.

[106] E. Liu, Q. Zhang, and K. Leung, "Asymptotic Analysis of Proportionally Fair Scheduling in Rayleigh Fading," *IEEE Transactions on Wireless Communications*, vol. 10, pp. 1764–1775, June 2011.

[107] A. Papoulis and S. U. Pillai, *Probability, random variables, and stochastic processes.* Tata McGraw-Hill Education, 2002.

[108] N. Michailow, M. Matthe, I. Gaspar, A. Caldevilla, L. Mendes, A. Festag, and G. Fettweis, "Generalized Frequency Division Multiplexing for 5th Generation Cellular Networks," *IEEE Transactions on Communications*, vol. 62, pp. 3045–3061, Sept 2014.

[109] V. Vakilian, T. Wild, F. Schaich, S. ten Brink, and J.-F. Frigon, "Universal-filtered multi-carrier technique for wireless systems beyond LTE," in *2013 IEEE Globecom Workshops (GC Wkshps)*, pp. 223–228, Dec 2013.

[110] R. Ayadi, M. Siala, and I. Kammoun, "Transmit/receive pulse-shaping design in BFDM systems over time-frequency dispersive AWGN channel," in *2007 IEEE International Conference on Signal Processing and Communications (ICSPC 2007)*, pp. 772–775, Nov 2007.